A NUMERICAL STUDY OF THE INTERACTION OF TIDAL FLOWS IN THE MERSEY ESTUARY AND LIVERPOOL BAY

QIN LI

Ph.D.

2004

A numerical study of the interaction of tidal flows in the Mersey estuary and Liverpool bay

Qin Li

A thesis submitted in partial fulfilment of the requirements of
London Metropolitan University
for the degree of
Doctor of Philosophy

December 2004

CONTENTS

Acknowledgements

I would like to thank Dr. Amir Khossousi, my director of studies, for his continuous help throughout this project. His patience and support have played an important role in the completion of my thesis. I am deeply grateful to Dr. Bryan Johns, for many invaluable discussions and suggestions. His advice and assistance was critical to the success of the project.

I also want to thank Dr. Jiuxing Xing of Proudman Oceanographic Laboratory, for his advice and especially for providing me opportunities to visit POL, Bidston Observatory over the years. His explanation helped me better understand the Irish Sea Model.

I would like to thank London Metropolitan University (formerly London Guildhall University) and the Proudman Oceanographic Laboratory for providing the funds and facilities. Specifically, I must mention Professor Ulf Ehrenmark and Dr. Alan Davies for their help and encouragement.

Finally, special thanks must go to my husband and parents for their constant love and support.

A numerical study of the interaction of tidal flows in the Mersey estuary and Liverpool bay

Qin Li

ABSTRACT

A numerical model for coastal and estuary waters has been developed to study the dynamic processes in estuaries and shallow water. The model is based on joining together a multi-level two dimensional river model with a three-dimensional hydrodynamic bay model. An interactive sigma coordinate splicing scheme is used to match the sigma coordinates with different vertical and time resolution so that the exchange of dynamic information between two models can be achieved.

The river model has been used for the modelling of the flow and relevant transport processes, including salinity and sediment transport in the estuary. The bay model has been used to provide real time tidal forcing information to the river model across the common boundary of two models.

After the joined model was set up and operated satisfactorily, the numerical experiments were carried out in Liverpool bay and the Mersey estuary to study the interaction of tidal flow in these two areas. The model was applied with real time tidal forcing due to an M_2 tidal constituent at the open boundary of the bay model and freshwater discharge from the Mersey estuary into Liverpool bay. The relevant results obtained from the numerical model have been compared with the data reported according to the observations and have shown good agreement with the data. It is shown that the M_2 tide plays an important role in the mixing of freshwater with the sea water in the Mersey estuary and Liverpool bay. The discharge of freshwater from Mersey into the bay leads to a plume of low salinity water around the mouth of river. The flow in the river driven by tidal forcing from Liverpool bay and the freshwater flow leads to the transport of suspended sediment from the Mersey estuary into Liverpool bay.

Chapter 1 Introduction

As an important part of Oceanography, sea waves have attracted the attention of researchers and have been the subject of study as early as around 300 BC. Tides are a special type of wave which are generated by the gravitational attractions of the Sun and the Moon, but constrained by the configuration of the ocean basins. Waves and tidal currents are responsible for sediment movement and deposition in the coastal region, but in estuaries the tidal processes are more important than wave processes.

Estuaries, can be defined as a partially enclosed body of water where freshwater from rivers and streams flows into the ocean, and mixing with the salty sea water. They are places where rivers meet the sea and are strongly influenced by the ocean dynamics in the shelf seas. Meanwhile they also have influence on the shelf seas.

The shelf sea influences the estuary through its dynamic forcing, such as tidal currents, wind stresses, surface waves and climate circulations. Among these, tidal currents are often the dominant force as they play an important part in determining the patterns of the currents and their dynamic structure. One important consequence of tidal currents in the coastal and nearshore regions is that some of their energy is transferred to the movement of sediment. Sediment transport plays a very important part among the processes in the coastal and shelf sea. A number of numerical studies have been reported in recent years (Chen and Dyke 1996, 1998; Xing and Davies, 2003). What sort of sediment is moved, how much and where it is moved to, depend significantly on the energy of the tidal currents and their direction of motion.

While rivers are influenced by the ocean dynamics from the shelf seas, they also have an effect on the processes in the shelf seas. The effects of freshwater discharge into a coastal region have attracted increasing attention in recent decades. For example, Duxbury (1965) and Bowden (1983) reported that the discharge from the Columbia River at a rate of order 7000 m^3/sec into the Pacific Ocean leads to the formation of a distinct plume of relatively low-salinity water at the surface of the adjacent shelf. Theoretical models have been developed to study the spread of an estuarial outflow over the adjacent shelf. Beardsley and Hart (1978) describe a two-layer analytical model which is characterized by there being a mean alongshore flow into which the river discharges. Observations by Gopala Krishna and Sastry (1985) along the East Coast of India show the extent of the southward spread of a low salinity plume and suggest the discharge of freshwater from the Hugli and Mahanadi rivers during the monsoon season has an inhibiting effect on the occurrence of upwelling. Johns et al. (1992a) studied the coastal wind-driven circulation in the western Bay of Bengal incorporating the effects of an estuarial discharge of relative freshwater using a numerical model. The results showed that the coastal upwelling off Visakhapatnam is expected to be in the presence of the local application of southwesterly surface wind-stress forcing. It is found to be suppressed by the northern fresh water discharge and is replaced by local sinking. Observations in Liverpool Bay by Sharples and Simpson (1993) also showed a semi-diurnal stratification cycle driven by tidal straining of a freshwater induced horizontal density gradient. The principal processes in the control of stratification have been identified by Simpson et al. (1990) as: (1) density-driven circulation caused by the freshwater run-off; (2) tidal straining of the density field by

vertical shear in the tidal currents; and (3) the springs-neaps cycle of tidal mixing allowing the possibility of stratification following neap tides and causing a return to vertical homogeneity by the following springs.

It is obvious that there are interactions between an estuary and the adjacent shelf sea region. The study of their interaction is necessary to improve our understanding of the processes in both the ocean and the river. However, our understanding of the detailed mechanism of the interaction between the processes in the ocean and the river is by no means complete due to the fact that in the coastal and shelf areas the circulation patterns are normally determined by combined forces and hence it is difficult to measure the effect of each individual force solely by observation. Numerical models are very useful in the study of the interaction between the estuary and shelf sea and a number of models have been developed over the past decade (Hsu et.al 1999; Davies and Xing 1999; Pietrzak et al., 2002).

1.1 The Hydrodynamic Equations

Numerical models have been used to describe the fields of velocity and density in the coastal and shelf sea (Davies et al., 1997a; Dyke, 2000), and are based on the hydrodynamic equations which incorporate the law of conservation of momentum, mass and energy.

The equation of the conservation of momentum can be written in the following format (Kowalik and Murty, 1993) :

$$\rho\frac{\partial u_i}{\partial t}+\rho u_j\frac{\partial u_i}{\partial x_j}+2\rho\varepsilon_{ijk}\Omega_j u_k=-\frac{\partial p}{\partial x_i}-\rho g\delta_{3i}+\frac{\partial \sigma_{ij}}{\partial x_j}. \qquad (1.1)$$

Here, a tensor summation notation is used, the three axes in Cartesian coordinate (x, y, z) are denoted by x_1 , x_2 and x_3 and the velocity components along each axes are denoted by u_1, u_2 and u_3 , respectively. In this notation system, an index appearing twice in a term implies summation over all three index values. In the above expression, ρ is the density of water, t is time, p is the pressure, Ω_j is the component of the Earth's angular velocity and σ_{ij} are the stress components due to the molecular viscosity. Also note that $\varepsilon_{ijk} = +1$ when i, j, k are in cyclic order, $\varepsilon_{ijk} = -1$ when i, j, k are in anticyclic order, and $\varepsilon_{ijk} = 0$ if any pair or all three have the same value; $\delta_{3i} = 1$ when $i = 3$, otherwise $\delta_{3i} = 0$.

The components of the stress tensor, σ_{ij} can be expressed in the form of:

$$\sigma_{ij}=\mu\left(\frac{\partial u_i}{\partial x_j}+\frac{\partial u_j}{\partial x_i}\right) , \qquad (1.2)$$

where μ is the molecular viscosity.

The conservation of mass can be expressed in terms of the continuity equation

$$\frac{\partial \rho}{\partial t}+\frac{\partial \rho u_i}{\partial x_i}=0 \qquad (1.3)$$

or $\frac{\partial u_i}{\partial x_i}=0$ for an incompressible fluid.

The conservation equation for any other property of the fluid such as salinity, temperature, etc., is given by

$$\frac{\partial \rho \Psi}{\partial t} + \frac{\partial \rho \Psi u_i}{\partial x_i} = -\frac{\partial F_i}{\partial x_i} + Q, \tag{1.4}$$

where F_i is the flux of the property Ψ due to internal forces or pressures and Q is the total internal source of Ψ.

Only in a few simple cases can the above equation be solved exactly, even so it needs to be simplified to determine which terms in the general equations are responsible for a particular phenomenon. One way to do so is to separate the motion of flow into two parts: the average motion and the departures from the average. The equations are consequently separated into two sets. This is usually used to separate the motion into the average and turbulent parts (Hinze 1975).

After the separation and modification, the equation of motion and continuity for the average motion can be written as

$$\frac{\partial \overline{\rho u_i}}{\partial t} + \frac{\partial \overline{\rho u}_j \overline{u}_i}{\partial x_j} - \frac{\partial R_{ij}}{\partial x_j} + 2\varepsilon_{ijk}\Omega_j \overline{\rho u}_k = -\frac{\partial \overline{p}}{\partial x_i} - g\overline{\rho}\delta_{3i} + \mu \frac{\partial^2 \overline{u}_i}{\partial x_j \partial x_j}, \tag{1.5}$$

$$\frac{\partial \overline{\rho}}{\partial t} + \frac{\partial \overline{\rho u_i}}{\partial x_i} - \frac{\partial Q_i}{\partial x_i} = 0 \quad . \tag{1.6}$$

Here

$$Q_i = -\overline{\rho' u_i'}, \tag{1.7}$$

here, the overbar signifies an average value over a short period of time T and is defined by

$$\overline{\Phi} = \frac{1}{T}\int_{t-T/2}^{t+T/2} \Phi dt \,. \tag{1.8}$$

The prime denotes a departure from the average.

The equations for the turbulent part of motion are

$$\bar{\rho}\frac{\partial u_i'}{\partial t} + \frac{\partial \overline{\rho u}_j u_i'}{\partial x_j} + \frac{\partial \bar{\rho} u_j' \bar{u}_i}{\partial x_j} - \frac{\partial R_{ij}'}{\partial x_j} + 2\varepsilon_{ijk}\Omega_j \bar{\rho} u_k' = -\frac{\partial p'}{\partial x_i} - g\rho'\delta_{3i} + \mu\frac{\partial^2 u_i'}{\partial x_j \partial x_j}, \tag{1.9}$$

$$\frac{\partial \rho'}{\partial t} + \bar{u}_i\frac{\partial \rho'}{\partial x_i} + u_i'\frac{\partial \bar{\rho}}{\partial x_i} - \frac{\partial Q_i'}{\partial x_i} = 0\,. \tag{1.10}$$

Where

$$R_{ij} = -\bar{\rho}\overline{u_i' u_j'}\,, \tag{1.11}$$

$$R_{ij}' = -\bar{\rho}(u_i' u_j' - \overline{u_j' u_j'})\,, \tag{1.12}$$

$$Q_j' = -(\rho' u_j' - \overline{\rho' u_j'})\,, \tag{1.13}$$

these two equations are not independent of each other due to their nonlinear nature. Here, R_{ij} is called Reynolds stress tensor and represents the influence of the turbulent flow upon the average motion and Q_i represents the mass transported by fluctuating motion.

The above equations of motion include a complete spectrum of motion. In order to use them in an application, a specific set which describes only certain types of motion has been derived from the general set of equations by means of dimensional analysis (Pedlosky 1982). It is assumed that certain information related to the temporal and spatial scale of motion is known as a priori. There are two examples for such priori, hydrostatic approximation and Boussinesq approximation.

The horizontal dimensions of the ocean are much larger than the vertical, so the vertical motion is much weaker than the horizontal motion. If the flow is predominantly horizontal and the vertical acceleration is small compared to the gravity acceleration, the simple hydrostatic law (Proudman 1953) can be applied to rewrite the vertical equation of motion as

$$0 = -g - \frac{1}{\rho}\frac{\partial p}{\partial z}, \tag{1.14}$$

where water is considered as incompressible and the variations in the density lead to a new term which is related to the buoyancy force (Landau and Lifshitz 1959) in the equation of motion. On making the Boussinesq (1903) approximation, the variation of density is only retained in the buoyancy force.

1.2 Hydrodynamic Models of Shallow Sea

The hydrodynamic models have been developed by solving the above equations in the specific area of interest, subject to appropriate simplifications and parameterizations. The approach used depends on the characteristics of the area. In the shallow sea

regions, the most common method for the tidal hydrodynamic modelling is to solve the equations with the tidal forcing input from the model's open boundary (Davies et al., 1997a), normally the tidal forcing is obtained from the measurements or output of a coarser grid model covering larger area. In this approach, the tide is prescribed as a co-oscillatory. In the shallow sea the water mass is small compared with that in deep ocean.

Due to the computational requirements, early numerical models of physical oceanography of shallow sea regions solved the two-dimensional vertically integrated hydrodynamic equations and were restricted to computing elevations and transports. Such models can be applied to solve problems which do not depend on the vertical structure and were ideal for examining the changes due to tides (e.g. Flather, 1976), and storm surges (e.g. Heaps, 1983), which involved essentially barotropic (a state of a fluid for which the density ρ is a function of only the pressure) processes and were confined to the continental shelf. These models have been applied to predict the surface elevations in time and averaged current in tides, storm surges and tsunamis (Murty 1984).

In the mean time, basin wide three-dimensional ocean circulation models were being developed. These models included important baroclinic (a state in which the variation with depth of motions associated with variation of density with depth) ocean effects. However, as computational limitations existed, they were available only with a coarse grid and could not resolve the shallow sea regions. In these models, the parameterisations of sub-grid scale processes are accomplished by using fixed

diffusivity parameters which are often artificially set a high value on coarse grid models to maintain stability.

In recent years the advances in computational power allow the development of three-dimensional shallow sea models. Leendertse and Liu developed and tested a full set of models (Leendertse et al., 1973; Leendertse and Liu 1975). Initially, a two-dimensional model was used for the long wave propagation, then a three-dimensional model and afterwards turbulent exchange processes were included (Liu and Leendertse 1978). One of the significant applications is in tidal modelling. The determination of tidal elevations and currents in shallow sea regions requires the solution of the hydrodynamic equations, subject to variations in bottom topography and appropriate parameterization of energy loss by frictional dissipation.

Blumberg and Mellor (1978) created a numerical model which included the turbulence closure sub-model (Mellor, 1973) to provide vertical mixing coefficients. The turbulence closure sub-model is based on the turbulence hypotheses by Rotta (1951) and Kolmogorov (1941) and has been extended to model stratified flows. As the results of subsequent contributions made by many others, the model has been developed and applied to oceanographic problems. The horizontal grid uses curvilinear orthogonal coordinates and an Arakawa C differencing scheme which is staggered (Mesinger and Arakawa, 1976). The vertical coordinate uses a sigma coordinate which is a necessary attribute in dealing with topographical variability. Together with the turbulence sub-model, the model produces a realistic bottom boundary layer which is important in coastal waters (Mellor and Blumburg, 1985).

The horizontal time differencing is explicit whereas the vertical differencing is implicit. The latter eliminates time stepping constraints for the vertical coordinate and allows the use of fine vertical resolution in the surface and bottom boundary layers. It has a free surface and a split time step.

Heaps (1972 and 1974) introduced a three dimensional hydrodynamic model of the Irish Sea which has been developed into sophisticated models. Whereas vertically integrated two-dimensional (in the horizontal) models were used for tidal storm and tsunami modelling, Heaps and researchers at Bidston Observatory first used three dimensional models for tidal and storm surge computation, this bridged the gap between two-dimensional coastal models and three-dimensional circulation models.

In recent years, with advances in computational power, more sophisticated three-dimensional shallow sea models have been developed. Unlike ocean circulation models in which the parameterisation of sub-grid scale processes is accomplished using fixed diffusivity parameters (which are often artificially high in order to maintain stability on the coarse grid), the fine grid nature of shallow sea models enables these processes to be included by using turbulence energy closure sub-models. Also, fine grid models incorporating turbulence closure schemes can both resolve the changes in topography associated with the shelf edge and the resulting boundary layer currents, as well as the turbulent mixing and across shelf exchange which occurs in this region.

A study by Pietrzak et al., (2002) presented a three dimensional hydrostatic model that combines a generalised vertical coordinate system with an efficient implicit solution for the free surface.

One of the major problems related to three dimensional modelling has been the excessive amount of time consumed in the computer simulations. One solution to this problem is using the time splitting scheme to solve the model equations. The velocity can be written into two parts which include the depth-mean velocity and the depth-dependent velocity. These two velocities are included in external and internal modes, respectively. The external mode represents the fast moving gravity waves and uses a small time step; the internal mode represents slower moving waves and larger time step can be used. This method was utilized by Simons (1974, 1980), Madala and Piacsek (1977), Berntsen et al., (1981), Blumberg and Mellor (1983) and Hess (1985).

In addition to splitting into physical modes, Berntsen et al., (1981) also used a time splitting into fractional time steps. The stability conditions of an external or barotropic model of motion in the numerical computation is governed by the CFL condition, which requires very short time step in computation (Ramming and Kowalik, 1980). This mode does not need to be described by the full three-dimensional equations, it can be studied by a two-dimensional, vertically averaged set of equations.

1.3 Numerical Models of Estuarial Circulation

In parallel with the development of these three-dimensional hydrodynamic models for shallow sea, numerical models of estuaries which are regions of transition from river to ocean were also developed. Estuaries are characterized by the possibility of tidal motions communicated from the sea, and by gradients of salinity and density associated with the progressive mixing of river water and sea water. The effect of gravity on the density difference between sea water and freshwater tends to bring about vertical salinity stratification and a convection flow known as estuarine circulation. The distribution of salinity, flow circulation within the estuary are dominantly determined by freshwater flow and tides. The interaction of tidal forcing, surface wind stress, irregular topography and density stratification results in complex flow and transport processes in estuaries. Numerical models used in estuarial studies should account in detail for both advective and turbulent transport. Early numerical models of estuaries have been used to investigate tidal dynamics using a one dimensional flow theorem (Harleman, 1971), but its application has severe limitations to a partially mixed estuary, and can not adequately describe the tidal current which has large vertical amplitude and phase variations.

A vertical two dimensional numerical model of a rectangular geometry has been developed by Hamilton (1975) in a study of circulation in the Rotterdam Waterway and vertical mixing within a tidal cycle. Blumberg (1975), Elliot (1976) and Rao (1995) had used nonuniform geometry in their two dimensional models; while Festa

and Hansen applied the steady-state, uniform geometry model to study internal circulation and turbidity. A semi-implicit two dimensional model for circulation in a partially mixed estuary was implemented by Wang and Kravitz (1980) to indicate large longitudinal and vertical changes in tide, density driven and wind driven circulations. These models appear to be able to reveal some major features characteristic of partially mixed estuary.

Johns (1978, 1983) developed a multi-level two-dimensional channel model using a turbulence energy equation in a scheme of turbulence parameter. The turbulence closure was achieved at the level of the turbulence energy equation. A transport equation had been added to the modelling system later on (Johns and Oguz, 1990) which describes how salinity is advected and diffused through the channel. The inclusion of this process leads to an extra term in the turbulence energy equation and this has its maximal effect in regions of strongly stable vertical salinity stratification where it has a marked suppressive influence on turbulence generation.

Hsu et al., (1999) suggested a laterally averaged two-dimensional numerical model and extended the model to handle the tributaries as well as the mainstream of an estuary.

1.4 Numerical Solution of the Modelling Equations

The first step towards the solution of the numerical models is discretization of the model equations. These include the discretization in the horizontal and vertical, as well as time stepping.

1.4.1 Horizontal Discretization

The traditional approach used in the horizontal is a uniform finite difference grid. In most of tidal hydrodynamic models, most commonly used scheme is space staggered grid. A well known scheme is the Arakawa C grid in which elevation and the two components of velocity are solved at different grid points. Another scheme is to compute the two components of velocity at the same grid point, while elevation is computed at a different point. This is known as 'the Arakawa B grid' (James, 1990 and Lardner and Song, 1992). The disadvantage of the uniform grid is that it can give rise to spurious residual flows in the near coastal region due to the irregular coastline. Johnson (1980) and Spaulding (1984) reported their work using boundary-fitted coordinates in which the grid is transformed to fit the coastline in a smooth regular manner. This significantly improved the representation of the coastline.

In recent years, the finite element method has been used in the horizontal by many researchers, among them there are: Foreman and Walters (1990); Lynch and Naimie (1993);Luettich and Westerink (1994); Lynch et al., (1995). The method is suited to problems involving tidal propagation from the ocean to the shallow sea where the wavelength of tide decreases and therefore enhanced resolution is required. Additionally, the higher harmonics of the tide are generated in the shallow sea through the nonlinear interactions (Xing and Davies, 1995). These higher harmonics have shorter wavelengths than the fundamental tide and hence the increased horizontal resolution is necessary to resolve them accurately. It has been shown that the finite element method with a progressive refinement of the grid at the near coastal

region can produce highly accurate solutions (Le Provost et al., 1995; Foreman et al., 1993; Luettich and Westerink 1994).

1.4.2 Vertical Discretization

The discretization in the vertical can use the similar techniques to those used in the horizontal, namely, finite difference grid along z coordinate. This scheme often fails to represent properly the near-bed region, where a very fine grid is needed. Koutitas and O'Connor (1980) applied the finite element method to the vertical discretization. The resolution can be improved by using finer elements in the near-bed region where the greatest shear of tidal currents exist and frictional effects are most important.

The difficulties are often encountered in the region of abrupt topography variations or in the surface of bottom boundary layers. To overcome these obstacles a coordinate dimensionless coordinate is introduced through the transformation:

$$\sigma = (B - A)\frac{z - \zeta}{h + \zeta} + B\,. \tag{1.15}$$

The new coordinate transforms the column of water from the surface ($z = \zeta$) to the bottom ($z = -h$) into a uniform depth ranging from A to B. The vertical discretization in σ-coordinate can be chosen in such manner as to provide an optimal vertical resolution. Using finite difference grid in σ-coordinates has the advantage of having the same number of grid points in the vertical at each horizontal location and avoiding the problem related to the free surface. The σ coordinate not only transforms the

vertical direction but it also depends on the horizontal coordinates. So all partial derivatives must be restated in the new system of coordinates.

It is obvious that in the tidal hydrodynamic models with σ-coordinate system the variables are calculated at non-fixed physical levels, because water column depth varies with time.

However, the use of σ-coordinates in regions of steep bottom topography can lead to spurious results (Gary 1973; Haney 1991). Sharp topographic change from one grid point to the next means that the pressure gradient calculation involves taking the difference between two large terms that can lead to large roundoff errors.

1.4.3 Time Discretization

The integration of the hydrodynamic equations through time is usually achieved by discrete time-stepping method in which the solution is integrated from one time level to the next (Aldridge and Davies, 1993).

In tidal problems where the solution is known to be periodic in time, an alternative approach is to use an expansion method in the time domain (Le Provost and Fornerrino,1985;Baptista et al., 1989; Westerink et al., 1989; Walters and Werner, 1991;). This approach describes the elevation and the two components of current as a time-dependent component P_0 and a sum of amplitudes of periodic components P_n with known frequencies ω_n.

$$P = P_0 + \frac{1}{2}\sum_{n=-N}^{N} P_n \exp(-i\omega_n t), \tag{1.16}$$

where P could denote ζ, u, or v. Tidal frequency for component P_n is denoted by ω_n. N is number of tidal harmonics in the expansion.

With the expansions for ζ, u and v, the time derivatives in the hydrodynamic equations are removed, leaving a complex set of equations without time variable. These can be solved using a finite element or finite difference mesh to determine the amplitude and phase of each tidal harmonic at each horizontal grid point.

1.4.4 Surface and Bottom Boundary Conditions

At the sea surface, the condition of the free surface is affected by specifying a zero stress surface boundary condition. At the seabed, the condition of zero flow at the bed is effected by specifying a no-slip condition.

In the three-dimensional model, the most common solution is to apply a slip condition at a reference height above the seabed and relate the bed stress to the currents at this reference height. It is found in the literature that the quadratic slip condition is one of the commonly used formulations:

$$F_B = \kappa \rho_0 u_h \sqrt{u_h^2 + v_h^2}\,, \tag{1.17a}$$

$$G_B = \kappa \rho_0 v_h \sqrt{u_h^2 + v_h^2}\,, \tag{1.17b}$$

where F_B,G_B are the bed stress components; u_h, v_h are currents at reference height $z = h$, κ is a constant coefficient given by

$$\kappa = \left(\frac{K}{\ln(z / z_0)} \right)^2, \tag{1.18}$$

where K is von Karman's constant and z_0 is the roughness of the seabed.

In the two-dimensional model the bed stress is usually related to the depth mean currents instead of currents at reference height. Davies (1988) used a convolution method to produce a bed stress that is equivalent to that in a three-dimensional model.

1.4.5 Diffusion Coefficients

Consideration needs to be given to the choice of diffusion coefficients. A good representation of turbulence is necessary for the simulation of flows in estuaries and coastal areas. Both surface and bottom mixing is considered an essential property of the choice, because wind and thermal forcing dominate the surface of the ocean, while in shallow sea the bed friction is important. A two-equation k-ε turbulence closure model has been applied by many researchers (Blumberg and Mellor, 1987; Burchard et al., 1998; Davies and Xing, 1999). The model involves prognostic equations for the turbulence energy and mixing length which can then be used in the computation of viscosity and diffusivity. Baumert and Radach (1992) have used prognostic equations for turbulence energy and dissipation rate.

1.5 Aims and Objective of Present Work

Although numerical models have been used to simulate processes in both estuaries and shallow sea, their space scales are different. If all the processes were resolved by a numerical model the computer time required to obtain the solution may be very large. This will be difficult when coastal engineers need to select a computational model to assess the impact of engineering works in coastal and estuarial waters. A solution to this problem is to subdivide the modelling domain into two subdomains, where spatial resolution can be different.

The overall aim of the work described in this thesis is to develop a numerical model based on joining together a two-dimensional river model with a three-dimensional shallow sea model. The model will be used to study the interaction of the tidal flow between the shelf sea and the estuary where the sea reaches the river valley. Both the role of shelf sea flow circulation in changing the flow in the river and the role of the river discharge in modifying the circulation in the shelf sea are involved. To achieve this, the following objectives need to be addressed.

(1) To select a two-dimensional river model which is able to describe the flow and relevant transport processes including advective and turbulent transport in estuaries. The high resolution in the horizontal direction is required for the hydrodynamic processes in the estuaries. The river model should be able to simulate the tidal elevation and allow the propagation of tidal motion through the seaward open boundary.

(2) To select a three-dimensional hydrodynamic model for the shallow sea (hereafter referred to as the bay model) to simulate the tidal current and provide the real-time variables to be used as boundary conditions of river model.

(3) To combine together the river model with the bay model to develop a joined model which enables combined modelling of tides, freshwater flow and sediment transport.

(4) To test the joined model against the observations of tidal component M_2.

In Chapter 2 and Chapter 3, the basic tools, namely, the river model and the bay model are described respectively. Using a turbulence energy equation in a scheme of turbulence parameterization, the river model is able to describe tidal and density driven circulations of flow, as well as sediment transport in the estuaries. The bay model is capable of simulating and predicting many of the complex flows in the shallow sea. It is used to produce real time tidal regimes and provide tidal forcing to the river model as open boundary condition.

The horizontal resolution in the river model has been increased and tested before it is joined with the bay model later in Chapter 4.

Chapter 4 presents the implementation of the joining work. The linkage is set up at the horizontal point where the river meets with the shallow sea. Two models are linked together dynamically by the surface elevations. The problems that are encountered and the methods of solution are described in detail. An interactive vertical grid splicing scheme is used for exchanging information between the river model and the

bay model along the common vertical boundary. This scheme converted the variables which are calculated at non-fixed physical levels into the variables at the same physical levels so that the time extrapolation can be carried out.

Results are given in Chapter 5 for test cases and several numerical experiments. Simulations from the joined model for the M_2 tidal amplitude are compared with the observations reported by Aldridge and Davies (1993). The significance of differences between the results of joined model and the bay model has also been tested by using a global estimator (Ozer et al., 2000). The following experiments are performed in Liverpool bay and Mersey estuary:

(1) River model without joining with bay model where a single harmonic with period of 12.4 hrs is used to produce the tidal amplitude imposed on the mouth of river.

(2) Bay model without joining with river model where the M_2 tidal component is input along the open boundary.

(3) Joined model driven by M_2 tidal force and freshwater discharge.

(4) Joined model driven by freshwater discharge only.

The results from above experiments are then used to investigate the ability of the joined model to simulate the relevant transport process in the estuary and shallow sea.

Chapter 6 contains the conclusions and suggestions for future research work.

Chapter 2 Two Dimensional Single River Model

The model used in the study is based on that initially developed by Johns and Oguz (1990) and applied in a study of the elevation of the flow and salinity distribution in the Bosphorus. It is a multi-level two-dimensional channel model with an energy-based turbulence closure scheme and topography following coordinates. Suspended sediment concentration has been incorporated into the present model.

2.1 Governing Equations

The model is set up on a two-dimensional analysis domain as shown in Fig.2.1. The water in the channel is considered to be a cross section frame (x,z) with the origin, O, at the equilibrium level of the free surface of the water. All conditions are referred to rectangular Cartestian coordinates. The axis OX points horizontally from the head of the estuary towards open sea along the channel. The positive z axis is directed vertically upwards from $z = 0$. The water motion is described by the velocity components u, w, and the pressure is denoted by p. We consider the water to be frictionless, inhomogeneous and incompressible. The external forces acting on a unit volume element will then be pressure gradient plus possible volume forces, primarily the gravity force. According to the theory of Newton's mechanics, the rate of change of momentum is related to the external force and has the form of

$$\frac{\partial u}{\partial t}+u\frac{\partial u}{\partial x}+w\frac{\partial u}{\partial z}=-\frac{1}{\rho}\frac{\partial p}{\partial x}\ , \tag{2.1}$$

and

$$\frac{\partial w}{\partial t}+u\frac{\partial w}{\partial x}+w\frac{\partial w}{\partial z}=-g-\frac{1}{\rho}\frac{\partial p}{\partial z}\ . \tag{2.2}$$

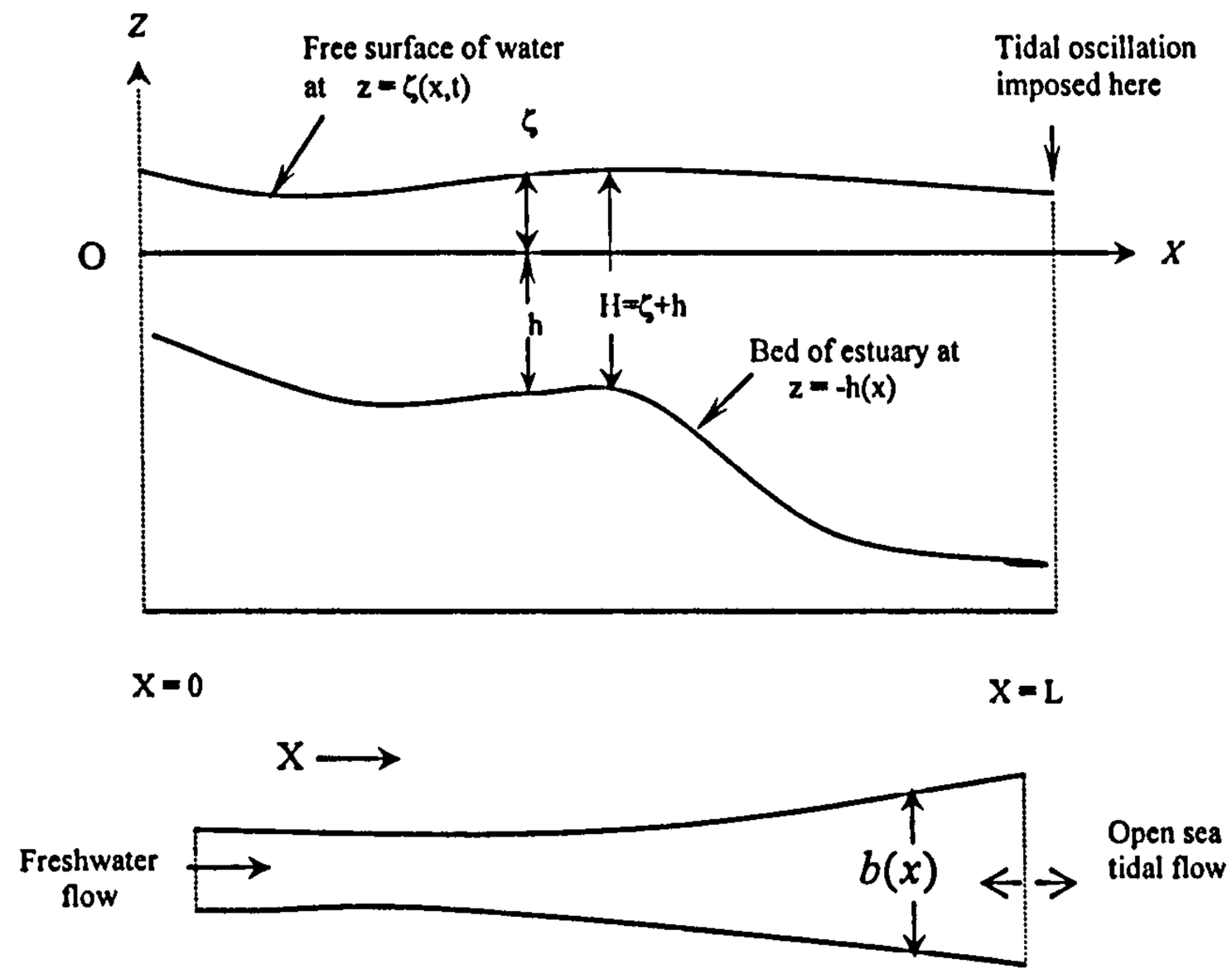

Fig. 2.1 The illustration of the analysis area along the river channel.

The fluid density ρ (x, z), velocity u, w, and pressure p are averaged across the channel with rectangular cross-section of breadth $b(x)$.

The equation of continuity for the unit volume element of water flow can be expressed in the form:

$$\frac{\partial}{\partial x}(bu)+\frac{\partial}{\partial z}(bw)=0\,. \tag{2.3}$$

The pressure is taken as hydrostatic, so the vertical equation of motion reduces to:

$$0=-g-\frac{1}{\rho}\frac{\partial p}{\partial z}\ . \tag{2.4}$$

Setting the cross-sectionally averaged position of the surface of the water at time t at $z = \zeta(x,t)$ and the cross-sectionally averaged position of the immobile bed to be at $z = -h(x)$, the integration of (2.4) from a general depth to the free surface will give:

$$p = p_a + \int_z^{\zeta} g\rho dz\,, \tag{2.5}$$

where p_a is the atmospheric pressure assumed constant.

Making partial differentiation on (2.5) w.r.t. x and simplifying with the Boussinesq approximation leads to

$$-\frac{1}{\rho}\frac{\partial p}{\partial x} = -g\frac{\partial \zeta}{\partial x} - \frac{1}{\rho_0}\int_z^{\zeta}\frac{\partial}{\partial x}(g\rho)dz\,, \tag{2.6}$$

where ρ_0 is the density of pure water.

Multiplying Equation (2.1) by b(x) together with continuity equation in flux form leads to:

$$\frac{\partial}{\partial t}(bu) + \frac{\partial}{\partial x}(bu^2) + \frac{\partial}{\partial z}(buw) = -gb\frac{\partial \zeta}{\partial x} - \frac{b}{\rho_0}\int_z^{\zeta}\frac{\partial}{\partial x}(g\rho)dz\,. \tag{2.7}$$

The salinity, S and the sediment concentration, C, satisfy the transport equations

$$\frac{\partial}{\partial t}(bS) + \frac{\partial}{\partial x}(buS) + \frac{\partial}{\partial z}(bwS) = 0\,, \tag{2.8}$$

and

$$\frac{\partial}{\partial t}(bC) + \frac{\partial}{\partial x}(buC) + \frac{\partial}{\partial z}[b(w - w_s)C] = 0\,, \tag{2.9}$$

where w_s is the settling velocity of typical sized sediment particle under consideration. Thus, the velocity at which particles are advected in the vertical is reduced by w_s. The

settling velocity is a crucial quantity governing the concentration distribution and it is proportional to the surface area of sediment particles. Following Johns (1997), its value is set to 10^{-4} m/sec for the sediment grains with a diameter of order 10μm for which the bulk density is 2100 kg m^{-3}.

Integrating the equation of continuity vertically from the bottom z = -h to the surface $z = \zeta$ will give another form of the continuity equation:

$$b\frac{\partial H}{\partial t}+\frac{\partial}{\partial x}(bH\langle u\rangle)=0, \tag{2.10}$$

where $H= \zeta + h$ is the total depth, and $\langle u\rangle$ is the depth-averaged velocity given by

$$\langle u\rangle=\frac{1}{H}\int_{-h}^{\zeta}udz\ . \tag{2.11}$$

The density ρ is related to the salinity, S, and the suspended sediment concentration in terms of

$$\rho=\rho_w+(1-\frac{\rho_w}{\rho_s})C, \tag{2.12a}$$

and

$$\rho_w=\rho_0(1+\gamma S), \tag{2.12b}$$

where ρ_0 is the density of pure water. ρ_s and ρ_w are the densities of the sediment material and the saline water. Here, we follow Johns *et al.* (1992) and take $\gamma =$ 7.5×10^{-4}/ppt.

Like most natural flows, the motion of water in the river is turbulent. The velocity and the pressure depend on space coordinates and time. These can be presented as the sum

of a time average and a time dependent fluctuating component. The instantaneous variables at a fixed point in space are expressed as,

$$u = \overline{u} + u' \,, \tag{2.13}$$

$$w = \overline{w} + w' \,, \tag{2.14}$$

$$p = \overline{p} + p' \,, \tag{2.15}$$

where a prime signifies the fluctuating part and an overbar denotes a time averaged value defined by

$$\overline{\Phi} = \frac{1}{T} \int_{-\frac{T}{2}}^{+\frac{T}{2}} \Phi dt \,. \tag{2.16}$$

In the above, T is the averaging period typically of the order of one minute and much less than a characteristic tidal period of M_2 tide (12.4 hours). Likewise, the densities, salinity and sediment concentration are decomposed as,

$$\rho = \overline{\rho} + \rho' \,, \tag{2.17}$$

$$\rho_w = \overline{\rho}_w + \rho'_w \,, \tag{2.18}$$

$$S = \overline{S} + S' \,, \tag{2.19}$$

$$C = \overline{C} + C' \,. \tag{2.20}$$

Substituting the flow parameters in (2.7), (2.8) and (2.9) by their mean and fluctuating components and taking time average lead to

$$\frac{\partial}{\partial t}(b\overline{u}) + \frac{\partial}{\partial x}(b\overline{u^2}) + \frac{\partial}{\partial z}(b\overline{uw}) = -gb\frac{\partial \zeta}{\partial x} - \frac{b}{\rho_0}\int_z^\zeta \frac{\partial}{\partial x}(g\overline{\rho})dz + \frac{\partial}{\partial x}(-b\overline{u'^2}) + \frac{\partial}{\partial z}(-b\overline{u'w'}) \tag{2.21}$$

$$\frac{\partial}{\partial t}(b\overline{S}) + \frac{\partial}{\partial x}(b\overline{u}\overline{S}) + \frac{\partial}{\partial z}(b\overline{w}\overline{S}) = \frac{\partial}{\partial x}(-b\overline{u'S'}) + \frac{\partial}{\partial z}(-b\overline{w'S'}) \,, \tag{2.22}$$

$$\frac{\partial}{\partial t}(b\overline{C})+\frac{\partial}{\partial x}(b\overline{u}\overline{C})+\frac{\partial}{\partial z}\left[b(\overline{w}-w_s)\overline{C}\right]=\frac{\partial}{\partial x}(-b\overline{u'C'})+\frac{\partial}{\partial z}(-b\overline{w'C'}). \qquad (2.23)$$

Here w_s is assumed constant and

$$\overline{\rho}=\overline{\rho}_w+(1-\frac{\overline{\rho}_w}{\rho_s})\overline{C}\ , \qquad (2.24a)$$

$$\overline{\rho}_w=\rho_0(1+\gamma\overline{S})\,. \qquad (2.24b)$$

The continuity equation when averaged becomes

$$\frac{\partial}{\partial x}(b\overline{u})+\frac{\partial}{\partial z}(b\overline{w})=0\,, \qquad (2.25a)$$

or

$$b\frac{\partial\zeta}{\partial t}+\frac{\partial}{\partial x}(bH\langle\overline{u}\rangle)=0\,. \qquad (2.25b)$$

In equations (2.21), (2.22), and (2.23), there are several terms which have similar formation and are related to turbulent flux. They are

$$-b\overline{u'u'},-b\overline{u'w'},-b\overline{u'S'},-b\overline{w'S'},-b\overline{u'C'},-\overline{w'C'}\,.$$

These terms are of fundamental importance in nearshore processes and need to be parameterised properly.

A conventional method is based on the gradient transfer law, in which the effect of the turbulent flux is expected to produce a shear in the Reynolds-averaged flow. Consequently:

$$-\overline{u'w'}=K_M\frac{\partial\overline{u}}{\partial z}\ , \qquad (2.26)$$

$$-\overline{w'S'}=K_S\frac{\partial\overline{S}}{\partial z}, \qquad (2.27)$$

$$-\overline{w'C'} = K_C \frac{\partial \overline{C}}{\partial z}, \tag{2.28}$$

where K_M, K_S, K_C are vertical coefficients of turbulent exchange of momentum, salinity and sediment concentration, respectively. In this work we prescribe that the diffusion coefficients for all transport processes are equal in value, thus

$$K_M = K_S = K_C = K. \tag{2.29}$$

All other turbulent flux terms represent a horizontal diffusive effect and will be ignored.

Now the equations (2.21)-(2.23) can be written as

$$\frac{\partial}{\partial t}(b\bar{u}) + \frac{\partial}{\partial x}\left(b\overline{u^2}\right) + \frac{\partial}{\partial z}\left(b\overline{uw}\right) = -gb\frac{\partial \zeta}{\partial x} - \frac{b}{\rho_0}\int_z^\zeta \frac{\partial}{\partial x}(g\bar{\rho})dz + \frac{\partial}{\partial z}(bK\frac{\partial \bar{u}}{\partial z}), \tag{2.30}$$

$$\frac{\partial}{\partial t}(b\bar{S}) + \frac{\partial}{\partial x}(b\bar{u}\bar{S}) + \frac{\partial}{\partial z}(b\overline{w}\bar{S}) = \frac{\partial}{\partial z}(bK\frac{\partial \bar{S}}{\partial z}), \tag{2.31}$$

$$\frac{\partial}{\partial t}(b\bar{C}) + \frac{\partial}{\partial x}(b\bar{u}\bar{C}) + \frac{\partial}{\partial z}\left[b(\overline{w} - w_s)\bar{C}\right] = \frac{\partial}{\partial z}(bK\frac{\partial \bar{C}}{\partial z}). \tag{2.32}$$

In above equations:

$-gb\frac{\partial \zeta}{\partial x}$ is the barotropic contribution to pressure gradient resulting from the slope of free surface.

$-\frac{b}{\rho_0}\int_z^\zeta \frac{\partial}{\partial x}(g\bar{\rho})dz$ is the baroclinic contribution to pressure gradient resulting from horizontal density gradient consequent upon the different ambient salinity of the water in the head and mouth of river.

$\frac{\partial}{\partial z}(bK\frac{\partial \overline{u}}{\partial z})$, $\frac{\partial}{\partial z}(bK\frac{\partial \overline{S}}{\partial z})$, $\frac{\partial}{\partial z}(bK\frac{\partial \overline{C}}{\partial z})$ are vertical turbulent transports of momentum, salinity and sediment, respectively.

Equations (2.25), (2.30), (2.31) and (2.32) have to be solved together with appropriate boundary conditions through which the system is driven. Additionally an appropriate assumption about K is also needed. For a homogeneous estuary flow, it may be acceptable to prescribe a constant value of K provided that appropriate boundary condition is applied at the outer limit of the bottom shear layer adjacent to $z = -h$. However, it is much more satisfactory to compute the value of K by an energy based turbulence closure scheme. This requires to derive the turbulent energy $\overline{E}$ from a prognostic equation. This equation can be obtained by inserting the velocity, pressure and density in form of mean plus turbulence into the basic hydrodynamic equations which now include the molecular viscous terms.

To do this it is necessary to define the Reynolds-averaged turbulence energy in the flow by

$$\overline{E} = \frac{1}{2}(\overline{u'^2} + \overline{w'^2}). \tag{2.33}$$

Multiply the equations with turbulent velocity and take Reynolds-average, then apply a lengthy manipulation to retain the dominant terms and ignore the rest of the items. This results in:

$$\frac{\partial}{\partial t}(b\overline{E}) + \frac{\partial}{\partial x}(b\overline{uE}) + \frac{\partial}{\partial z}(b\overline{wE}) + \frac{\partial}{\partial z}\left\{\overline{bw'(p'/\rho_0 + \frac{1}{2}u'^2)}\right\} = b\left(-\overline{u'w'}\right)\frac{\partial \overline{u}}{\partial z} + \frac{gb}{\rho_0}\left(-\overline{\rho'w'}\right) - b\varepsilon \tag{2.34}$$

Here ε is the dissipation rate of turbulent kinetic energy which specifies the loss of turbulence energy by dissipative processes.

The expression $\left\{-b\overline{w'(p'/\rho_0+\frac{1}{2}u'^2)}\right\}$ represents the redistribution of turbulence energy by turbulence itself and can be replaced by

$$bK\left(\frac{\partial \overline{E}}{\partial z}\right). \tag{2.35}$$

The first term on the right hand side in equation (2.34) represents the production of turbulence energy from the mean flow. It will always be positive so is a source of turbulence energy. From (2.26) and (2.29), this term can be parameterised by

$$b(-\overline{u'w'})\frac{\partial \overline{u}}{\partial z} = bK\,(\frac{\partial \overline{u}}{\partial z})^2. \tag{2.36}$$

The second term on the right hand side of (2.34) represents the vertical transfer of density fluctuations by the fluctuating vertical turbulent velocity. This term could be either positive or negative and will act as either a source or sink of turbulence energy. Again it is frequently parameterised according to the gradient transfer law applied to density fluctuation, hence

$$\frac{gb}{\rho_0}(-\overline{\rho'w'}) = \frac{gb}{\rho_0}K\frac{\partial \overline{\rho}}{\partial z}. \tag{2.37}$$

All the transfer processes are therefore contributing to the vertical gradients in the corresponding Reynolds-averaged quantities. Consequently equation (2.34) is equivalent to:

$$\frac{\partial}{\partial}(b\overline{E})+\frac{\partial}{\partial x}(b\overline{u}\overline{E})+\frac{\partial}{\partial z}(b\overline{w}\overline{E}) = bK(\frac{\partial \overline{u}}{\partial z})^2+\frac{\partial}{\partial z}[K\frac{\partial}{\partial z}(b\overline{E})]+\frac{gbK}{\rho_0}\frac{\partial \overline{\rho}}{\partial z}-b\varepsilon, \tag{2.38}$$

According to Johns(1978), the exchange coefficient is related to the turbulent energy density by

$$K = c^{1/4} l \overline{E}^{1/2} . \tag{2.39}$$

The turbulent energy density, E, satisfies (2.39) and ε is the dissipation rate and given by

$$\varepsilon = \frac{c^{3/4} \overline{E}^{3/2}}{l_D}, \tag{2.40}$$

where c is an empirical constant and its value is recommended by Launder and Spalding (1972) as 0.08. The vertical mixing length, l, is given by Johns et al. (1991) as:

$$l = \frac{\kappa\beta}{1/(z+h+z_0)+1/(\zeta-z+z_s)}, \tag{2.41}$$

where κ is Von Karman's constant, z_0 is bottom roughness length, z_s is a surface roughness length whose primary role is to prevent the occurrence of a zero in l at z =ζ The damping coefficient, β, is defined by local Richardson number:

$$\beta = [\frac{1}{R_i + (1+R_i^2)^{1/2}}]^2 , \tag{2.42}$$

$$R_i = -g\gamma \frac{\partial \overline{S} / \partial z}{(\partial \overline{u} / \partial z)^2} . \tag{2.43}$$

2.2 Boundary Conditions

The boundary conditions at the free surface and the floor of channel are defined by:

$$\frac{D}{Dt}(\zeta - z) = 0 \qquad \text{at} \quad z = \zeta , \tag{2.44}$$

$$\frac{D}{Dt}(h + z) = 0 \qquad \text{at} \quad z = -h, \tag{2.45}$$

where

$$\frac{D}{Dt} = \frac{\partial}{\partial t} + u\frac{\partial}{\partial x} + w\frac{\partial}{\partial z} \ . \tag{2.46}$$

A condition of no-slip and zero normal velocity at the topography is prescribed.

$$\bar{u} = 0 \qquad \text{at z = -h ,} \tag{2.47}$$

$$\bar{w} + \bar{u}\frac{\partial h}{\partial x} = 0 \qquad \text{at z = -h .} \tag{2.48}$$

No momentum transfer across free surface:

$$K\frac{\partial \bar{u}}{\partial z} = 0 \qquad \text{at z = } \zeta \ , \tag{2.49}$$

$$K\frac{\partial \bar{E}}{\partial z} = 0 \qquad \text{at z = -h and z = } \zeta \ , \tag{2.50}$$

which means no vertical transfer of turbulence energy across topography or free surface.

The boundary conditions on the salinity and sediment concentration at the topography and free surface are:

$$K\frac{\partial \bar{S}}{\partial z} = 0 \qquad \text{at z = -h and z = } \zeta, \tag{2.51}$$

this means no vertical transfer of salinity across topography or free surface.

The boundary conditions on the concentration at the topography are prescribed according to the following two cases:

Case A: when the bottom friction velocity, u^*, is less than some critical value, u^*_c, there is a flux of concentration across the bed due to the settling; when u^* exceeds that critical value, u^*_c, there is no flux across the bed, thus

$$\frac{\partial \overline{C}}{\partial z} = 0 \quad \text{for } u^* \leq u^*_c, \tag{2.52}$$

and

$$K\frac{\partial \overline{C}}{\partial z} + \overline{w}_s \overline{C} = 0 \quad \text{for } u^* > u^*_c. \tag{2.53}$$

Case B: when the bottom friction velocity u^* is less than some critical value, u^*_c, there is a flux of concentrate across the bed due to the settling; when u^*, exceeds the critical value, u^*_c, it allows sediment pickup,

$$\frac{\partial \overline{C}}{\partial z} = 0 \quad \text{for } u^* \leq u^*_c, \tag{2.54}$$

$$-K\frac{\partial \overline{C}}{\partial z} = P \quad \text{for } u^* > u^*_c, \tag{2.55}$$

where P is a pick up function which is suggested by Van Rijn (1984) which is defined as

$$P = C_{ref} w_p O^{3/2}, \tag{2.56}$$

where

$$\theta = 0 \text{ for } u^* \leq u^*_c, \tag{2.57}$$

$$\theta = [u^*/ u^*_c]^2 - 1 \quad \text{for } u^* > u^*_c. \tag{2.58}$$

C_{ref} is a reference concentration whose value is determined by the available erodible bed material and must be prescribed. In this study $C_{ref}=10^{-4}$ (Johns 1997). The pickup velocity, w_p, is defined by:

$$w_p = [\{(\rho_s - \rho_0)/\rho_0\} g D_{50}]^{1/2}, \tag{2.59}$$

where D_{50} is the median grain diameter of the concentrate.

The critical friction velocity, u^*_c, is suggested to have a value of 16.3×10^{-3} m/sec by Van Rijn (1984,1986).

At the head and mouth of channel, radiation boundary conditions are used (Johns et al.,1983), they have the following forms:

$$\bar{u} - (\frac{g}{h})^{1/2}\zeta = -2(<\bar{u}>)_{x=L} \quad \text{at} \quad x = L, \tag{2.60}$$

and

$$\bar{u} + (\frac{g}{h})^{1/2}\zeta = 2(<\bar{u}>)_{x=0} \quad \text{at} \quad x = 0, \tag{2.61}$$

where $(<\bar{u}>)_{x=0}$ is set equal to a quantity, u_0, which must be able to reflect the freshwater flow across the landward end of the channel or estuary.

The value of $(<\bar{u}>)_{x=L}$ will be set to reflect the effect of tidal wave with period, t_P, propagating from seaward end of the estuary, and it is chosen to produce the tidal amplitude at x = L. Here the tidal wave is considered as a single harmonic.

Consequently the boundary conditions become:

$$\zeta = (\frac{h}{g})^{1/2}[2u_0 - <\bar{u}>] \quad \text{at} \quad x = 0, \tag{2.62}$$

and

$$\zeta = (\frac{h}{g})^{1/2}[2u_L \sin(2\pi t / t_P) + <\bar{u}>] \quad \text{at } x = L. \tag{2.63}$$

A streamfunction ψ is introduced in the model to illustrate the circulation pattern in the river, this is defined by:

$$\frac{\partial \psi}{\partial z} = -b\bar{u}\,, \tag{2.64}$$

$$\frac{\partial \psi}{\partial x} = b\bar{w}\,. \tag{2.65}$$

The application of the boundary conditions at $z = -h(x)$ and $z = \zeta(x,t)$ results in the choice of z as a vertical coordinate unsuitable, it is often unable to reproduce the processes in the region of abrupt topography variations or in the surface or bottom boundary layers. As presented by Johns (1978), a dimensionless coordinate is introduced through the transformation

$$\sigma = \frac{z+h}{\zeta+h} \tag{2.66}$$

In σ-coordinates, the vertical differentiation has the form:

$$\frac{\partial \psi}{\partial \sigma} = -bH\bar{u}\,, \tag{2.67}$$

and taking $\psi = 0$ at $\sigma = 0$, we have

$$\psi = -bH\int_0^{\sigma} \bar{u}\, d\sigma\,. \tag{2.68}$$

By using the value of u at the discrete σ-levels in above equations, the integral in (2.68) may be evaluated numerically to provide corresponding values of ψ. The streamlines of the volume transport in the river can be delineated by plotting the contours along which ψ is a constant.

The new coordinate converts the column of water from bottom ($z = -h$) to the surface ($z = \zeta$) into a uniform depth ranging from 0 to 1. The illustration of it is shown in Fig. 2.2. The vertical discretization in σ coordinates can be chosen in such a way that an optimal vertical resolution can be provided. It follows smoothly the contours of the variable topography with the number of the vertical layers being conserved over the computational domain. This method was originally introduced into meteorology by Phillips (1957) and has been applied in marine modelling by Freeman et al. (1972)

and Nihoul (1977) and many others since. Its application in free-surface channel modelling has also been considered by Smith and Takhar (1977).

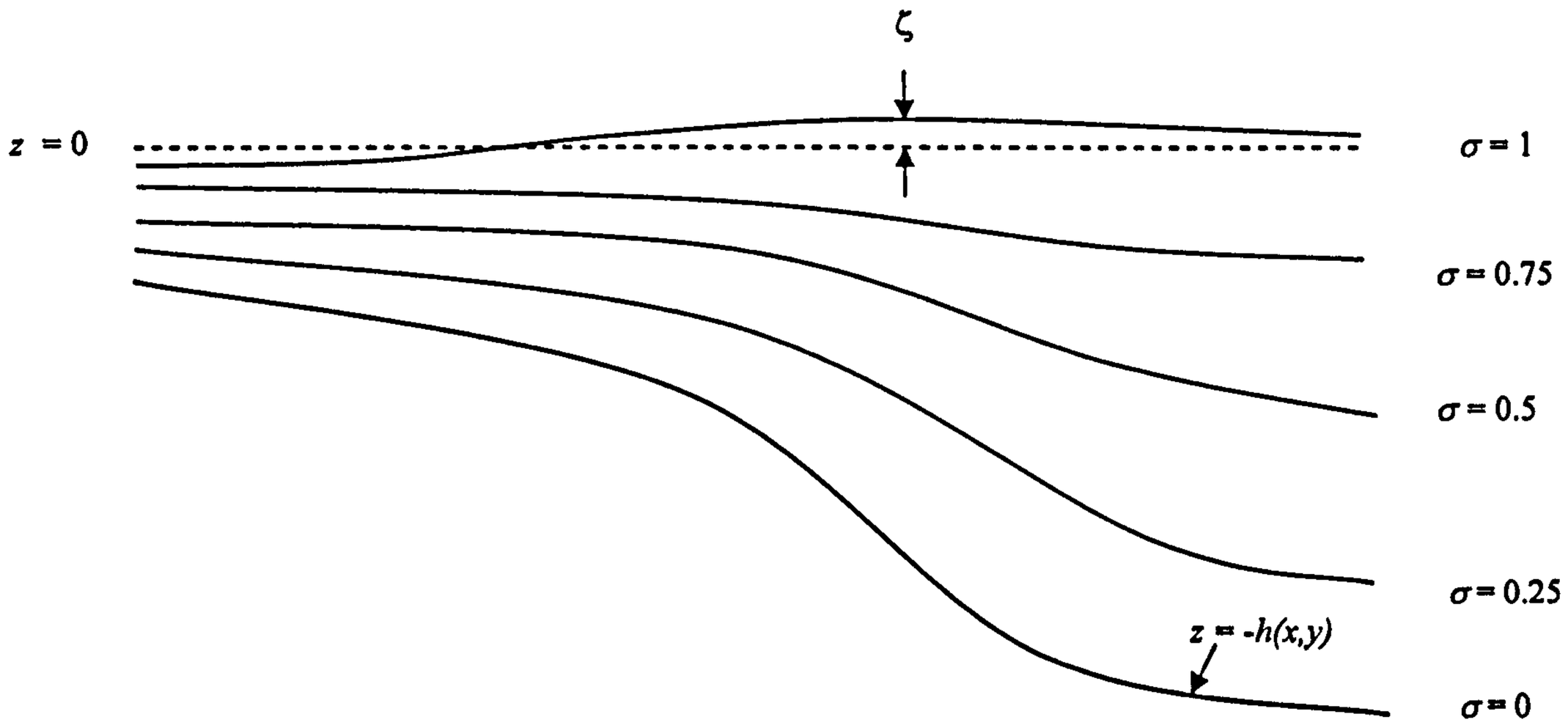

Fig. 2.2 The sigma coordinate system

It is clear that the sigma coordinates not only transform the vertical direction but also depends on horizontal coordinates. Therefore all partial derivatives must be transferred into the new system of coordinates. Derivatives with respect to z transform according to:

$$\frac{\partial \phi}{\partial z} = \frac{1}{\zeta + h} \frac{\partial \phi}{\partial \sigma}, \tag{2.69}$$

where ϕ represents a dependent variable. The derivative with respect to the horizontal coordinate in the old system is transformed according to

$$\left.\frac{\partial \phi}{\partial x}\right|_z = \left.\frac{\partial \phi}{\partial x}\right|_\sigma - \frac{1}{(\zeta + h)}\left(\sigma \frac{\partial (\zeta + h)}{\partial x} + \frac{\partial \zeta}{\partial x}\right)\frac{\partial \phi}{\partial \sigma} . \tag{2.70}$$

The time derivatives transform according to

$$\left.\frac{\partial \phi}{\partial t}\right|_z = \left.\frac{\partial \phi}{\partial t}\right|_\sigma - \frac{1}{(\zeta + h)}(1+\sigma)\frac{\partial \zeta}{\partial t}\frac{\partial \phi}{\partial \sigma}. \tag{2.71}$$

The previous equations are now transferred into new coordinates with the definition of the following prognostic variables:

$$\hat{u} = bH\bar{u} , \tag{2.72}$$

$$\hat{S} = bH\bar{S} , \tag{2.73}$$

$$\hat{E} = bH\bar{E} , \tag{2.74}$$

$$\hat{C} = bH\bar{C} . \tag{2.75}$$

Using new variables in (2.72)-(2.75) and substituting for the density from (2.24), equation (2.30) becomes:

$$\begin{aligned} &\frac{\partial \hat{u}}{\partial t} + \frac{\partial}{\partial x}(\bar{u}\hat{u}) + \frac{\partial}{\partial \sigma}(\bar{\omega}\hat{u}) \\ &= -gbH\frac{\partial \zeta}{\partial x} - g\gamma bH^2 \int_\sigma^1 \frac{\partial \bar{S}}{\partial x} d\sigma + g\gamma bH\left[\left\{(1-\sigma)\bar{S} - \int_\sigma^1 \bar{S} d\sigma\right\}\frac{\partial h}{\partial x}\right. , \\ &\left. + \left\{\bar{S}_{\sigma=1} - \sigma\bar{S} - \int_\sigma^1 \bar{S} d\sigma\right\}\frac{\partial \zeta}{\partial x}\right] + \frac{1}{H^2}\frac{\partial}{\partial \sigma}\left(K\frac{\partial \hat{u}}{\partial \sigma}\right) \end{aligned} \tag{2.76}$$

where new dependent variable, ϖ, is defined by:

$$\bar{\omega} = \sigma_t + \bar{u}\sigma_x + \bar{w}\sigma_z , \tag{2.77}$$

here a subscript denotes a partial differentiation.

The continuity equation (2.29) leads to a diagnostic equation for ϖ:

$$\frac{\partial}{\partial x}\{bH(\bar{u}-\langle\bar{u}\rangle)\}+\frac{\partial}{\partial\sigma}(bH\varpi)=0, \tag{2.78}$$

where $\varpi=0$ at σ=0 and σ=1, and $\langle\bar{u}\rangle$ is given by:

$$\langle\bar{u}\rangle=\int_0^1\bar{u}d\sigma\ . \tag{2.79}$$

Equations (2.31) and (2.32) now become

$$\frac{\partial\hat{S}}{\partial t}+\frac{\partial}{\partial x}(\bar{u}\hat{S})+\frac{\partial}{\partial\sigma}(\bar{\varpi}\hat{S})=\frac{1}{H^2}\frac{\partial}{\partial\sigma}(K\frac{\partial\hat{S}}{\partial\sigma}), \tag{2.80}$$

and

$$\frac{\partial\hat{C}}{\partial t}+\frac{\partial}{\partial x}(\bar{u}\hat{C})+\frac{\partial}{\partial\sigma}[(\bar{\varpi}-\frac{\overline{w}_s}{H})\hat{C}]=\frac{1}{H^2}\frac{\partial}{\partial\sigma}(K\frac{\partial\hat{C}}{\partial\sigma}). \tag{2.81}$$

The turbulence energy equation is also transformed to

$$\frac{\partial\hat{E}}{\partial t}+\frac{\partial}{\partial x}(\bar{u}\hat{E})+\frac{\partial}{\partial\sigma}(\bar{\varpi}\hat{E})=\frac{bK}{H^3}(\frac{\partial\hat{u}}{\partial\sigma})^2+gb\gamma K(1-\frac{\hat{C}}{\rho_s})\frac{\partial\hat{S}}{\partial\sigma}+gbK(\frac{1}{\rho_0}-\frac{1+\gamma\hat{S}}{\rho_s})\frac{\partial\hat{C}}{\partial\sigma}$$
$$+\frac{1}{H^2}\frac{\partial}{\partial\sigma}(K\frac{\partial\hat{E}}{\partial\sigma})-bH\varepsilon \tag{2.82}$$

The boundary conditions to accompany this set of transformed equations are now expressed as:

$$\bar{u}=0 \text{ at } \sigma=0, \tag{2.83}$$

$$\frac{\partial\bar{u}}{\partial\sigma}=0 \text{ at } \sigma=1, \tag{2.84}$$

$$\frac{\partial E}{\partial\sigma}=0,\frac{\partial S}{\partial\sigma}=0 \text{ at } \sigma=0 \text{ and } \sigma=1. \tag{2.85}$$

2.3 Numerical Solution

The governing equations are solved by finite difference numerical scheme over a discrete grid in a x-σ domain.

$$x = (i-1)\Delta x, \quad i = 1, 2, \ldots, m, \quad \Delta x = \mathrm{L}/(m\text{-}1), \tag{2.86}$$

$$\sigma = (j-1)\Delta\sigma\,, \; j = 1, 2, \ldots, n, \; \Delta\sigma = 1/(n\text{-}1)\,. \tag{2.87}$$

In the horizontal dimension, staggered finite differencing grids are used, the odd value of i correspond to the points at which surface elevation, ζ, and salinity, S, are calculated; the even value of i correspond to the point at which velocity u and the turbulent energy density $\overline{E}$ are calculated. m is selected to be odd so that the ends of horizontal domain correspond to ζ points. A non staggered grid is used in the vertical dimension.

The finite difference form of equations are solved by a combined centred finite differencing and averaging method. For the horizontal advective terms in the salinity and sediment concentration equations a globally conserving upstream scheme of differencing is applied that guarantees the positive advected quantity. The evaluation of vertical derivatives is derived by the use of simple centred difference replacements.

The elevations, ζ, at the grid points $i = 3, 5, 7, \ldots\ m\text{-}2$ are calculated from:

$$\frac{\zeta_i^{p+1} - \zeta_i^{p}}{\Delta t} + \frac{\left(\int \hat{u}_{i+1,j}^{p} d\sigma - \int \hat{u}_{i-1,j}^{p} d\sigma\right)}{2b_i \Delta x} = 0\,. \tag{2.88}$$

The value of ζ at $i = 1$ is specified according to (2.62), and at $i = m$ it is specified according to (2.63).

At each time step, p, the horizontal velocity u is computed at $i = 4, 6, \ldots\ m\text{-}3$ by discretized form of the momentum equation:

$$\frac{\tilde{u}_{i,j}^{p+1}-\tilde{u}_{i,j}^{p}}{\Delta t}+\frac{(\overline{\tilde{u}\tilde{u}})_{i+2,j}^{p}-(\overline{\tilde{u}\tilde{u}})_{i-2,j}^{p}}{4\Delta x}+\frac{(\varpi_{i,j}^{p}+\varpi_{i,j+1}^{p})(\tilde{u}_{i,j}^{p}+\tilde{u}_{i,j+1}^{p})-(\varpi_{i,j}^{p}+\varpi_{i,j-1}^{p})(\tilde{u}_{i,j}^{p}+\tilde{u}_{i,j-1}^{p})}{4\Delta\sigma}$$

$$=-gb_i(\zeta_i^{p+1}+h_i)\frac{(\zeta_{i+1}^{p+1}-\zeta_{j-1}^{p+1})}{2\Delta x}-gb_i\gamma(\zeta_i^{p+1}+h_i)[(\frac{(\zeta_{i+1}^{p+1}+h_{i+1})\bar{S}_{i+1,j}^{p}-(\zeta_{i-1}^{p+1}+h_{i-1})\bar{S}_{i-1,j}^{p}}{2\Delta x})\Delta\sigma$$

$$-\frac{\zeta_{i+1}^{p+1}-\zeta_{j-1}^{p+1}}{2\Delta x}\bar{S}_{i,n}^{p}-(1-\sigma_j)\frac{(h_{i+1}-h_{i-1})}{2\Delta x}\bar{S}_{i,j}^{p}+\sigma_j\frac{(\zeta_{i+1}^{p+1}-\zeta_{i-1}^{p+1})}{2\Delta x}\bar{S}_{i,j}^{p}+\frac{1}{2(\zeta_i^{p+1}+h_i)^2(\Delta\sigma)^2}[(K^{p}{}_{i,j}$$

$$+K_{i,j-1}^{p})\tilde{u}_{i,j-1}^{p+1}-(K_{i,j+1}^{p}+2K_{i,j}^{p}+K_{i,j-1}^{p})\tilde{u}_{i,j}^{p+1}+(K_{i,j+1}^{p}+K_{i,j}^{p})\tilde{u}_{i,j+1}^{p+1}]$$

(2.89).

The turbulence energy is calculated by the discretized form of energy equation:

$$\frac{\hat{E}_{i,j}^{p+1}-\hat{E}_{i,j}^{p}}{\Delta t}+\frac{(\overline{u}\hat{E})_{i+2,j}^{p}-(\overline{u}\hat{E})_{i-2,j}^{p}}{4\Delta x}+\frac{(\overline{\omega}_{i,j}^{p}+\overline{\omega}_{i,j+1}^{p})(\hat{E}_{i,j}^{p}+\hat{E}_{i,j+1}^{p})-(\overline{\omega}_{i,j}^{p}+\overline{\omega}_{i,j-1}^{p})(\hat{E}_{i,j}^{p}+\hat{E}_{i,j-1}^{p})}{4\Delta\sigma}$$

$$=\frac{K_{i,j}^{p}}{b_i^{3}(\zeta_i^{p}+h_i)^{3}}\frac{(\hat{u}_{i,j+1}^{p}-\hat{u}_{i,j-1}^{p})^2}{(2\Delta\sigma)^2}+\frac{gK_{i,j}^{p}}{2\Delta\sigma}[\gamma(1-\frac{\overline{C}_{i,j}^{p}}{\rho_s})(\bar{S}_{i,j+1}^{p}-\bar{S}_{i,j-1}^{p})+(\frac{1}{\rho_0}-\frac{1+\gamma\bar{S}_{i,j}^{p}}{\rho_s})(\overline{C}_{i,j+1}^{p}-\overline{C}_{i,j-1}^{p})]$$

$$-\frac{(K_{i,j-1}^{p}+K_{i,j}^{p})\hat{E}_{i,j-1}^{p+1}}{2(\zeta_{i,j}^{p}+h_i)^2(\Delta\sigma)^2}+[\frac{K_{i,j-1}^{p}+2K_{i,j}^{p}+K_{i,j+1}^{p}}{2(\zeta_{i,j}^{p+1}+h_i)^2(\Delta\sigma)^2}+\frac{c^{3/4}(\overline{E}_{i,j}^{p})^{1/2}}{l_{i,j}^{p}}-Xb]\hat{E}_{i,j}^{p+1}-\frac{(K_{i,j}^{p}+K_{i,j+1}^{p})\hat{E}_{i,j+1}^{p+1}}{2(\zeta_{i,j}^{p+1}+h_i)^2(\Delta\sigma)^2}$$

(2.90),

where

$$Xb=\frac{c^{1/4}l_{i,j}^{p}g}{2\Delta\sigma(\zeta_{i,j}^{p}+h_i)(\overline{E}_{i,j}^{p})^{1/2}}[\gamma(1-\frac{\overline{C}_{i,j}^{p}}{\rho_0})(\bar{S}_{i,j+1}^{p}-\bar{S}_{i,j-1}^{p})+(\frac{1}{\rho_0}-\frac{1+\gamma\bar{S}_{i,j}^{p}}{\rho_s})(\overline{C}_{i,j+1}^{p}-\overline{C}_{i,j-1}^{p})] \tag{2.91}$$

and

$$K_{i,j}^{p}=c^{1/4}l_{i,j}^{p}(\overline{E}_{i,j}^{p})^{1/2}. \tag{2.92}.$$

In the salinity transport equation, the treatment of all terms except the horizontal advection is analogous to the evaluation of the corresponding terms in the momentum equation shown as above. We simply describe the basic form of the solution process to be:

$$\frac{\partial\hat{S}}{\partial t}+\frac{\partial}{\partial x}(\hat{u}\bar{S})=\Re \tag{2.93}$$

where $\Re$ incorporates the effects of vertical advection, vertical diffusion and horizontal diffusion.

The salinity transport equation now has the form

$$\frac{\hat{S}_{i,j}^{p+1}-\hat{S}_{i,j}^{p}}{\Delta t}+\frac{\left\{\left(\hat{u}_{i+1,j}^{p}-\left|\hat{u}_{i+1,j}^{p}\right|\right)\bar{S}_{i+2,j}^{p}+\left(\hat{u}_{i+1,j}^{p}+\left|\hat{u}_{i+1,j}^{p}\right|-\hat{u}_{i-1,j}^{p}+\left|\hat{u}_{i-1,j}^{p}\right|\right)\bar{S}_{i,j}^{p}+\left(-\hat{u}_{i-1,j}^{p}-\left|\hat{u}_{i-1,j}^{p}\right|\right)\bar{S}_{i-1,j}^{p}\right\}}{4\Delta x}=\Re_{ij} \tag{2.94}$$

where $\Re_{ij}$ are calculated partly implicitly and partly explicitly.

Similarly, for the sediment transport we have:

$$\frac{\partial \hat{C}}{\partial t}+\frac{\partial}{\partial x}(\hat{u}\bar{C})=\aleph \tag{2.95}$$

and therefore:

$$\frac{\hat{C}_{i,j}^{p+1}-\hat{C}_{i,j}^{p}}{\Delta t}+\frac{\left\{\left(\hat{u}_{i+1,j}^{p}-\left|\hat{u}_{i+1,j}^{p}\right|\right)\bar{C}_{i+2,j}^{p}+\left(\hat{u}_{i+1,j}^{p}+\left|\hat{u}_{i+1,j}^{p}\right|-\hat{u}_{i-1,j}^{p}+\left|\hat{u}_{i-1,j}^{p}\right|\right)\bar{C}_{i,j}^{p}+\left(-\hat{u}_{i-1,j}^{p}-\left|\hat{u}_{i-1,j}^{p}\right|\right)\bar{C}_{i-1,j}^{p}\right\}}{4\Delta x}=\aleph_{ij} \tag{2.96}$$

$\aleph_{ij}$ has a similar character as $\Re_{ij}$.

Eq. (2.88) is used to provide an updating in time of ζ. This updated value of ζ is then used in (2.89) with a one-sided replacement of $\partial u/\partial t$. The last term on the right hand side of (2.89) is the discretized form of $\frac{1}{H^2}\frac{\partial}{\partial\sigma}\left(K\frac{\partial\hat{u}}{\partial\sigma}\right)$. It is evaluated at the advanced time level $p+1$, and the process leads to the determination of u by solving a linear system:

$$a_{1,j}X_{j-1}+a_{2,j}X_{j}+a_{3,j}X_{j+1}=a_{4,j} \tag{2.97}$$

The turbulence energy equation (2.90) is solved consequently using the same scheme with the updated ζ and u for time level $p+1$.

The eddy viscosity coefficient K is updated by (2.92) when the evaluation of turbulence energy density for the advanced time level $p+1$ is completed.

This chapter described a two-dimensional single-section estuary model which is capable of describing the tidal flow in a channel using a turbulence energy closure scheme and topography following coordinates. The governing equations are solved on a staggered finite-difference grid in the horizontal. A combination of centred-differencing and averaging is used to evaluate the horizontal derivatives for elevation, velocity and energy. The evaluation of vertical derivatives is achieved by simple centred-difference replacements although the discretization of the boundary conditions involves the use of second-order accurate forward and backward replacements. The equations are integrated ahead in time from an initial state of rest with the periodic tidal forcing at the mouth of river and the integration is continued until the initial transient response is dissipated by the friction and radiated out of the analysis domain. The final cycle of integration may then be analysed.

Chapter 3 Shelf Sea Model

This chapter describes a high resolution, three-dimensional shelf sea model based on the eastern Irish Sea model developed by Proudman Oceanography Laboratory (POL). This model is highly advanced and is capable of accurately describing the current circulation driven by tidal and meteorological forcing (Aldridge and Davies, 1993; Xing and Davies, 1995b). In the latter part of this thesis this model is applied to join with the river model as bay model and study the interaction of the tidal flow between two models.

3.1 The Description of Model

3.1.1 Basic Equations

The model is a three dimensional, free surface, baroclinic sigma(σ) system model.

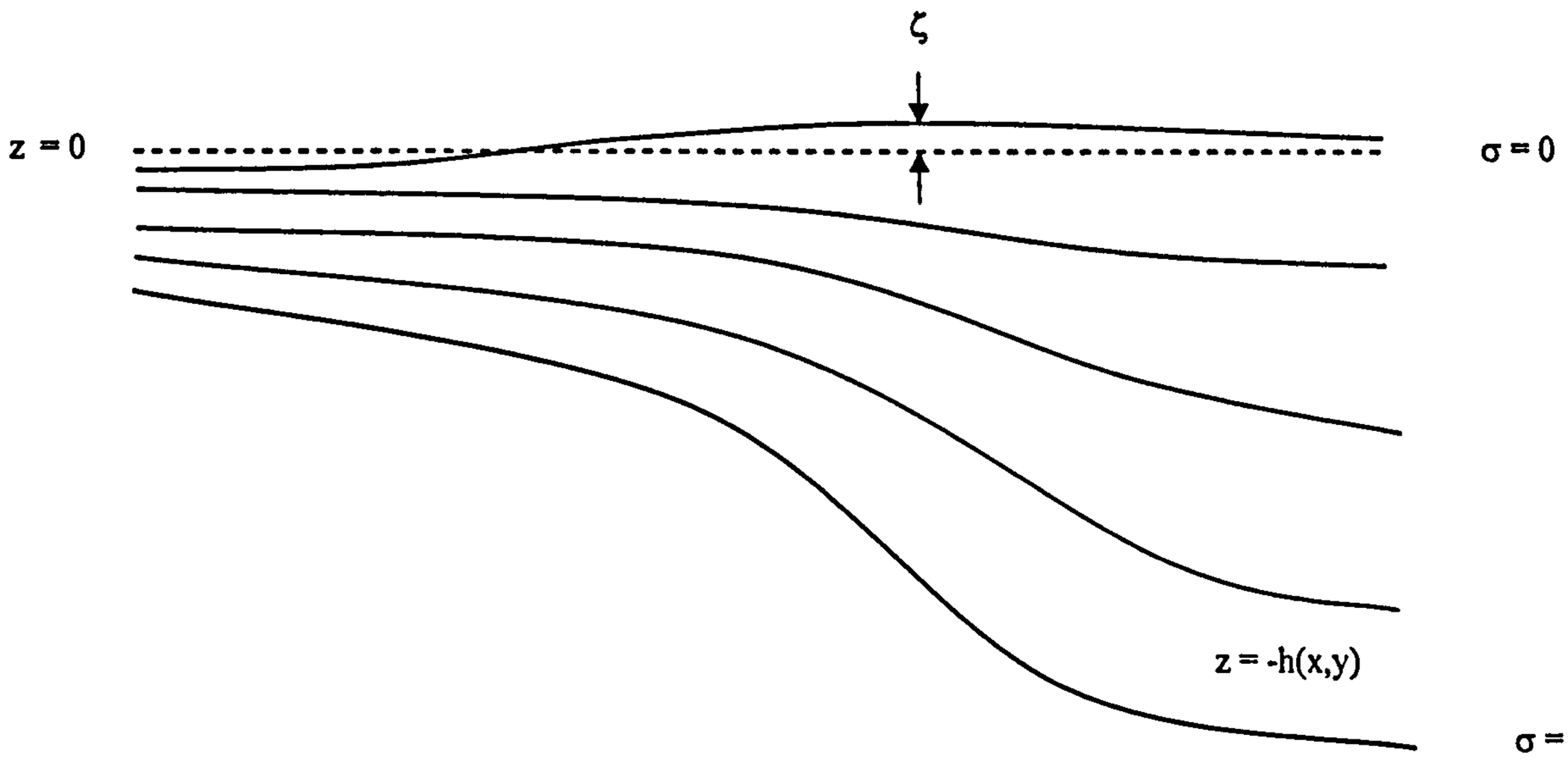

Fig. 3.1. The σ coordinate system

The model equations are described in a spherical coordinate system with σ given by

$$\sigma = \frac{z-\zeta}{H}, \tag{3.1}$$

where $H = h+\zeta$, $h(x,y)$ is the bottom topography and $\zeta(x,y,t)$ is the surface elevation.

Thus σ ranges from $\sigma = 0$ at $z = \zeta$ to $\sigma = -1$ at $z = -h$ (Fig. 3.1). The σ coordinate system was first introduced into meteorology by Phillips (1957). For the derivation of the sigma coordinate equations, the reader is referred to Blumberg and Mellor (1980, 1987).

After coordinate transformation to σ coordinates, the basic equations are written as:

Momentum equations:

$$\frac{\partial Hu}{\partial t} + \nabla\cdot(\vec{V}Hu) + \frac{\partial Hu\omega}{\partial\sigma} - fHv = -\frac{gH}{R\cos\theta}\frac{\partial\zeta}{\partial\lambda} + BPF_\lambda + \frac{1}{H^2}\frac{\partial}{\partial\sigma}(K_m\frac{\partial Hu}{\partial\sigma}) + F_u,$$

(3.2)

$$\frac{\partial Hv}{\partial t} + \nabla\cdot(\vec{V}Hv) + \frac{\partial Hv\omega}{\partial\sigma} - fHu = -\frac{gH}{R}\frac{\partial\zeta}{\partial\theta} + BPF_\theta + \frac{1}{H^2}\frac{\partial}{\partial\sigma}(K_m\frac{\partial Hv}{\partial\sigma}) + F_v.$$

(3.3)

Continuity equation:

$$\frac{\partial\zeta}{\partial t} + \nabla\cdot\left(\int_{-1}^{0} H\vec{V}d\sigma\right) = 0 \quad . \tag{3.4}$$

Temperature equation:

$$\frac{\partial HT}{\partial t} + \nabla\cdot(\vec{V}HT) + \frac{\partial H\omega T}{\partial\sigma} = \frac{1}{H^2}\frac{\partial}{\partial\sigma}(K_h\frac{\partial HT}{\partial\sigma}) + F_T + \frac{\partial I}{\partial\sigma}\ , \tag{3.5}$$

$$\frac{\partial HS}{\partial t} + \nabla\cdot(\vec{V}HS) + \frac{\partial H\omega S}{\partial\sigma} = \frac{1}{H^2}\frac{\partial}{\partial\sigma}(K_h\frac{\partial HS}{\partial\sigma}) + F_S\ . \tag{3.6}$$

Hydrostatic approximation:

$$\frac{\partial P}{\partial \sigma} = -\rho g H \,. \tag{3.7}$$

The density is related to salinity and temperature by

$$\rho = 1000.0 + \sigma_t \,, \tag{3.8}$$

where

$$\sigma_t = 28.152 - 0.75T - 0.00469T^2 + (0.802 - 0.002T)(S - 35) \,. \tag{3.9}$$

In the above equations:

$\vec{V} = (u,v)$, (u,v,ω) are the velocity components corresponding to the (λ,θ,σ) coordinates with λ the longitude and θ the latitude; H is the total water depth; ∇ is the horizontal divergence operator; t is time; f is the Coriolis parameter; R is the radius of the earth; T is the temperature; S is the Salinity; ζ is the sea surface elevation above the equilibrium level; z is water depth increasing vertically upwards; ρ is the density; K_m, K_h are the vertical eddy viscosity and diffusivity coefficient respectively; I is the incoming solar radiation and P is the pressure field.

F_u, F_v, F_T, F_S are the horizontal diffusion terms, and have the Laplacian form using a transformation suggested by Mellor and Blumberg (1985),

$$F_{(u,v)} = A_m \nabla \cdot (H \nabla (u,v)), \tag{3.10}$$

$$F_{(T,S)} = A_h \nabla \cdot (H \nabla (T,S)). \tag{3.11}$$

Here A_m, A_h are coefficients of horizontal diffusion terms for momentum and density (temperature and salinity) respectively.

BPF_λ, BPF_θ are the baroclinic pressure gradient force terms having the forms:

$$BPF_{\lambda} = -\frac{H\partial P_{bi}}{\rho_0 R\cos\theta\partial\lambda}\Big|_z - \frac{H}{\rho_0}\left(\frac{\partial(P_b - P_{bi})}{R\cos\theta\partial\lambda} + \frac{\sigma}{H}\frac{\partial(P_b - P_{bi})}{\partial\sigma}\frac{\partial H}{R\cos\theta\partial\lambda} + \frac{\partial(P_b - P_{bi})}{H\partial\sigma}\frac{\partial\zeta}{R\cos\theta\partial\lambda}\right) \tag{3.12}$$

$$BPF_{\theta} = -\frac{H\partial P_{bi}}{\rho_0 R\partial\theta}\Big|_z - \frac{H}{\rho_0}\left(\frac{\partial(P_b - P_{bi})}{R\partial\theta} + \frac{\sigma}{H}\frac{\partial(P_b - P_{bi})}{\partial\sigma}\frac{\partial H}{R\partial\theta} + \frac{\partial(P_b - P_{bi})}{H\partial\sigma}\frac{\partial\zeta}{R\partial\theta}\right). \tag{3.13}$$

P_{bi} is a reference baroclinic pressure or initial baroclinic pressure field. The first terms on the right hand of above two equations are the pressure gradient forces calculated in z coordinates, therefore only deviations of the pressure gradient force are calculated in σ coordinates. In this way the errors due to the vertical coordinates transformation can be reduced (Xing et al, 1999).

3.1.2 Turbulence Mixing

A one-equation turbulence model (Johns and Oguz 1990; Davies and Xing 1995) is applied to calculate the vertical eddy viscosity (K_m) and eddy diffusivity (K_h), it includes a prognostic equation for turbulence energy and an algebraic form of the length scale.

Turbulence kinetic energy prognostic equation in σ coordinates is given by:

$$\frac{\partial HE}{\partial t} + \nabla\cdot(\vec{V}HE) + \frac{\partial HE\omega}{\partial\sigma} = \frac{K_m}{H}\left[\left(\frac{\partial u}{\partial\sigma}\right)^2 + \left(\frac{\partial v}{\partial\sigma}\right)^2\right] + \frac{g}{\rho_0}K_h\frac{\partial\rho}{\partial\sigma} - \varepsilon H + \frac{1}{H}\frac{\partial}{\partial\sigma}(K_h\frac{\partial HE}{\partial\sigma}) + F_E \tag{3.14}$$

Where F_E is the horizontal diffusion term and has the same form as F_T. The parameters required by the equation are:

$$\varepsilon = \frac{C_1 E^{3/2}}{l}, \tag{3.15}$$

$$K_m = K_h = \frac{C_0 E^{1/2}}{l}, \tag{3.16}$$

where ε is the turbulence dissipation. $C_0=C^{1/4}$, $C_1=C_0^3$ and C= 0.046 (Davies et al, 1988). l is the mixing length scale. Xing and Davies (1995b, 1996a, 1996b) use a turbulence energy closure scheme of this form to simulate M_2 and M_4 in the Irish Sea.

The length scale is prescribed diagnostically by an algebraic expression proposed by Xing and Davies (1995):

$$l = \frac{1}{1/l_1 + 1/l_2}, \tag{3.17}$$

where

$$l_1 = \kappa(\sigma H + H + z_0)\exp(\beta_1 \sigma), \tag{3.18}$$

$$l_2 = \kappa(z_s - \sigma H), \tag{3.19}$$

κ= 0.4, is Von Karman's constant ; β_1 is an empirical constant. z_0 is the bed roughness length; z_s is the surface roughness length, which controls the σ value at the sea surface.

In the above formulations the influence of vertical stratification on the length scale is not included, but it is important to adjust the length scale under stratified conditions. Following Beckers (1991) the length scale is modified with the Richardson number (R_i) as:

$$l = l_0 \Psi, \tag{3.20}$$

here l_0 is determined as l in (3.17) and

$$\Psi = [(R_i^2 + 1)^{1/2} + R_i]^{-2}. \tag{3.21}$$

where

$$R_i = -\frac{g}{\rho_0}\frac{H\partial\rho}{\partial\sigma}\left[\left(\frac{\partial u}{\partial\sigma}\right)^2 + \left(\frac{\partial v}{\partial\sigma}\right)^2\right]^{-1}. \tag{3.22}$$

Together with a range of turbulence energy models, above formulation was used to study the sensitivity of the internal tide to the parameterization of vertical viscosity and diffusivity (Xing and Davies 1998).

3.2 Boundary Conditions

3.2.1 Surface and Bed Boundary Conditions

At the sea surface the internal stress is set equal to the externally applied wind stress components τ_x and τ_y. Thus the boundary conditions of velocity are:

$$\rho_0 K_m \frac{\partial u}{H\partial\sigma} = \tau_x, \tag{3.23}$$

$$\rho_0 K_m \frac{\partial v}{H\partial\sigma} = \tau_y. \tag{3.24}$$

Here, τ_x, τ_y are calculated from wind data following Davies and Flather (1987).

At the sea bed, a quadratic bottom friction condition (Davies 1986) is applied:

$$\rho_0 K_m \frac{\partial u}{H\partial\sigma} = C_D u_b (u_b^2 + v_b^2)^{1/2}, \tag{3.25}$$

$$\rho_0 K_m \frac{\partial v}{H\partial\sigma} = C_D v_b (u_b^2 + v_b^2)^{1/2}. \tag{3.26}$$

Here, u_b, v_b are components of bottom velocity and C_D is a coefficient of bottom friction which is determined from:

$$C_D = \left[\frac{\kappa}{\ln(z_r / z_0)}\right]^2. \tag{3.27}$$

In the above formula, z_r is the reference height above the bed at which C_D and bed currents u_b and v_b are calculated, in practice it takes the value according to the height of the first grid box from the bottom.

The sea surface boundary condition for the turbulence energy equation is:

$$K_h \frac{\partial E}{H \partial \sigma} = \mu(\frac{\tau}{\rho_0}). \tag{3.28}$$

Where τ is the surface wind stress and μ a constant (taken as 100) for parameterizing the input of turbulence kinetic energy from breaking wave surface waves (Craig 1996). The equation (3.28) introduces a gradient of turbulence energy in the surface layer, with the product of the turbulence energy and the mixing length (3.15, 3.16) determining the profile of viscosity and diffusivity in this layer. Recently Stacey and Pond (1997) have proposed an increase in the value of the mixing length in the surface layer to reflect enhanced roughness due to wind waves. Calculations by Davies et al (2001) have shown that this reduces the near surface current and shear although the current at a depth of about 5 meters below the surface does not change.

The boundary condition for the turbulence energy equation at the seabed is:

$$K_h \frac{\partial E}{H \partial \sigma} = \frac{\delta}{K_m}(C_0 C_1 E^2 - u_*^4), \tag{3.29}$$

where δ is the lowest model level height; u_* is the bottom friction velocity.

The boundary condition for temperature at sea surface is:

$$K_h \frac{\partial T}{H \partial \sigma} = \frac{Q}{c_p \rho_0}, \tag{3.30}$$

with $Q = Q_s + K_q(T_d - T_s)$; Q_s is the observed surface insulation; T_s is the modelled sea surface temperature. T_d is the dew point temperature; K_q is the heat loss coefficent and $K_q(T_d\text{-}T_s)$ is the heat loss and heat gain at the sea surface

The short wave solar insolation I($ms^{-1}K$) is given by:

$$I = \frac{Q_s}{c_p \rho_0}(\alpha e^{\sigma H/\lambda_1} + (1-\alpha)\alpha e^{\sigma H/\lambda_2}), \tag{3.31}$$

here α is a constant with value 0.62.

λ_1, λ_2 are extinction depths and λ_1=1.5m ,λ_2=20m.

The lateral boundary conditions at the coast are no-slip for velocity and no flux for temperature and turbulence.

At the sea surface and the sea bed there is no salinity flux, so

$$\left.\frac{\partial S}{\partial \sigma}\right|_0 = 0, \left.\frac{\partial S}{\partial \sigma}\right|_{-1} = 0. \tag{3.32}$$

3.2.2 Lateral Boundary Conditions

Along the closed boundaries the normal component of the current was set equal to zero.

$$u\cos\psi + v\sin\psi = 0, \tag{3.33}$$

where ψ is the inclination of the normal to the direction of increasing x.

In very shallow water, regions flood and dry at various stages of the tidal cycle and this dynamic lateral boundary condition was considered by an algorithm of Flather and Heaps (1975). The review of incorporating drying conditions into the nearshore models has been given by Flather and Hubbert (1990).

Along open boundaries a radiation condition is applied, the six dominant tidal constituents are introduced. It has the form (Davies and Furnes 1980)

$$q = q_r + \frac{\sqrt{gh}}{h}(\zeta - \zeta_r), \tag{3.34}$$

where q is the normal component of depth mean current and

$$q_r = \sum_i Q_i(\chi,\phi)\cos[\omega_i t - \gamma_i(\chi,\phi)], \tag{3.35}$$

$$\zeta_r = \sum_i H_i(\chi,\phi)\cos[\omega_i t - G_i(\chi,\phi)], \tag{3.36}$$

where ω_i the speed of the various tidal constituents, H_i and G_i are the amplitude and phase of tidal elevation; Q_i and γ_i are the tidal currents. Index i denotes each tidal constituent such as M_2, M_4, M_6, S_2, N_2.

An alternative way to apply a radiation condition is to use an elevation specified open boundary with ζ prescribed by ζ_r at ζ points along the boundary.

3.3 Numerical Solution

The model equations are solved numerically using a mixed spectral-finite difference approach given by Davies (1983b, 1986, 1987b).

In the spectral-finite difference approach, a regular finite-difference grid in the horizontal, namely the Arakawa C grid (Arakawa and Lamb, 1977) in which ζ, u, v are evaluated at different points. Fig. 3.2 shows the sample of Arakawa C grid, grid at ζ points in the middle the elevation ζ, and pressure p are calculated and at the corners the vorticity q is treated, velocities u and v are calculated in the middle of the sides between the q points.

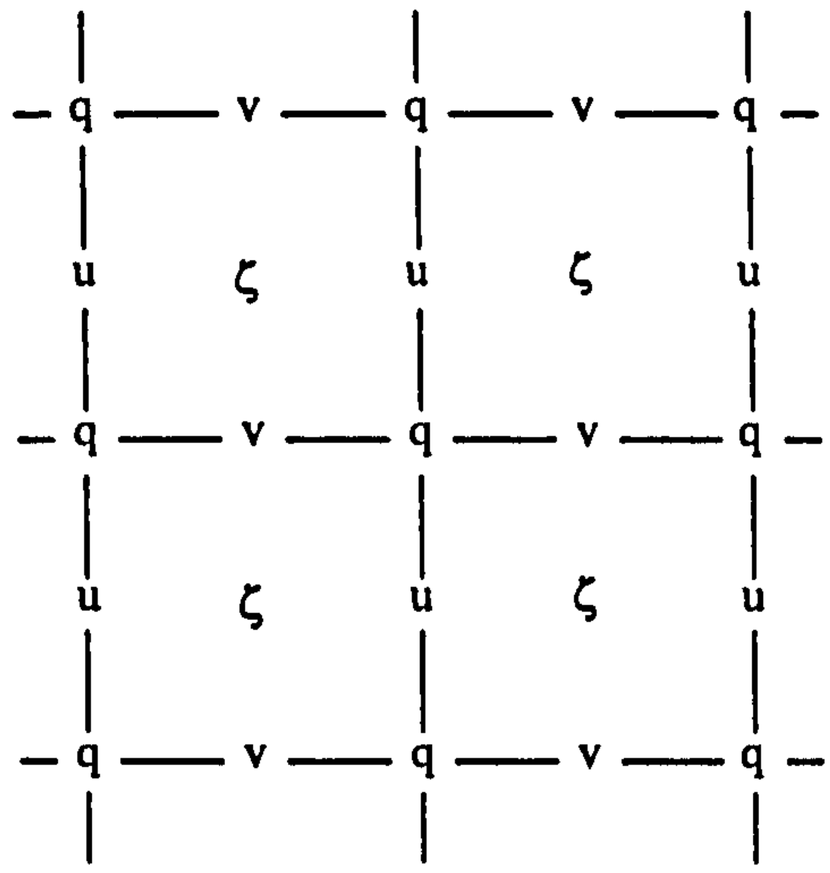

Fig. 3.2 The Arakawa C-grid

In the vertical, the Galerkin method with a basis set of functions is employed and gives a continuous current profile from sea surface to sea bed. A range of basis functions can be used with the Galerkin method, for example, Legendre Polynomials (Gordon and Spaulding 1987; Spaulding and Isaji 1987). In this model, however, a basis set of eigenfunctions (Davies 1983a; Furnes 1983;Furnes and Mork 1987) of the eddy viscosity profile is employed, in the linear case this gives an uncoupled set of equations and is computationally economic (Davies and Stephens 1983) and ideal for integration on the new generation of multiprocessor vector computers.

The discretization of the model equations is implemented in the modelling domain and the equations are integrated forward in time.

The full set of the equations is solved by an alternating direction implicit (ADI) method (Stelling et al. 1986; Wilders et al. 1988; Wolf 1983). By this means an unconditionally stable set of equations can be obtained that can be solved with a larger time step than that required by the Courant-Friedrichs-Lewy (CFL) condition.

The equations, governing the dynamics of coastal circulation, contain fast moving external gravity waves and slow moving internal gravity waves. It is desirable in terms of computer economy to separate the vertically integrated equations (external mode) from the vertical structure equations (internal mode).

The velocities can be separated in to:

$$u = U + u', \tag{3.37}$$

$$v = V + v', \tag{3.38}$$

where U, V are the depth-mean velocity (barotropic or external mode) represent the motions related to fast moving gravity waves, it requires a small time step DTS for integration to satisfy the CFL condition. u', v' are the depth-dependent velocity (baroclinic or internal mode) represent the velocities related to slower moving waves, larger time steps can be used.

This technique, known as time-split method (Simons, 1974; Madala and Piacsek, 1977) allows the calculation of the free surface elevation with little sacrifice in computational time by solving the velocity transport separately from the three-dimensional calculation of the velocity and the thermodynamic properties.

The velocity transport, external mode equations are obtained by integrating the internal mode over the depth, thereby eliminating all vertical structure.

The calculation of the external mode results in updates for surface elevation and the vertically averaged velocities. The internal mode calculation results in updates for u, v, t, S and the turbulence quantities.

The time stepping process for the external and internal mode in simplified form is shown in Fig. 3.3. Assume everything is known at time t^{n-1} and t^n, the previous leap

frog time step have just been finished. Integrals involving the baroclinic forcing and the advective terms are supplied to the external mode along with the bottom stress; their values are held constant during $t^n < t < t^{n+1}$. The external mode 'leap frogs' many times, with the time step, dts, that is much smaller than that for the internal mode, until $t=t^{n+1}$. The vertical and time averaged velocities and those from the previous time step, are time averages of the external variables. The internal and external modes have different truncation errors so that the vertical integrals of the internal mode velocity may depart slightly from the external variables during the course of a long integration. Therefore the internal velocities are adjusted.

In order to avoid errors in mass conservation as a result of using the time splitting method, the sea surface elevation is recomputed using the temporal mean of the depth mean velocities in the smaller time steps prior to the solution of the internal mode. Therefore equation (3.4) is numerically satisfied not only during the integration of the external mode but also in the larger time step integration of the internal mode. The vertical velocity is calculated using the internal mode solution only, therefore:

$$\nabla \cdot (H\vec{V}') + \frac{\partial H\omega}{\partial \sigma} = 0, \tag{3.39}$$

where $\vec{V}' = (u', v')$ is depth-dependent velocity (internal mode).

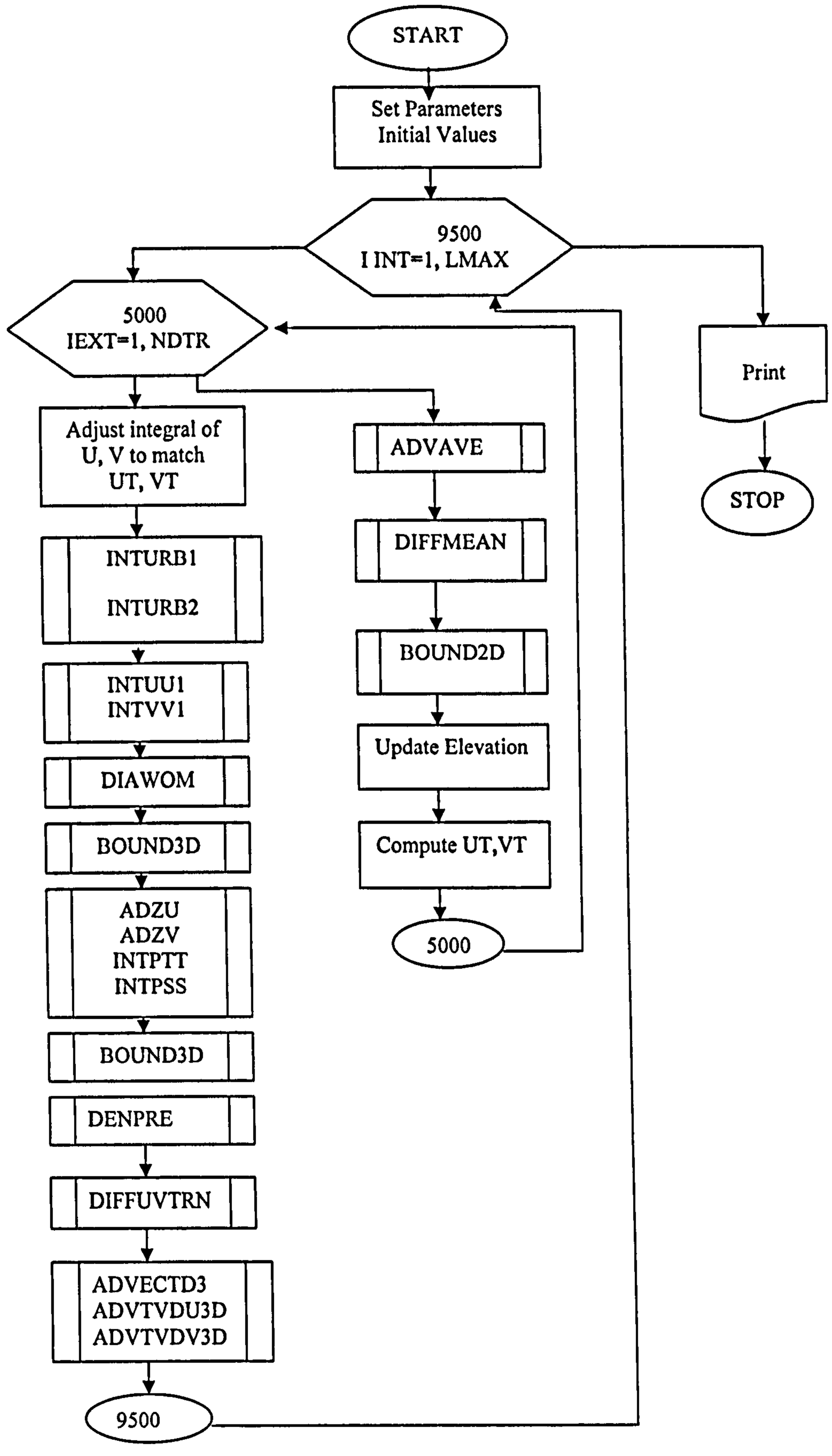

Fig. 3.3 Flow chart of the code of the time stepping process for the external and internal modes. The boxes with sidebars contain subroutines.

The finite difference equations are solved by a central difference scheme except for the advection of density(temperature) where a total variation diminishing (TVD) method is applied to preserve the sharp gradients in the temperature field as they are advected by the tidal flow.

Calculation starts from an initial condition of zero elevation and motion. A tidal regime is set up in the region by tidal forcing across the western open boundary.

Chapter 4 Development of Joined Model

The work presented here describes the joining together of the two models that were described in chapters 2 and 3. A joined model is developed for the exchange of water flow between the Mersey Estuary and Liverpool Bay. The essential part of the joining procedure is to link together the models dynamically through the elevation at the meeting point. The linkage of salinity is achieved by matching the sigma (σ) coordinates with the different vertical and time resolution, so that a linear interpolation/extrapolation of computed values of salinity at the meeting point can be carried out from one set of computational levels to the other.

The main feature of the method is to match the variables along the vertical boundary between the two models. Both models use vertical σ coordinate systems which are defined differently and have a different number of computational levels in the vertical. The variables are calculated at topography-following coordinates in the vertical. They are not located at a fixed physical z level and their locations vary with time. This is the main problem that has to be considered and solved in this work.

4.1 Combined Model with Identical Time Resolution

In this section, we construct the joining scheme using a simple method. An identical time step of 200sec is used when the two models are linked together.

In the bay model, the computational domain covers the region of the Eastern Irish Sea as shown in Fig. 4.1. The Cartesian coordinates (x, y) in the horizontal, combined with σ coordinate in the vertical are used. So that the model variables have a general

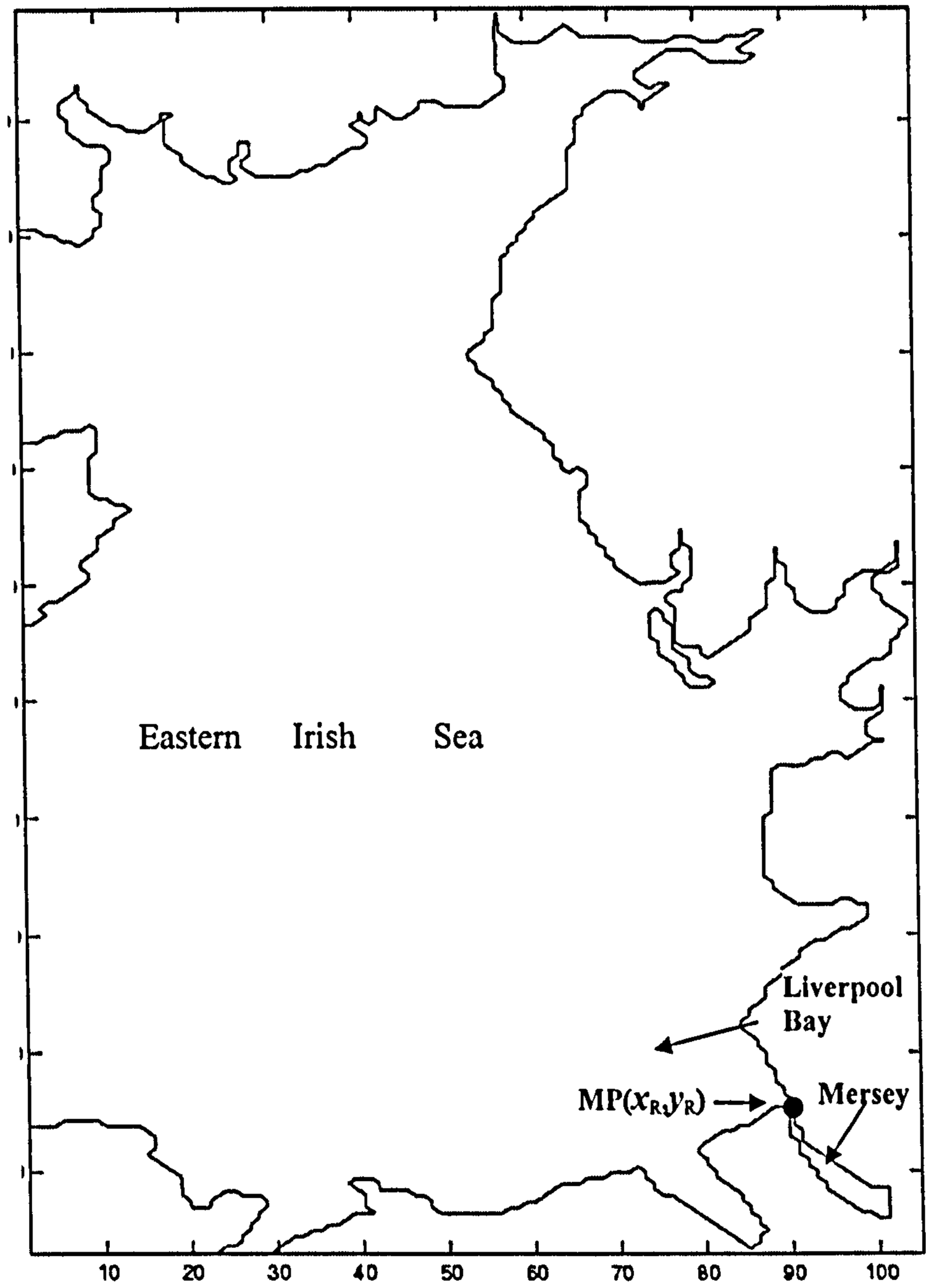

Fig. 4.1 Computational area and the location of the meeting point MP(x_R, y_R).

form of f(x, y, σ, t). The horizontal resolution in the north-south direction is 0.5', and as there are 120 grid boxes per degree of latitude this leads to a resolution of order 0.9 km. In the east-west direction it is 1.0' and there are 60 grid boxes per degree of longitude leading to a resolution of order 1.0 km. There are 104×214 grid-points in a horizontal computational plane and 18 computational levels in the vertical.

The meeting point between the Mersey and Liverpool bay corresponds to (53° 26″N, 3° 01″W) where the breadth of the Mersey is 1.6 km. The coordinate of the point where the river model is linked to the bay model is (x_R, y_R) (hereafter referred to the meeting point as MP). The river model uses an arrangement of horizontal grid-points that is identical to that described in chapter 2, Fig. 2.1. The origin, O, of the axis Ox' is located at the head of the Mersey and points toward Liverpool bay. The seaward end of the Mersey, $x' = L$, corresponds to the MP in Liverpool bay. This requires that the MP is an elevation point in both models.

The bay model runs to provide real time information of tidal elevation and salinity at the MP and then updates the water elevation and salinity values in the Mersey at $x' = L$. However, when the river model is run alone without joining, the surface elevation at $x' = L$ is prescribed to represent the form of tidal amplitude as a simple sinusoidal oscillation on the open boundary, as described by equation (2.63). The flow chart of joining processes is presented in Fig. 4.2.

It is necessary to describe the notation used in defining the variables this chapter. Subscripts are used to refer to the location where a quantity is calculated; For example, r for the river and b for the bay. The superscript notation, p, refers to the time level .

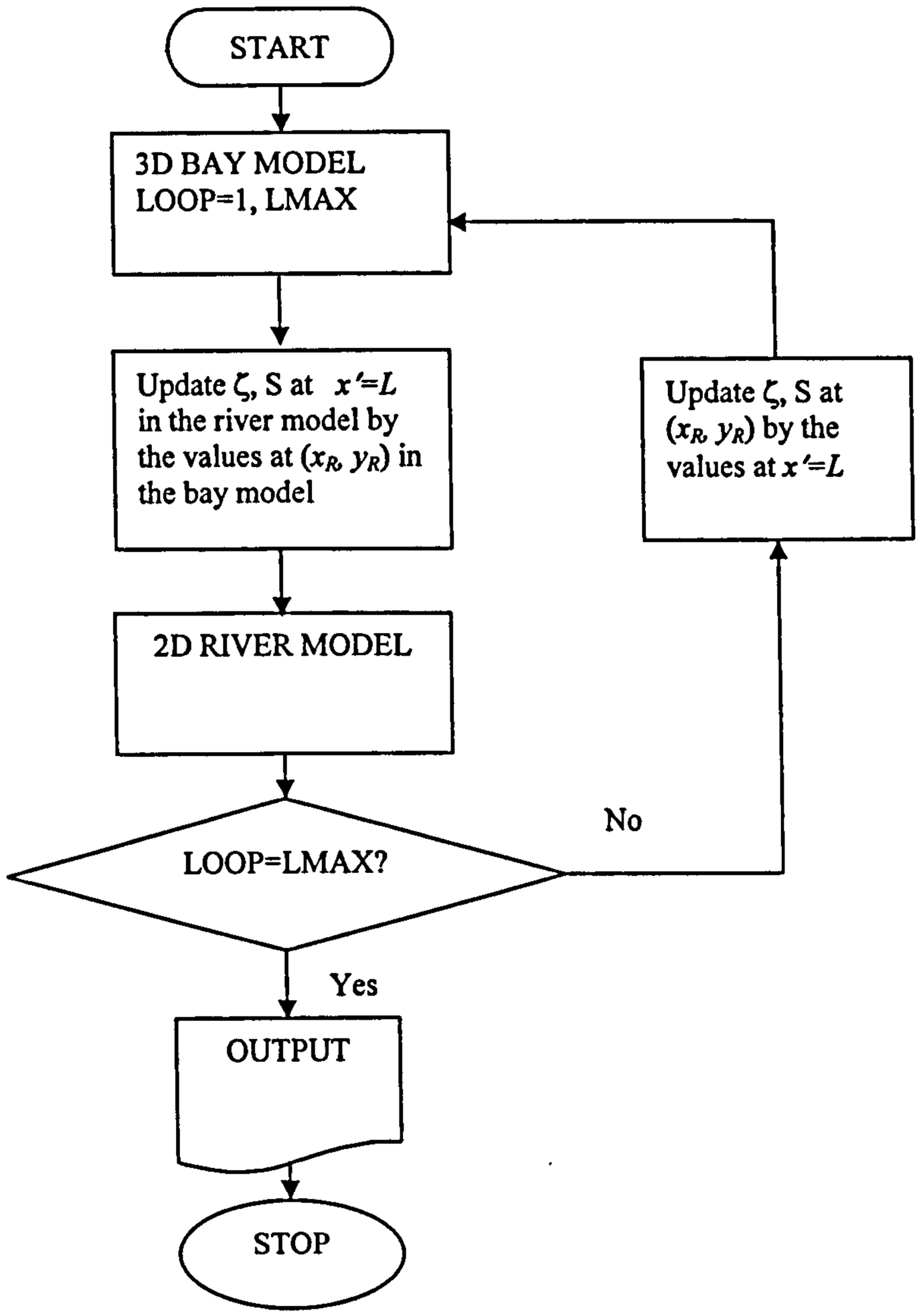

Fig. 4.2 Flow diagram of the joining process

For example, ζ_b^p represents the elevation in the bay model at time level p, and ζ_r^{p+1} represents the elevation in the river model at time $p+1$.

In the bay model, the σ coordinate is denoted as σ_b, the elevation at MP is ζ_b.

In the river model, the sigma coordinate is σ_r, the elevation at the MP (where $x' = L$) is ζ_r.

The sigma in the river model is defined as

$$\sigma_r = \frac{z+h}{\zeta+h} \quad . \tag{4.1}$$

Thus $\sigma_r = 1$ refers to the surface and $\sigma_r = 0$ refers to the bottom.

In the bay model, sigma is defined as

$$\sigma_b = \frac{z-\zeta}{\zeta+h} \quad . \tag{4.2}$$

Thus $\sigma_b = 0$ refers to the surface and $\sigma_b = -1$ refers to the bottom.

From (4.1) and (4.2), we obtain

$$\sigma_b = \sigma_r - 1 \ . \tag{4.3}$$

The computation of salinity involves more detailed work. A two-way linkage of the salinity in the vertical direction from bay to river and from river to bay is required. The exchange of information regarding the salinity between the river and bay models is much more complex. This is mostly because in the vertical, the salinity is calculated

at a discretized set of computational levels which are not located at a fixed physical position. Another problem is caused by different number of computational levels in the river model and the bay model. Fig. 4.3 gives an example of the relative grid layout between the two models.

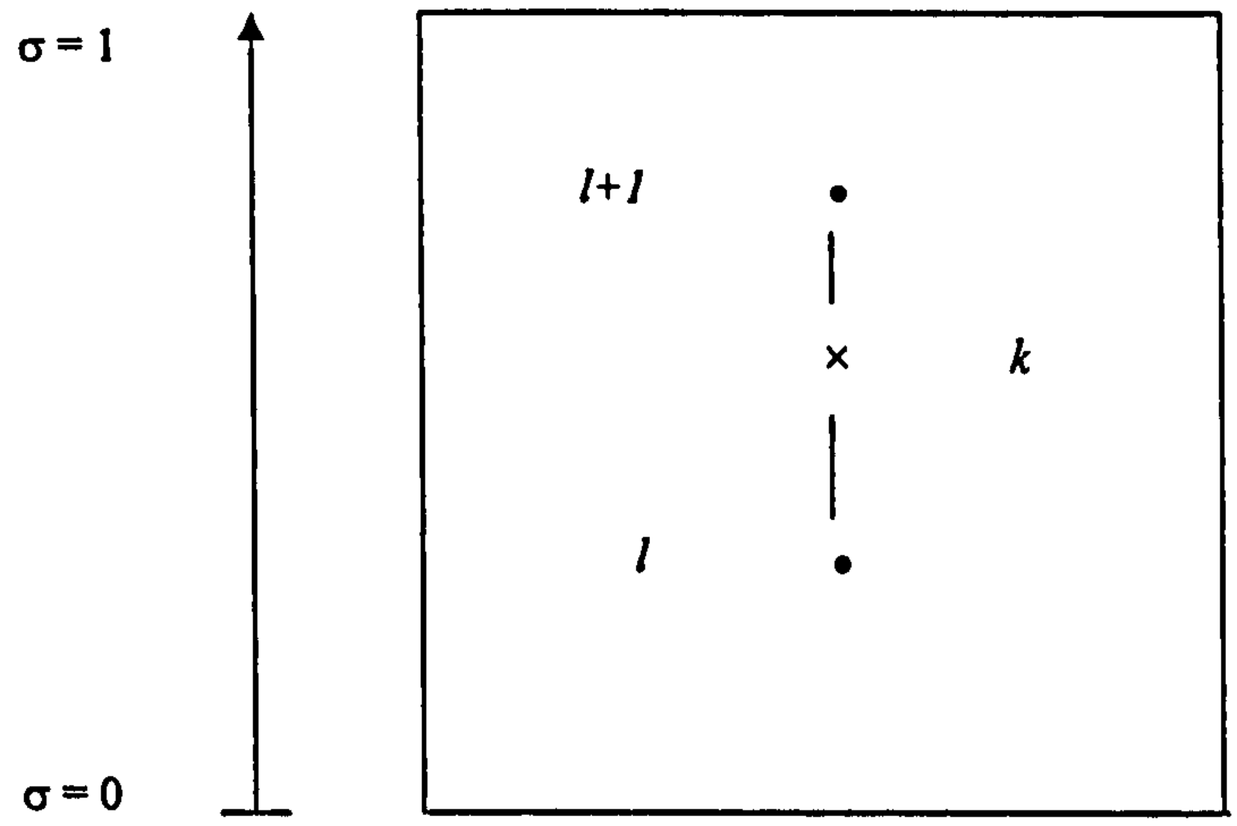

Fig. 4.3 The vertical grid distribution for $S_b^{p+1}(l)$ and $S_r^{p+1}(k)$

Using expression (4.3), the salinity at the MP can be exchanged between the two models. At this stage the processes of integration in both models are carried out at the same time level.

Let us depict the derivative of salinity at MP when the integration is developed from time level p to $p+1$, the salinity in the river model at $x'=L$ is denoted by

$S_r^p(k)$, $k=1, 2, 3\ldots n$,

where k is the computational level index for σ_r. There are n levels for the river model.

The salinity in the bay model at the MP is denoted by

$S_b^p(l)$, $l=1, 2, 3\ldots m$,

where l is the computational level index of σ_b. There are m levels for the bay model.

Assuming everything is known at time p, then at time $p+1$, the first step is to calculate the new values in the bay model, including those at the MP, namely, ζ_b^{p+1} and $S_b^{p+1}(l)$.

The next step is to calculate the variables in the river model at time level $p+1$. The boundary conditions at the river mouth, $x'=L$, must be determined through the calculation of ζ_b^{p+1} and $S_b^{p+1}(l)$.

The river model is dynamically linked to the bay model at the MP by elevation, ζ.

At first, the elevation at each grid-point in the river model is updated by the surface elevation at the MP, i.e., $x'=L$. This is supplied by the bay model in which

$$\zeta_r^{p+1} = \zeta_b^{p+1} \quad . \tag{4.4}$$

The next step is to calculate the salinity in the river model. This requires using the input from the bay model, $S_b^{p+1}(l)$, to update the salinity in the river model at its open boundary at $x'=L$, $S_r^{p+1}(k)$.

The salinity from the bay model, $S_b^{p+1}(l)$, is calculated at each discretised level of σ_b, where the thickness between each level, $\Delta\sigma_b$ is not constant (Table 4.1). But in the river model $S_r^{p+1}(k)$ is calculated at discretised levels of σ_r (Table 4.2) with $\Delta\sigma_r = 0.05$. The physical z level of σ_b is different from that of σ_r. In order to obtain $S_r^{p+1}(k)$ from $S_b^{p+1}(l)$, they have to be transferred using a common coordinate system. The method used here is to convert σ_b, using (4.3), into the sigma system of the river model and denote it by σ_{rb}. The last step is to define the derivative $S_r^{p+1}(k)$ by linear interpolation according to the sigma coordinate of the river model, σ_r. First of all, we need to find the location of $\sigma_r(k)$ in the σ_{rb} coordinate, let us assume that

$$\sigma_{rb}(l) \le \sigma_r(k) < \sigma_{rb}(l+1),$$

where $\sigma_{rb}(l)$ and $\sigma_{rb}(l+1)$ are the σ coordinates for $S_b^{p+1}(l)$ and $S_b^{p+1}(l+1)$, respectively. The following expression is then used to find $S_r^{p+1}(k)$,

$$\frac{S_r^{p+1}(k)-S_b^{p+1}(l)}{\sigma_r(k)-\sigma_{rb}(l)} = \frac{S_b^{p+1}(l+1)-S_b^{p+1}(l)}{\sigma_{rb}(l+1)-\sigma_{rb}(l)} \qquad (4.5)$$

Rearranging above formula leads to

$$S_r^{p+1}(k) = \frac{S_b^{p+1}(l)\sigma_{rb}(l+1)+(S_b^{p+1}(l+1)-S^{P+1}{}_b(l))\sigma_r(k)-S_b^{p+1}(l+1)\sigma_{rb}(l)}{\sigma_{rb}(l+1)-\sigma_{rb}(l)} \qquad (4.6)$$

The following prescriptions are necessary to satisfy the interpolation,

At the surface

$$S_r^{p+1}(1) = S_b^{p+1}(1) \tag{4.7}$$

At the bottom

$$S_r^{p+1}(n) = S_b^{p+1}(m) \tag{4.8}$$

The flow diagram for implementing the expression (4.6) is shown in Fig. 4.4.

The river model is then called by the bay model as a subroutine. The dynamic variables, u, w and E, in the river are subsequently updated in the time stepping process.

When the calculation in the river model at time level $p+1$ is completed, the joined model returns to the main program, and the water elevation and salinity in the bay model at the MP are recalculated using the new ζ_r^{p+1} and $S_r^{p+1}(k)$ from the river model. Thus the exchange of the information between the river model and the bay model is interactive. A similar procedure is carried out for the interpolation of salinity values from the river model to the bay model.

The finite-difference analogue of the salinity transport equation in the river model, equation (2.90), shows that the horizontal advection scheme has a desirable upstream property. When the river model is joined with the bay model in this study, this scheme implies that at the mouth of the river where $x' = L$, if there is an inflow into the river, the bay model supplies salinity for updating the corresponding quantities in the river. On the other hand, if there is an outflow from the river into the bay, the river model supplies salinity to update the corresponding quantities in the bay.

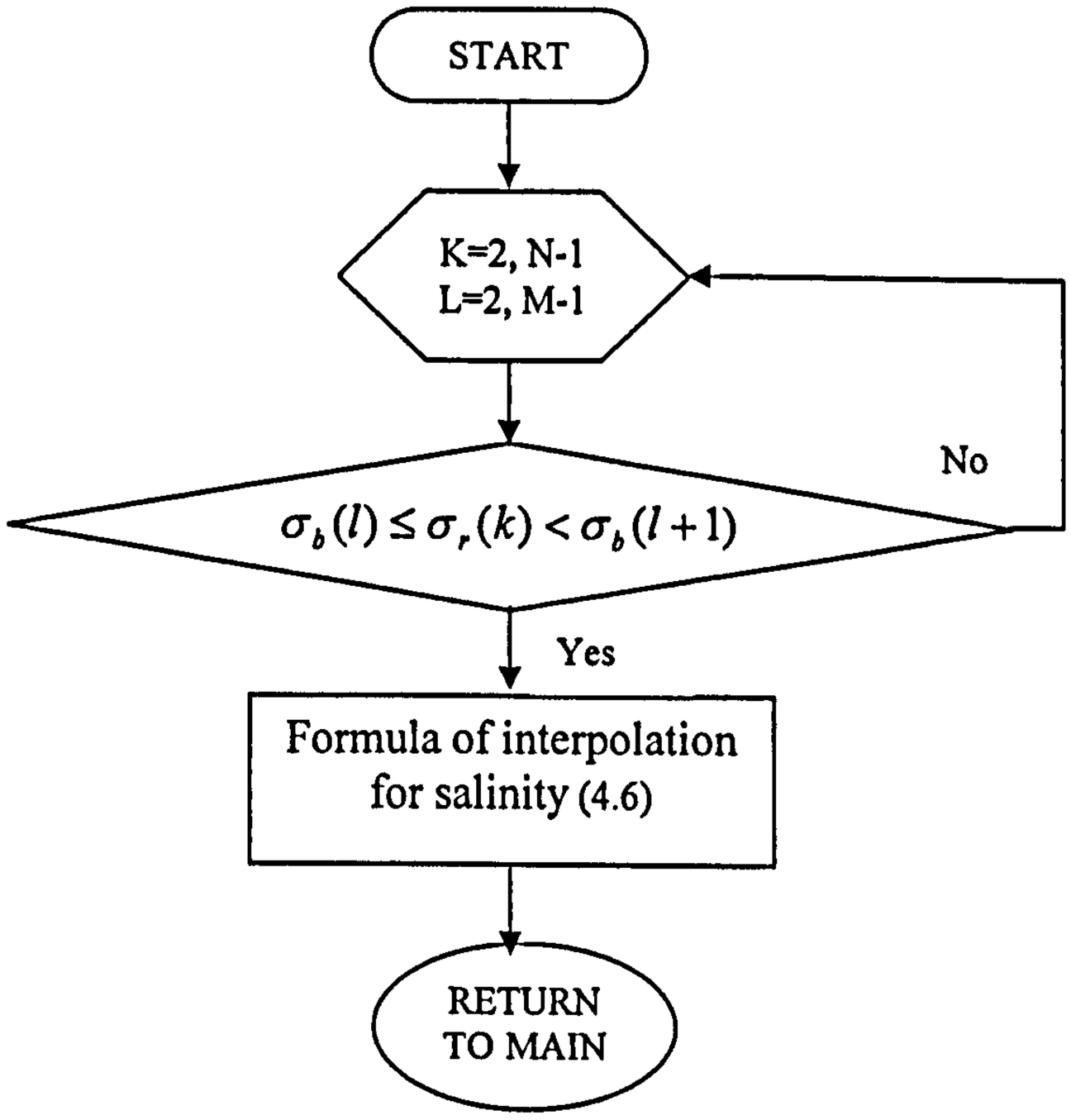

Fig. 4.4 The interpolation procedure of salinity from the bay model to the river model at time level $p+1$

Table 4.1 The vertical discretization of σ_b from the surface ($\sigma_b = 0$) to the seabed ($\sigma_b = -1$) and transferred σ_{rb}.

Level l	σ_b	σ_{rb}
14	0	1
13	-0.02	0.98
12	-0.06	0.94
11	-0.12	0.88
10	-0.19	0.81
9	-0.3	0.70
8	-0.41	0.59
7	-0.52	0.48
6	-0.63	0.37
5	-0.74	0.26
4	-0.84	0.16
3	-0.91	0.09
2	-0.96	0.04
1	-1.0	0

Table 4.2 The vertical discretization of from the surface ($\sigma_r = 1$)to the bottom($\sigma_r = 0$)

Level k	σ_r
21	1
20	0.95
19	0.9
18	0.85
17	0.8
16	0.75
15	0.7
14	0.65
13	0.6
12	0.55
11	0.5
10	0.45
9	0.4
8	0.35
7	0.3
6	0.25
5	0.2
4	0.15
3	0.1
2	0.05
1	0

4.2 Increase the Horizontal Spatial Resolution in the River

In section 4.1, the length of the river used in the computation is 30 km, and there are 21 staggered grid-points in the horizontal dimension. This results in a distance of 3.0 km between successive elevation computational points. The hydrodynamic processes involved in the river usually occur at small scales, and a fine resolution will be required. This is the main motivation for increasing the horizontal spatial resolution in the river.

Furthermore, in order to increase the spatial resolution in the river model, 89 staggered grid points in the horizontal are used in the calculation. So the horizontal distance between successive elevation computational points is reduced. For the river with a length of 30 km, the spatial grid increment is reduced from 3.0 km to 0.68 km. As the requirement of numerical stability, the following CFL condition needs to be satisfied:

$$\Delta t < \frac{\Delta x}{\sqrt{g h_{\max}}} \tag{4.9}$$

In the above Δt is the time step and Δx is the space step, and $h_{\max}$ is the maximum water depth in the computation domain. With the decrease of the space step, the time step also needs to be reduced to satisfy the stability condition.

Different time steps are to be implemented in the river model and the bay model in this section. The integration time step in the bay model is much longer than that needed in the river model. One way to achieve the linkage of the two models with

different time steps is to split the integration process in the river model into several shorter steps during each successive integration in the bay model. Therefore, each model has a time step of its own which should be matched at MP.

At the time level p, the bay model provides updated values for the surface elevation and salinity, ζ_b^p and S_b^p, for the river model at the MP. The integration in the river model from time level p to $p+1$ is performed at several shorter steps, and the number of the steps is denoted by ns. The time step index in the river model, denoted by inr, is expressed as

$$inr = p + \frac{in}{ns}, \qquad in = 1, 2, \ldots n_s, \tag{4.10}$$

The calculation in the river model requires the input of elevation and salinity from the bay model as boundary conditions at each small time step defined above. They are referred to as ζ_r^{inr} and S_r^{inr}.

Care is needed in constructing the derivatives of ζ_r^{inr} and S_r^{inr}, as they can not be derived directly from ζ_b^p and S_b^p by the approach used in section 4.1. The boundary conditions that are needed at each of the small time steps are not provided by the bay model values of ζ_b^p and S_b^p alone. However, as the elevation and salinity at previous time level p-1 are also known, then it is possible to apply the elevation and salinity in the previous two steps p-1, and p to construct the derivatives of ζ_r^{inr} and S_r^{inr}.

If ζ_b and S_b are known at the time levels p-1 and p, stored as ζ_b^{p-1}, S_b^{p-1}, ζ_b^p and S_b^p, then the derivatives of ζ_r^{inr} and S_r^{inr} can be deduced from ζ_b^{p-1}, S_b^{p-1}, ζ_b^p and S_b^p by means of extrapolation.

The extrapolation formula for ζ_r^{inr} is given by

$$\zeta_r^{inr} = \zeta_b^p + (\zeta_b^p - \zeta_b^{p-1})\frac{in}{ns} . \qquad (4.11)$$

Because the elevation is changing with time, the physical level of sigma is changing as well. Therefore the salinity S_b^{p-1} and S_b^p are calculated at different physical z-levels.

Let us use Fig. 4.5 to illustrate the displacement of the location where salinity is computed in the bay model at MP. We shall consider the vertical j and j+1 levels in σ coordinates at time p-1 and p. The computed values of salinity at these levels are denoted by S_j^{p-1}, S_j^p, S_{j+1}^{p-1} and S_{j+1}^p. The physical positions for j and j+1 levels in fixed z coordinates are denoted by, z_j^p, z_{j+1}^{p-1} and z_{j+1}^p. At time p-1 and p the computed elevations at MP are ζ_b^{p-1} and ζ_b^p.

According to (4.2), we have

$$z_j^p = \sigma_j(\zeta_b^p + h) + \zeta_b^p \qquad (4.12).$$

And

$$z_j^{p-1} = \sigma_j(\zeta_b^{p-1} + h) + \zeta_b^{p-1} \qquad (4.13).$$

From (4.12) and (4.13), it is clear that $z_j^{p-1} \neq z_j^p$, because $\zeta_b^{p-1} \neq \zeta_b^p$. In order to predict salinity value at z_j^p for the next time level by means of extrapolation, we need to know the previous value of salinity at z_j^p (i.e. for time p-1).

Assuming the previous salinity is S_q^{p-1} and its σ coordinate is σ_q. The following expression shall be true:

$$z_j^p = z_q = \sigma_q(\zeta_b^{p-1} + h) + \zeta_b^{p-1} \tag{4.14}$$

Therefore

$$\sigma_q = \frac{\sigma_j(\zeta_b^p + h) + \zeta_b^p - \zeta_b^{p-1}}{\zeta_b^{p-1} + h} \tag{4.15}$$

Next step is to find out the location of σ_q at the σ levels, and if

$$\sigma_{j+1} > \sigma_q > \sigma_j,$$

then S_q^{p-1} can be estimated from an interpolation using S_j^{p-1}, S_{j+1}^{p-1}, σ_j, σ_{j+1} and σ_q, the following formulas are used

$$\frac{S_q^{p-1} - S_j^{p-1}}{S_{j+1}^{p-1} - S_j^{p-1}} = \frac{\sigma_q - \sigma_j}{\sigma_{j+1} - \sigma_j} \quad , \tag{4.16}$$

hence

$$S_q^{p-1} = \frac{S_{j+1}^{p-1}(\sigma_q - \sigma_j) + S_j^{p-1}(\sigma_{j+1} - \sigma_q)}{\sigma_{j+1} - \sigma_j} \tag{4.17}$$

As the calculation proceeds in time, S_q^{p-1} is replaced by S_j^p at z_j^p, so we can predict the value of salinity at next time step, p+1, by using S_q^{p-1} and S_j^p.

The surface and bottom boundary conditions are:

At the surface

$$S_q^{p-1} = S_1^{p-1} \tag{4.18}$$

at the bottom

$$S_q^{p-1} = S_n^{p-1} \tag{4.19}$$

When S_q^{p-1} is known, the salinity at z_j^p for time level *inr* of the river model, S_b^{inr}, can be calculated by extrapolation using an expression similar to (4.11):

$$S_b^{inr} = S_b^p + (S_b^p - S_q^{p-1}) \frac{in}{ns} \tag{4.20}$$

Here the salinity S_b^{inr} refers to the value at the MP and are input to river model as a boundary condition at $x \leftarrow L$. It should be an array of n elements to prescribe the value at each σ level in the bay model. When calculation is proceeded in the river model, these values need to be transferred according to the σ coordinate of the river model. The method used is similar to that in section 4.1.

After the calculation in the river model has been processed from p to $p+1$, the values of the surface elevation and salinity at the mouth of the river are recalculated by the river model and used to update the variables in the bay model at the MP.

4.3 Problem of Non-linear Instability in Joined Model

In section 4.1, the length of the time step for the bay model is taken to be the same as that of the river model, namely 200 sec. When the horizontal space resolution of the river model is increased in section 4.2, the total number of grid-point increases from 21 to 89, which is approximately four times as many as the total number in the case of low resolution as in section 4.1. During each integration in the bay model, the integration in the river model is subdivided into several smaller time steps, and initially five steps are chosen. Therefore, if the time step used in the bay model is 200

seconds, the time step in the river model will be 40 seconds. But running the joined model with these values generates an exception, due to the floating-point overflow in the river model, and results in the termination of the programme.

In order to overcome this problem, the joined model was run several times using different time steps in the river model. It has been found that the stability of calculation is achieved after the integration in the river model is subdivided into 20 time steps of shorter integration, which means the time step in the river model is reduced to 10 seconds.

The reason for this instability may be the input of short wave components from the bay model into the river model, which leads to a rapid spatial variation that can not be resolved if the time-step is too long. In the single river model, the surface elevation is prescribed to represent the form of tidal amplitude as a simple sinusoidal oscillation on the open boundary. In the joined model, it is updated by the real time elevation that is provided by the bay model.

This chapter describes an interactive grid-splicing scheme capable of exchanging information between two models with different sigma coordinate systems along the vertical common boundary. In order to achieve the interaction, the variables that are calculated at the same sigma level, but different physical levels, are converted into variables at the same physical levels, so that the time extrapolation can be carried out. In the joining of the higher resolution in the river model, the integration is divided into smaller time steps, which reduces the horizontal resolution of the river model. The next chapter presents the application of this joining technique to link together the

2D single river model with a 3D shelf sea model to study the interaction of the tidal flow between Liverpool Bay and the Mersey Estuary.

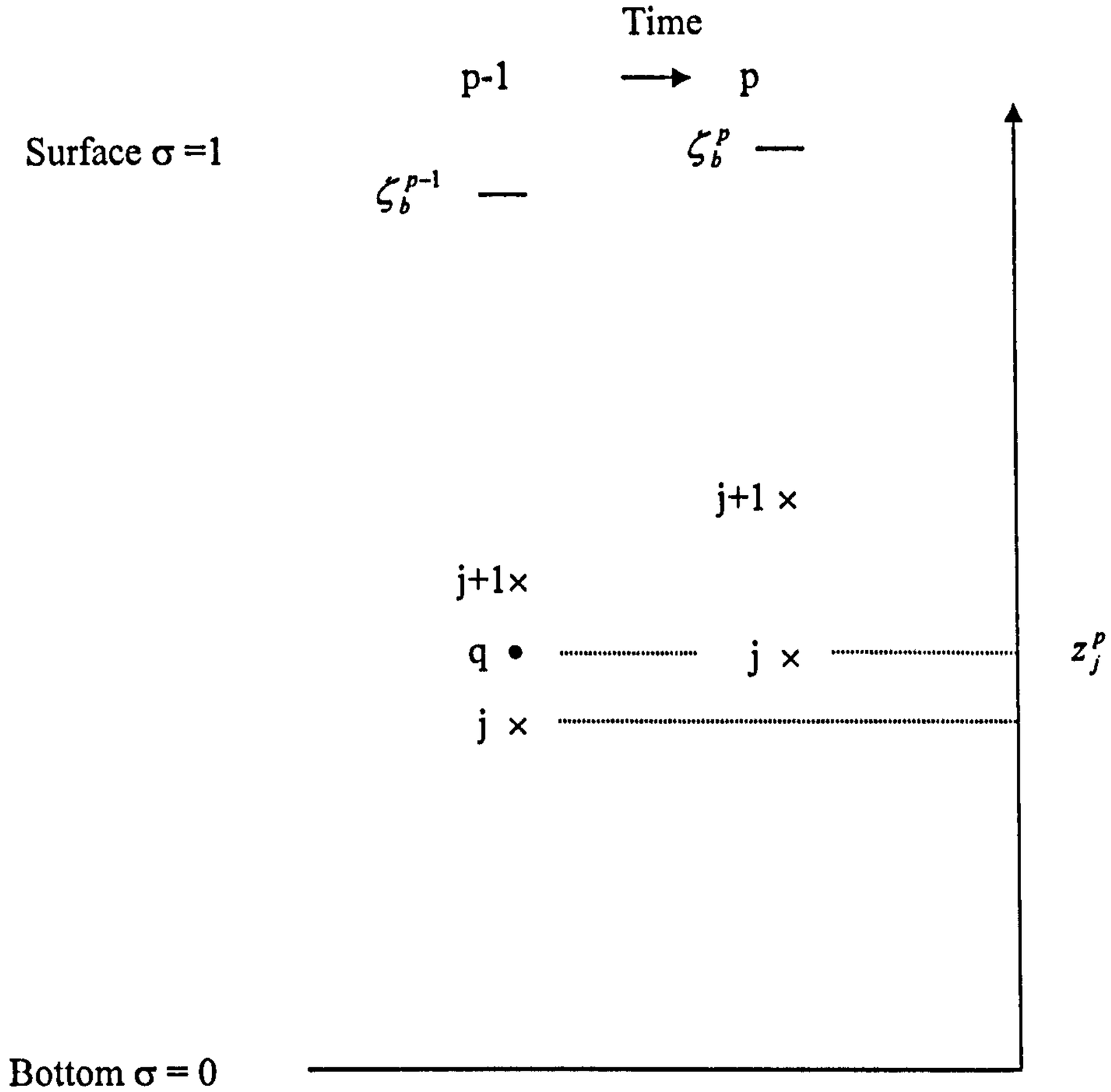

Fig. 4.5 The displacement of vertical levels in time process

Chapter 5 Application of the Joined Model to Liverpool Bay and the Mersey Estuary

In this chapter, the joined model described in chapter 4 is used to investigate the tidal flow interaction between Liverpool bay and the Mersey estuary.

An estuary is a partly enclosed coastal body of water. It has a free connection with the open sea but its salty sea water is diluted with freshwater from inland rivers. The estuary is usually divisible into three sectors: (i) a marine or lower estuary, in free connection with the open sea; (ii) a middle estuary, subject to strong salt and freshwater mixing; and (iii) an upper estuary, characterized by freshwater but subject to tidal action. (Fairbridge, 1980).

In the regions of estuary and its adjacent open shallow sea, the freshwater is discharged into a region of more saline and dense sea water. The features of the dynamic structure of the estuary are strongly influenced by the tidal features involved. The main features are:

1) Salt wedge estuaries develop in virtually tideless seas and where the sediment discharge is low.

2) Partially mixed estuaries develop where there is a moderate tidal range.

3) Well mixed estuaries develop where the tidal range is high.

The area of interest in this study, namely, the Mersey estuary and Liverpool bay are dominated by the tidal currents and during the spring-neap tidal cycle the ranges at the

mouth vary from 4 to 10 m. The Mersey is a macrotidal estuary and usually in well-mixed conditions.

5.1 Implementation

In the river model, the parameters are chosen to represent the Mersey estuary. The estuary is described as four main sections (Fig. 5.1.1). An important feature is that the river at the seaward end is deeper and narrower than the remaining section. The

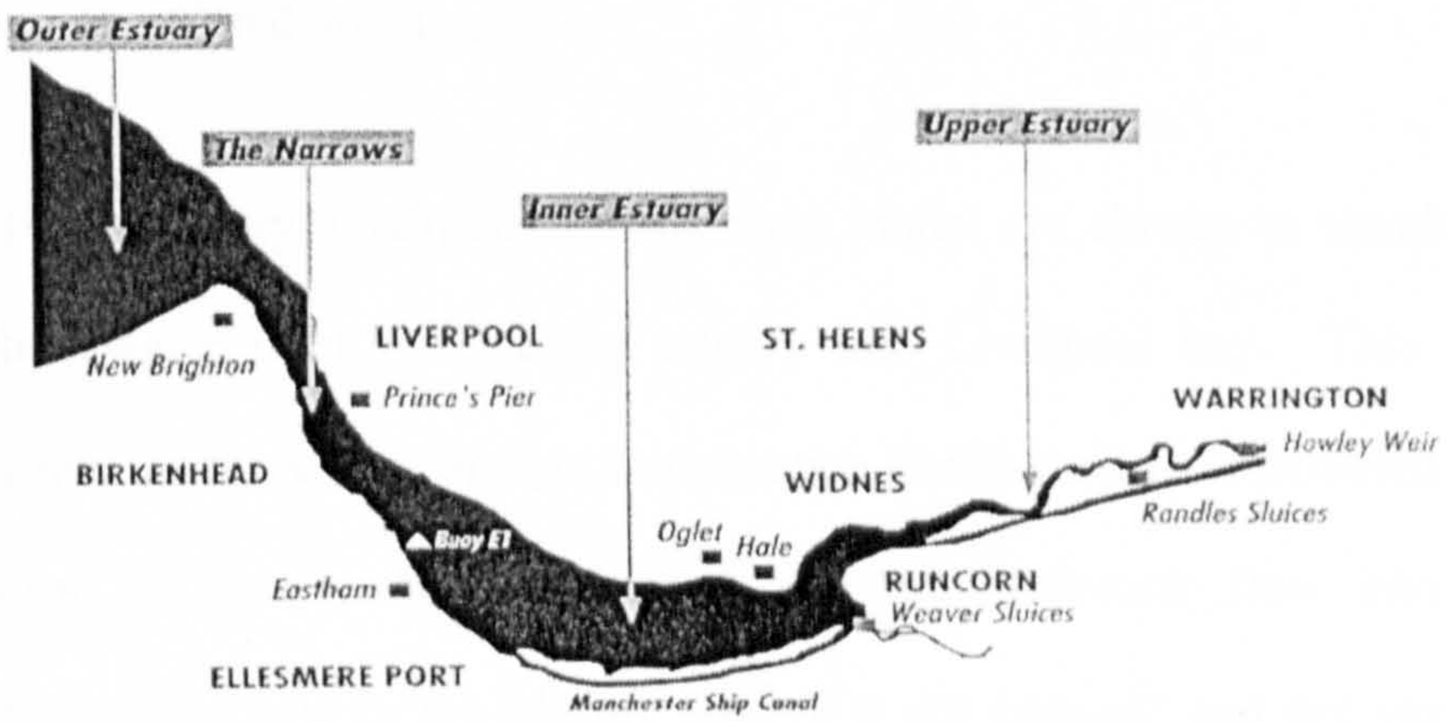

Fig. 5.1.1 The Mersey estuary

narrow mouth results in high velocity tidal currents, giving the estuary a strong tidal scour and high suspended particulate matter. In the upper estuary the river becomes a meandering channel from Runcorn. In this work, the Mersey is modelled as a rectangular domain, where the origin of the axis is located at landward end of the inner estuary. The Ox axis is directed towards the seaward end along the main channel of the river, the Oz axis is directed vertically upwards. The computation section starts at Weston near Runcorn and ends at New Brighton. The length of the calculation domain is 30 km with 89 finite grid points along the domain in the horizontal, and 21 computational levels through the depth in the vertical. The implied distance between

computational elevation points (or current points) is about 0.68 km. The bottom topography of the Mersey Estuary is unusually irregular, and it is difficult to determine the depth at discrete grid points. The depth and breadth data cross main channel are taken from the Chart of River Mersey surveyed by the Mersey Docks and Harbour Company and HR Wallingford Ltd (1997). The depth varies from approximate 19.0m at the deepest section near the mouth to around 2.2m at the landward end. The breadth varies between 825 m and 4875 m along the computational domain.

The boundary conditions for the river model are chosen to simulate a discharge of freshwater from the Mersey estuary into Liverpool bay. This is carried out by adjusting the values of u_0 in the equation (2.62) until the calculated mean value at the head of river yields the desired input of freshwater flow into the bay. As the freshwater flow in the Mersey estuary is not constant and can vary from 10 m^3/s to 600 m^3/s. To test the sensitivity with respect to the freshwater discharge rate a wide range of values between 300 m^3/s and 1000 m^3/s is used. The salinity of the oceanic water into which the freshwater is discharged is set at 35 ppt. The salinity at the landward end of the river during the freshwater inflow is set at 5 ppt.

Sediment concentration at both ends of the river channel are set initially to zero, this implies that the sediment concentration flux in the river will solely be result of the concentration pickup across the bed of the channel by the dynamic processes related to the freshwater and tidal current.

The point of communication between the Mersey and Liverpool bay corresponds to (53° 26″N, 3° 01″W) where the breadth of Mersey is 1.6 km.

In the bay model, the calculation domain is chosen to represent the region of the eastern Irish Sea (Fig. 5.1.2 and Fig. 5.1.3). The western boundary of the modelling domain is open at a location about 4°30″ W. The real time tidal forcing due to M_2 tidal component is used to produce tidal currents in the modelling domain. All other boundaries are closed to represent the coast of East Irish sea. The horizontal resolution is approximately 1.0× 0.9 km. In the vertical there are 14 σ levels used. The integration proceeds with a time step of 200s for the depth-dependent variables (internal model) and 10s for the depth-mean flow (external model) in the bay model.

The bay model is driven by tidal current and the real time tidal forcing due to the M_2 tidal component imposed at the western boundary of the domain.

In the following part of this chapter, a series of calculations are performed to examine the joined model's ability to simulate the interaction between local and offshore processes.

Figure 5.1.2 Model area for the eastern Irish Sea. Depths in metres.

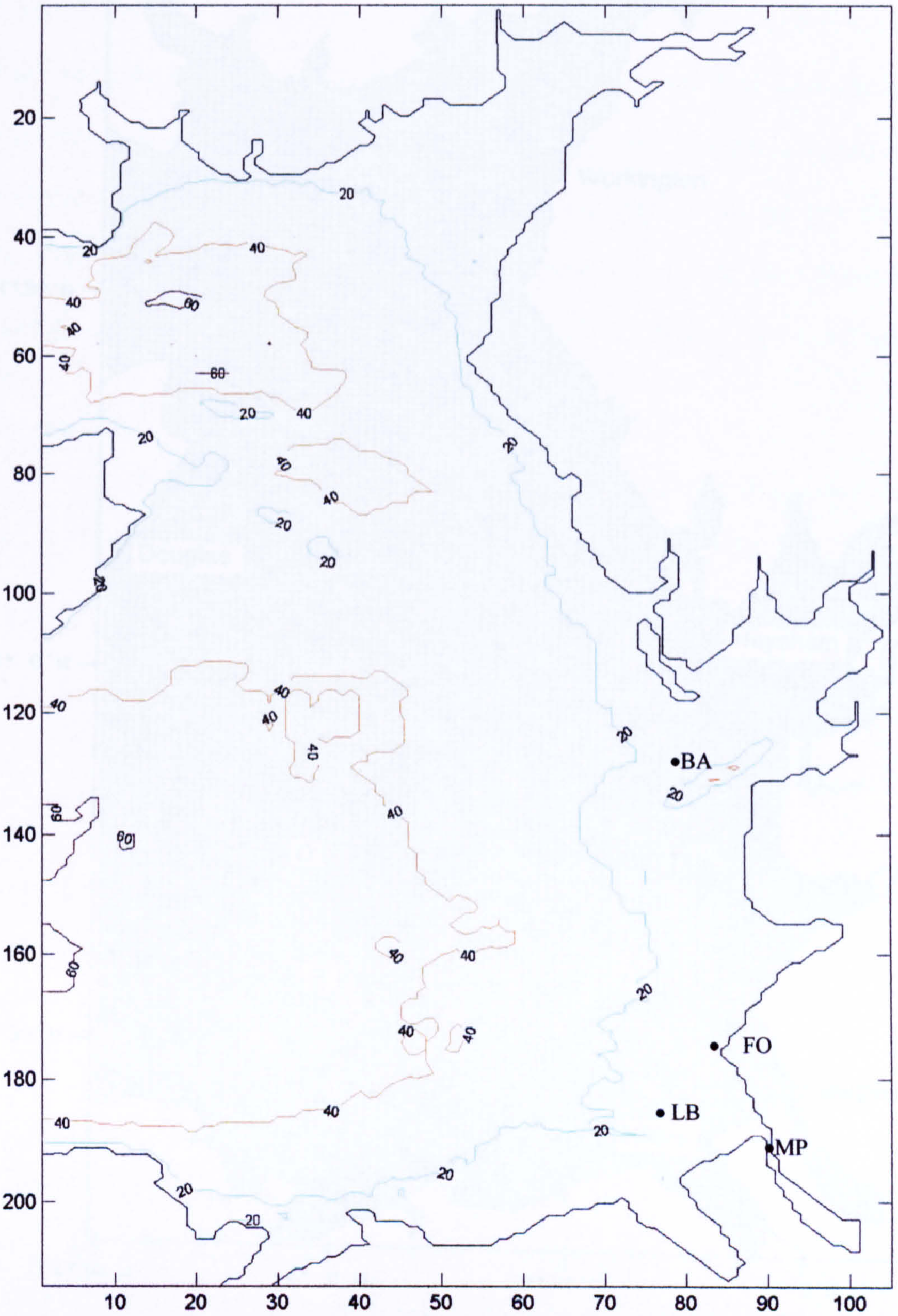

Fig. 5.1.3 Finite-difference grid of the bay model for eastern Irish Sea

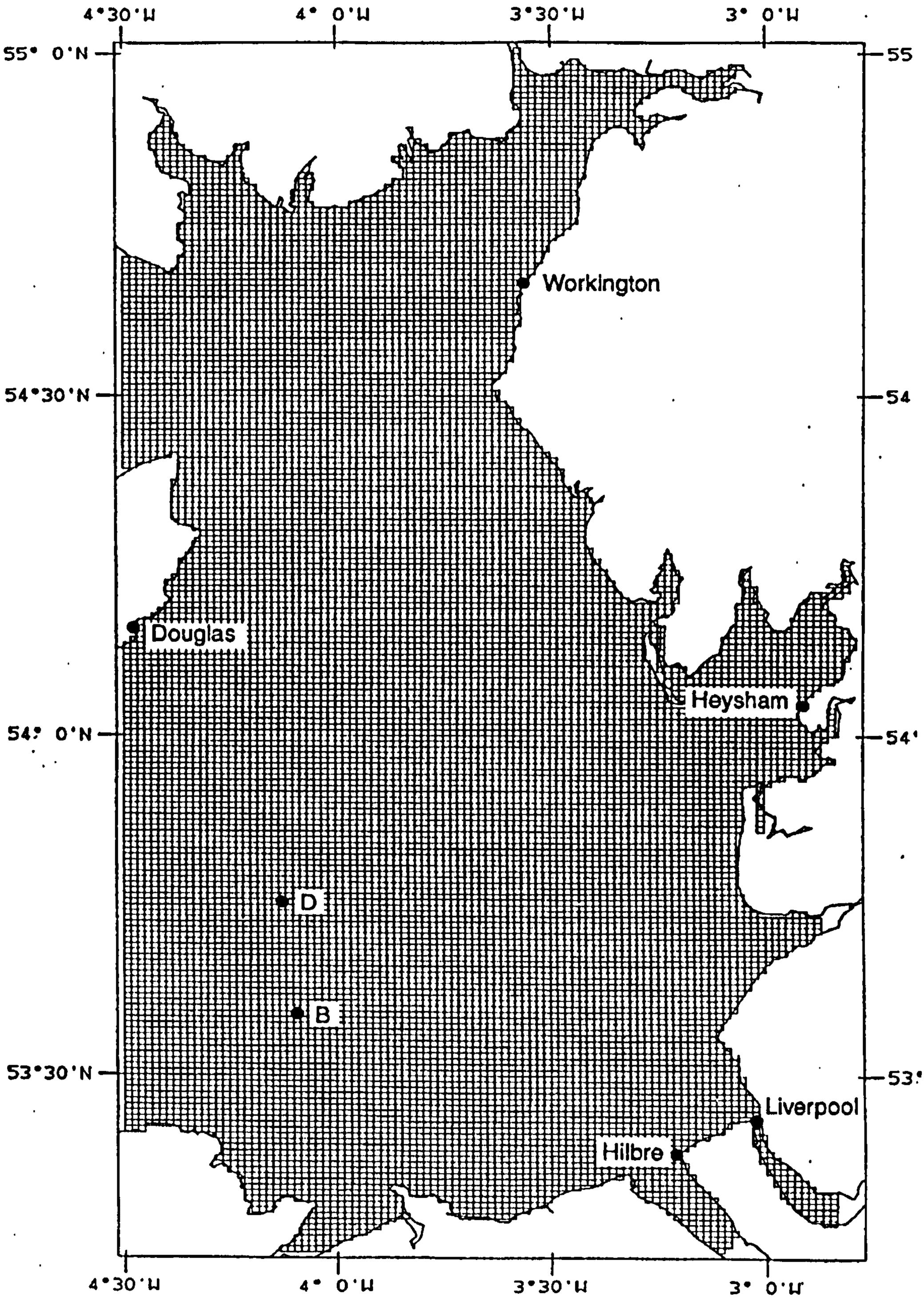

5.2 Test of Joined Model

The initial calculations are performed with the joined model to test the model's ability to predict the M_2 tidal elevations and currents. Calculations start from an initial state of zero elevation and motion and tidal component M_2 is input at the open boundary. At this stage, the results are analysed during the fourth tidal cycle. Four places located in the model domain including Formby(FO), Liverpool Bay (LB), Barrow (BA) and Liverpool (MP) where the river model is linked with bay model are selected to analyse the tidal elevations and currents. The observations of M_2 tidal elevations are available at these locations which are shown on Fig. 5.1.2 (Aldridge and Davies 1993).

Fig. 5.2.1 and Fig. 5.2.2 show the computed time series of M_2 tidal elevations at MP and LB. The time series for M_2 tidal currents are presented in Fig. 5.2.3.

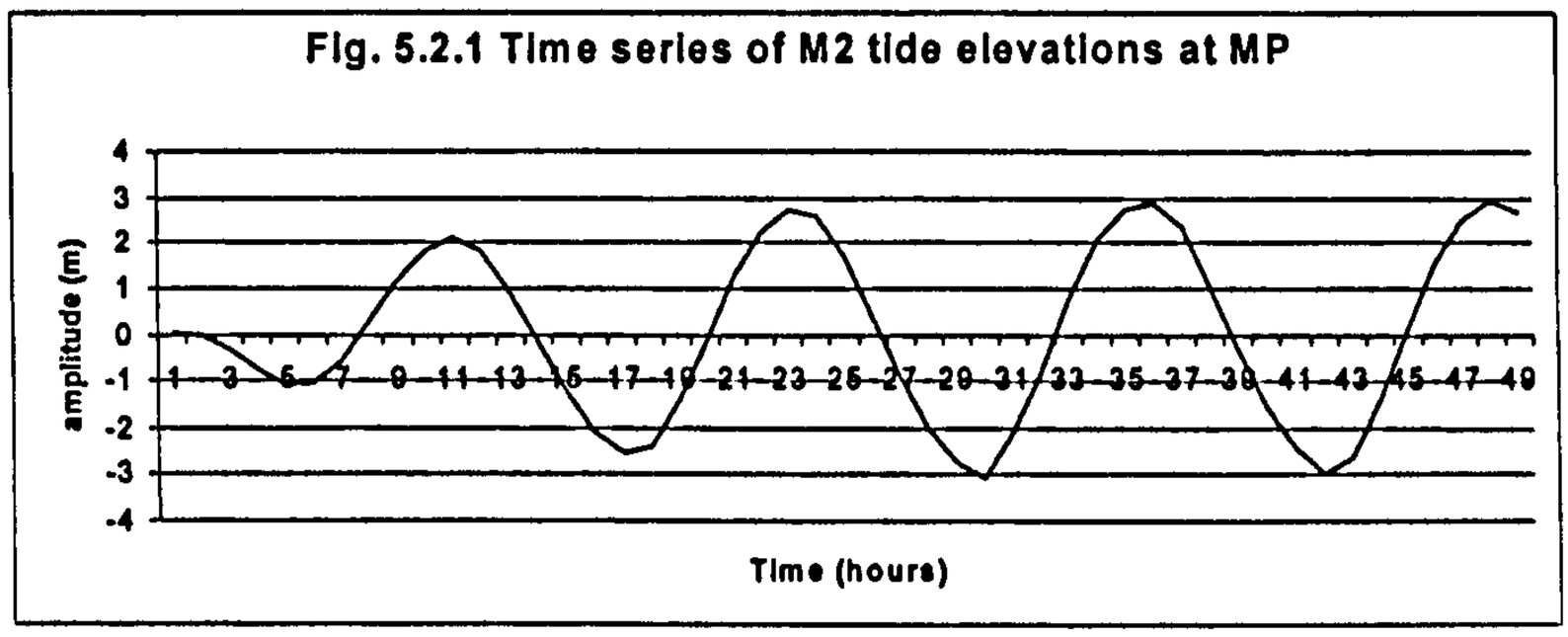

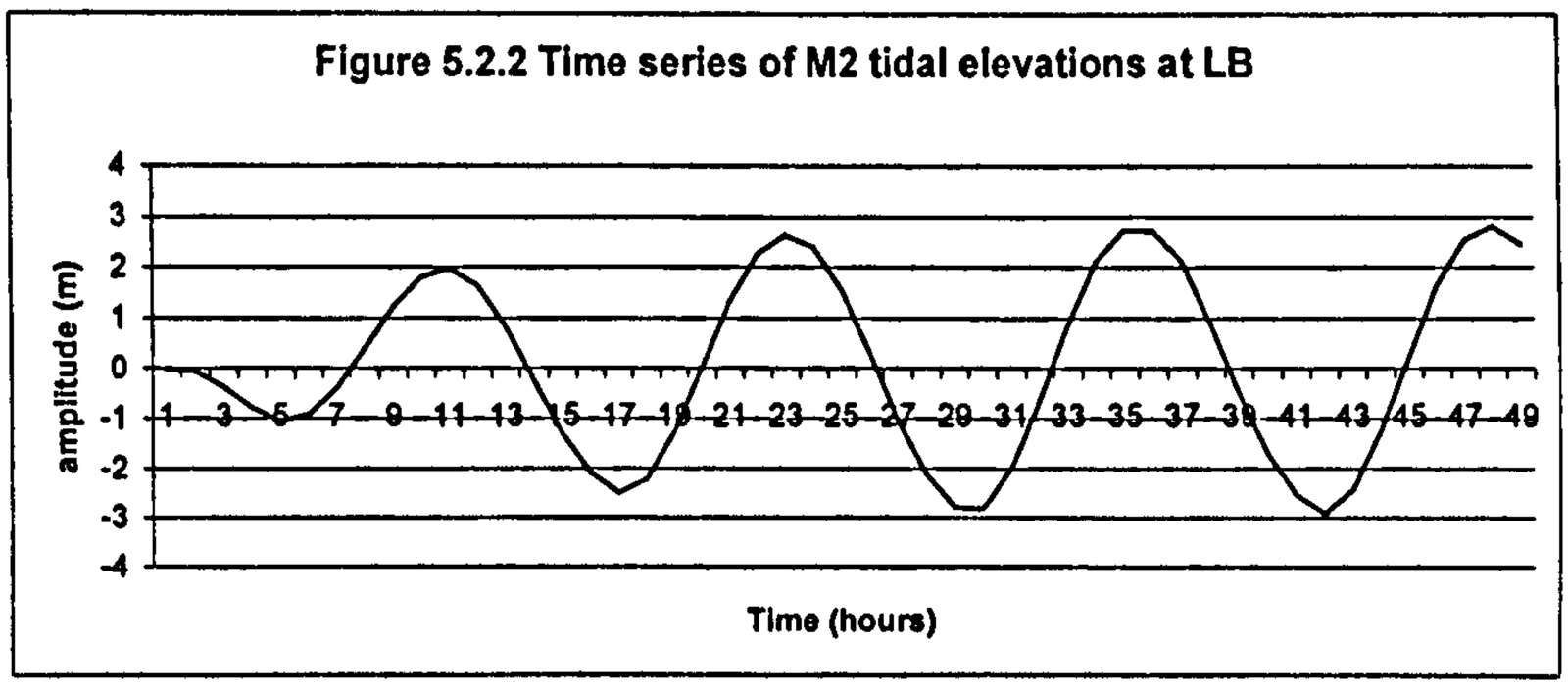

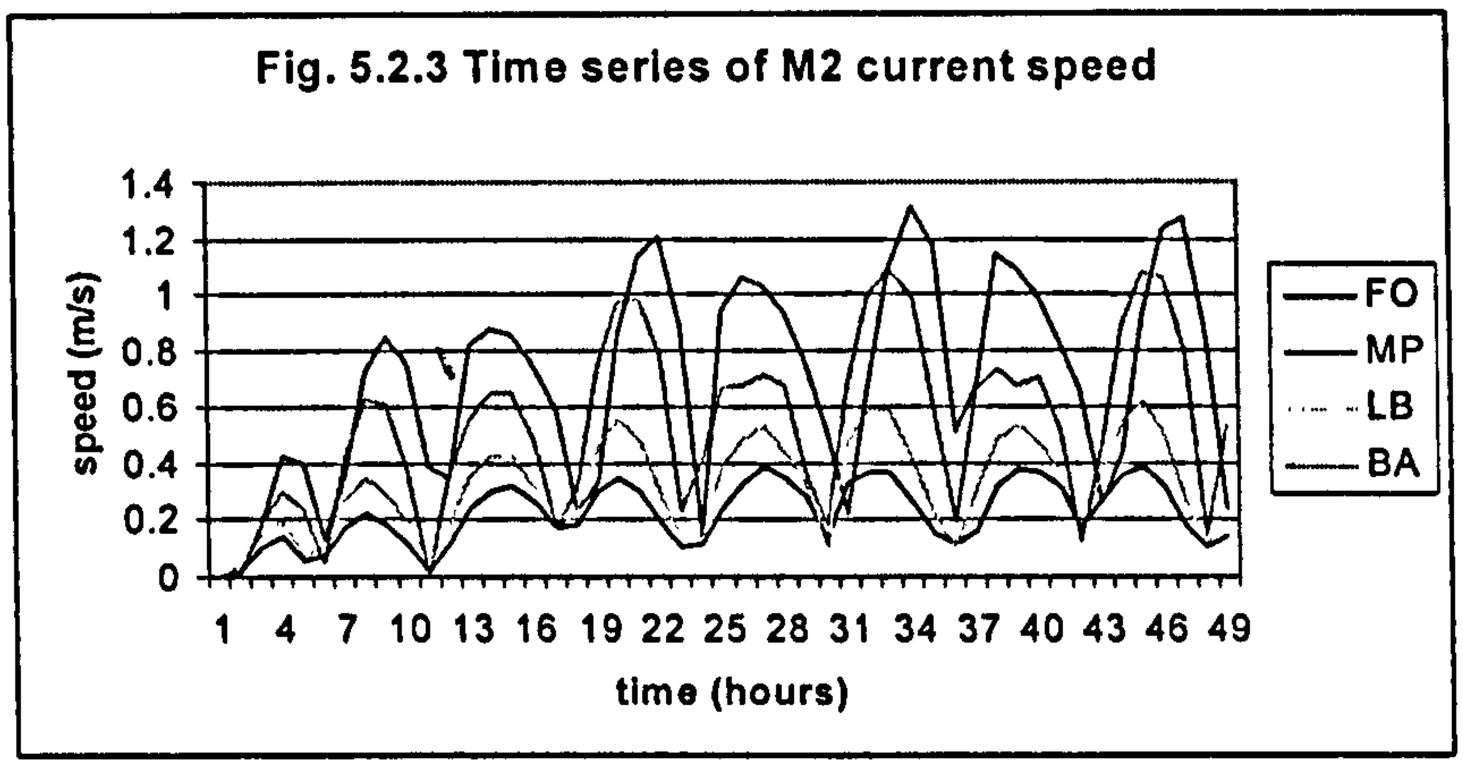

From the time series plots for elevations, we can see that elevations at both MP and LB present a semi-diurnal harmonic. The tidal range is 6.0 m at MP and 5.7 m at LB.

Table 5.2.1 Comparison of computed M_2 tidal amplitude (m) against observations (Aldridge and Davies 1993)

	MP	*LB*	*FO*	*BA*
Computation	2.93	2.81	2.89	3.02
Observation	3.08	2.62	3.13	2.97

From the above table, it is noted that the overall fit with the observations is good. The joined model is able to reproduce the main features of M_2 tidal elevations and currents.

Apart from this test of the joined model for M_2 tidal features, another test has been made to deal with the significance of differences between the joined model and the bay model. The test is based on time series of differences between results of these two models. Hourly values of three parameters at four positions (MP, LB, FO, BA in Figure 5.1.2) in the bay area have been computed by both models. Here, a global estimator is used (J.Ozer *et al.* 2000):

$$G(x) = 100 \frac{\sqrt{\frac{1}{n}\sum_{k=1}^{n}(x_j(k) - x_b(k))^2}}{\sqrt{\frac{1}{n}\sum_{k=1}^{n}x_b^2(k)}} \quad , \tag{5.1}$$

where x is a model parameter, n is the number of values in the time series, $x_j(k)$ and $x_b(k)$ are the values of x at time t_k in the joined model and the bay model, respectively.

Table 5.2.2 The global estimator G for the differences between the joined model and the bay model at four positions over the period of 10 days integration.

	MP	LB	FO	BA
Current	18.92	32.52	4.78	22.2
Elevation	10.84	5.41	3.36	2.82

From Table 5.2.2, we note that the joined model has introduced a change from 5% to 33% in current speeds, and a change from 3% to 11% in surface elevations. Therefore, the result of the joined model is different from that of the bay model.

5.3 Numerical Experiments

5.3.1 Introduction

In the following sections, a series of numerical experiments is performed to assess the ability of the joined model to produce various features of tidal flow interaction between the bay model and the river model.

The following cases are considered in the calculation:

(1) Single river model without joining with bay model.

(2) Bay model without joining with river model.

(3) Joined model with the bay model is driven by tidal forcing and freshwater is discharged from the river.

(4) Joined model with the tidal forcing is absent from the bay model and freshwater is discharged from the river.

The results from above cases then are analysed and compared.

In case (1), the river model is run without being linked to bay model. At the mouth of the river, a current of 1.5 m/s is used to characterise the river Mersey. The current speed at the head of the river, u_0, is chosen so that a desired freshwater discharge rate can be obtained. It is found that u_0 has to be set to a value between 0.2 m/s and 0.35 m/s to support the discharge rate between 300 m^3/s to 1000 m^3/s.

5.3.2 Comparison of Results in the Mersey Estuary

In this section, the flow fields in the Mersey is analysed both with and without the input of tidal elevation from the bay model. All the results correspond to 10 days of integration from a state of rest at $t = 0$. In the subsequent comparative descriptions, panel (a) represents the case of single river model without joining with bay model, and panel (b) represents that of the joined model. Both panels are applied for the freshwater discharge rate of 300 m^3/s.

The computed salinity distribution in the channel is shown in Fig. 5.3.1(a, b). It is clear from Fig. 5.3.1(a) that a strong horizontal salinity gradient exists in the channel and there is salinity transportation from the seaward end. There is very little variation of salinity with depth, and it became uniform on the bottom of the channel. It also

shows that the salinity is vertically mixed up by the tidal current. Fig. 5.3.1(b) shows the tidal forcing from the bay model has led to a well mixed structure in the vertical and there is no variation at all with the depth.

The computed streamlines of instantaneous volume transport in the river channel are shown in Fig. 5.3.2(a, b). The different colours refer to the numbers representing transport rates in m^3s^{-1}. In Fig. 5.3.2(a), there is an inflow from the seaward end into the river. This flow dominates the most part of the channel and turns around at about 8-12km from the head of the river, where the depth is less than 10m. At the head of the river where there is an inflow into the channel, the streamlines direct towards the surface as it entering the channel. In Fig. 5.3.2 (b), however, the whole river channel is dominated by a seaward outflow, indicating the existence of an ebb tide.

In Fig. 5.3.3(a, b), we show the associated velocity profiles at a sequence of positions along the channel. In Fig. 5.3.3(a), the velocity profile is directed towards the seaward end of the river and it becomes weaker along the channel. It is clear that the seaward flow effectively controls the channel as far as about 8 km from the head of the river. From here to about 13 km away from the head, the profile reverses at mid depth. This corresponds to the location where the streamlines are turning back in Fig. 5.3.2(a). The remaining part of the river which covers the channel beyond 13 km is controlled by the inflow from the open sea. Comparison with Fig. 5.3.3(a), Fig. 5.3.3(b) shows the velocity profile towards the seaward end over the whole of the channel with no reversal. The maximum computed velocity is about 1.5 m/s at the surface, while in Fig. (a) it is about 0.5m/s.

Sediment transport and deposition are affected where the tidal current dominates the dynamic processes. The distribution of sediment concentration over the river channel is presented in Fig. 5.3.4(a, b). It appears that after 10 days of integration there is a net pick up of sediment concentration from the bed of the channel. In Fig. 5.3.4(a), there is a maximum concentration of 117mg/litre near the shallow landward end. The concentration in the deeper section close to the mouth of the river is much lower and less than 20 mg/litre. In Fig. 5.3.4(b), however, the maximum concentration is over 2800 mg/litre and it appears at the deeper part of channel near the mouth of the river. It is clear that the strong influence of tidal flow from Liverpool bay has led to a significant sediment transport within the Mersey.

Fig 5.3.5(a, b) are the plots of mean flux of sediment concentration settling at the bed of the river. From this we can see that the downward sediment concentration flux is negative at the landward end indicating net pick up in this region. This is transported towards the seaward end of the river. The concentration is settling down to the bed while it is transported.

From above discussion, we can note that the tidal range in this region is high and the tidal flow is strong relative to the river flow, the water column becomes completely mixed. The tidal movements in the estuary caused by predicted M_2 tide in Liverpool bay using the bay model are large. They give rise to the well mixing of the fresh and saline water in the vertical. The M_2 tide plays an important role in the transport of suspended sediment concentration in the river flow.

5.3.3 Comparison of Results in Liverpool Bay

The computational tidal elevations and currents, as well as salinity contours after 10 days of integration of the joined model are used to describe the processes in Liverpool bay. This shows the influence of the river flow upon the shelf sea as feedback of tidal current.

Shown in Fig 5.3.6(a, b) are computed M_2 tidal currents using (a) bay model alone and (b) joined model with freshwater of 300 m^3/s discharged from the Mersey. By comparing (a) and (b) it is possible to evaluate the influence of freshwater from the Mersey on the current field in Liverpool bay. This is seen as an enhancement of the surface current at the 10 to 15 km west of the mouth of the river. Table 5.3.1 gives the surface currents at selected positions at the west-east cross- shelf zone off the river mouth. Here, positions are selected at 1.0 km interval of distance from the MP. It can be noted that the current speeds predicted by the joined model are slightly higher than that by the bay model at a location within 3 km from the mouth of the river. The currents calculated by bay model become stronger than that of the joined model from 3km to 9 km with maximum difference of 0.137 m/s at about 4 km. From about 10 to 15 km, there is a region where the joined model predicts stronger currents and at 13 km from the mouth of river the highest current difference between the joined model and the bay model is found to be 0.2 m/s. Fig. 5.3.6(c) is the plot of currents similar to Fig. 5.3.6(b), but with freshwater discharge from the Mersey set at 1000 m^3/s. The enhancement of surface currents in the above region becomes stronger.

Table 5.3.1 Surface currents at selected position. (m/s)

Distance from MP (km)	Results of bay model	Results of joined model	Difference between the two models
2	0.87	0.91	0.04
3	1.12	1.14	0.02
4	0.40	0.34	-0.06
5	0.83	0.69	-0.14
6	0.71	0.57	-0.13
7	0.64	0.53	-0.11
8	0.52	0.45	-0.07
9	0.51	0.43	-0.08
10	0.50	0.49	-0.01
11	0.51	0.65	0.14
12	0.53	0.72	0.19
13	0.53	0.72	0.19
14	0.50	0.70	0.20
15	0.51	0.60	0.09

It is noted that in most parts of the region there is a small variation of the current fields between both models. This implies that the computational region is dynamically dominated by tidal currents and the influence of the river flow is outweighed by the tidal flow.

Fig 5.3.7(a, b, c) show the contours of salinity at the surface, middle and bottom of the region of Liverpool bay when the freshwater discharge rate is 300 m^3/sec. The distribution of the salinity presents a character of bulge in the region around the mouth of the Mersey estuary, indicating a dispersion of freshwater from the Mersey into Liverpool bay. The low saline flow plume spreads out towards the coastal sides of the estuary with the contours of 34 and 33 ppt extending northward along the coastline. Although the region of the bulge is slightly reduced from the surface to the bottom, there is a very small difference of salinity variation with depth. This is consistent with the result in the river (see section 5.3.1).

We also run the joined model with higher freshwater discharge(1000m^3/s) with the rest of the parameters remaining the same as previous runs.

Contours of salinity in Fig 5.3.8(a, b, c) show a similar structure to Fig 5.3.7, but the value of the contour is lower. The 30 ppt contour extended to the region where the value is between 32 to 34 ppt in low freshwater case.

5.3.4 Results of Numerical Experiment without Tidal Forcing

From the discussion above we note that with the M_2 tide as the driving force of the model, the salinity distribution in Liverpool bay and the Mersey estuary is vertically well mixed. It implies the importance of tidal currents in the mixing of salt and freshwater. In a subsequent calculation, the joined model was run without including the tidal forcing across the open boundary of the bay model and the freshwater discharge from the river model was set to 1000 m^3/sec. As stated previously the amount of freshwater discharge was given by the adjustment of u_0 in the river model. This value was chosen to be 0.85 m/sec to support 1000 m^3/sec of freshwater

discharge when tidal forcing is involved in the model. When the tidal forcing is absent, such a high value for u_0 is not required and it can be reduced to 0.18 m/s.

In the absence of tide, the contours of salinity after 10 days of integration (Fig 5.3.9(a)-(c)) show that the freshwater distributes as a plume spreading on the surface layer away from the discharge point. From the surface to the sea bed, the area that is covered by the 34 ppt contour is diminished rapidly towards the Mersey estuary. The plume extends northwards as far as approximately 40 km from the Mersey estuary. The spreading of the plume in the east-west direction remains the same as was in Fig 5.3.8. It implies that the low salinity plume tends to spread to the right as a result of the Coriolis effect and is confined by the coastline.

The results in the Mersey when there is no tidal current included as a driving force are also presented here (see Fig 5.3.10). A consequence of the absence of the tide in the river shows the existence of a strong vertical gradient of isohalines. The salinity of the bottom water near mouth of the Mersey is of the order of 40 ppt and the salinity of the surface water is reduced below 24 ppt.

A feature of dynamics in the river can be noted from the associated streamlines of volume transport (Fig. 5.3.11) and corresponding velocity profiles (Fig 5.3.12) and presents a three-layer structure of flow. The surface seaward flow has a velocity of order 0.5 m/sec while the bottom seaward flow is very weak and extends 13 km from the open sea. In the middle layer across the whole computational channel of Mersey, there is an inflow from Liverpool bay into the river.

The comparison shows that the dispersion of freshwater discharge from the Mersey into Liverpool bay is held back and mixed vertically by the tidal current. The existence of tidal currents in Liverpool bay has a dominant effect on the local coastal dynamics.

The contours of salinity in Fig. 5.3.10 show a maximum salinity of 46.9 ppt near the bottom of the river at the seaward end. This implies a transport of salinity from Liverpool bay into the Mersey in the case considered here. In theory, if the model is initialized with no forcing, zero velocity and horizontal isopycnals, there should be no velocity developed in the integration. However, we noted that in our study here, the model has produced non-zero velocities in Liverpool bay when there is no forcing involved. This might be related to an error caused by the use of sigma coordinates. A disadvantage of using sigma coordinates is that there exists a numerical, baroclinic pressure gradient error (Mellor *et al.* 1998). The pressure gradient force in the sigma coordinate model consists of two terms, one term involves the pressure gradient along the σ- surface, the other involves the pressure gradient due to bottom topography. These terms can be large on the steep topography, comparable in magnitude and opposite in sign. In this case a small truncation error can result in a large error in the pressure gradient force (Mellor *et al.* 1994; Haney 1991). Fig 5.3.13(a,b) shows a time series of surface and seabed current speed at location MP in the bay model. The seabed velocity at this location has a peak value of 0.3 m/sec with a mean value of 0.15 m/sec. The maximum surface velocity reaches as high as 0.43 m/sec with mean value of 0.31m/sec. From these results we can identify that there are velocity errors caused by sigma coordinate error and they may give rise to a salinity transport from the bay model into the river model.

5.3.5 Sediment Transport from the Mersey Estuary into Liverpool Bay

One of the important features of the river model is that it includes the process of sediment transport. The movement of sediments occur when the force that water current exerts on the sediment is sufficiently large to overcome the gravity force acting on the sediment particles and the friction between the particles and underlying bed. The river model can calculate the flux of the sediment concentration across the bed of the estuary. When the sediments are picked up by the motion of the flow, they are transported with the flow in a form of suspended particles and may settle down to the bed during the movement or they may be transported out to the sea with the outflow. In the calculation here, the mean flux of sediment concentration across the seaward end of channel in the last day of integration is estimated. This indicates the amount of sediment concentration that may be transported out of the Mersey estuary and into Liverpool bay. The results show that when the joined model is run with M_2 tidal forcing along the western open boundary of bay model and with a freshwater discharge from the estuary into the bay of 300 m^3/sec, the total mean flux of sediment into Liverpool bay from Mersey is 9.846 kg/sec. When the freshwater discharge is increased to 1000 m^3/sec, the total mean flux of sediment is increased to 12.282 kg/sec. We also calculated the sediment flux when the tidal forcing is absent, and the corresponding sediment flux out of Liverpool bay is nearly reduced to zero. Obviously, the influence of tidal current on the sediment transport in the Mersey estuary and Liverpool bay is significant.

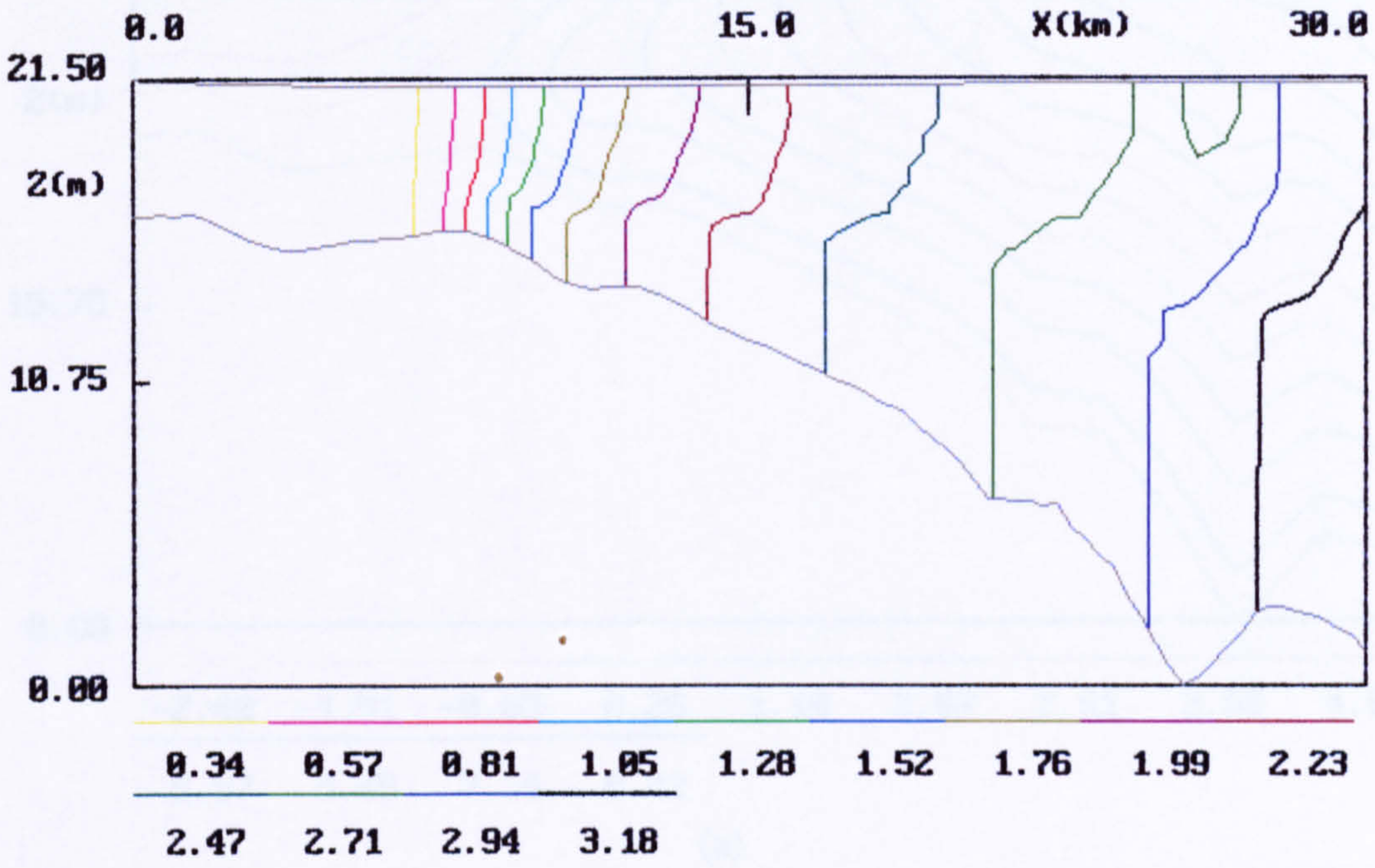

(a)

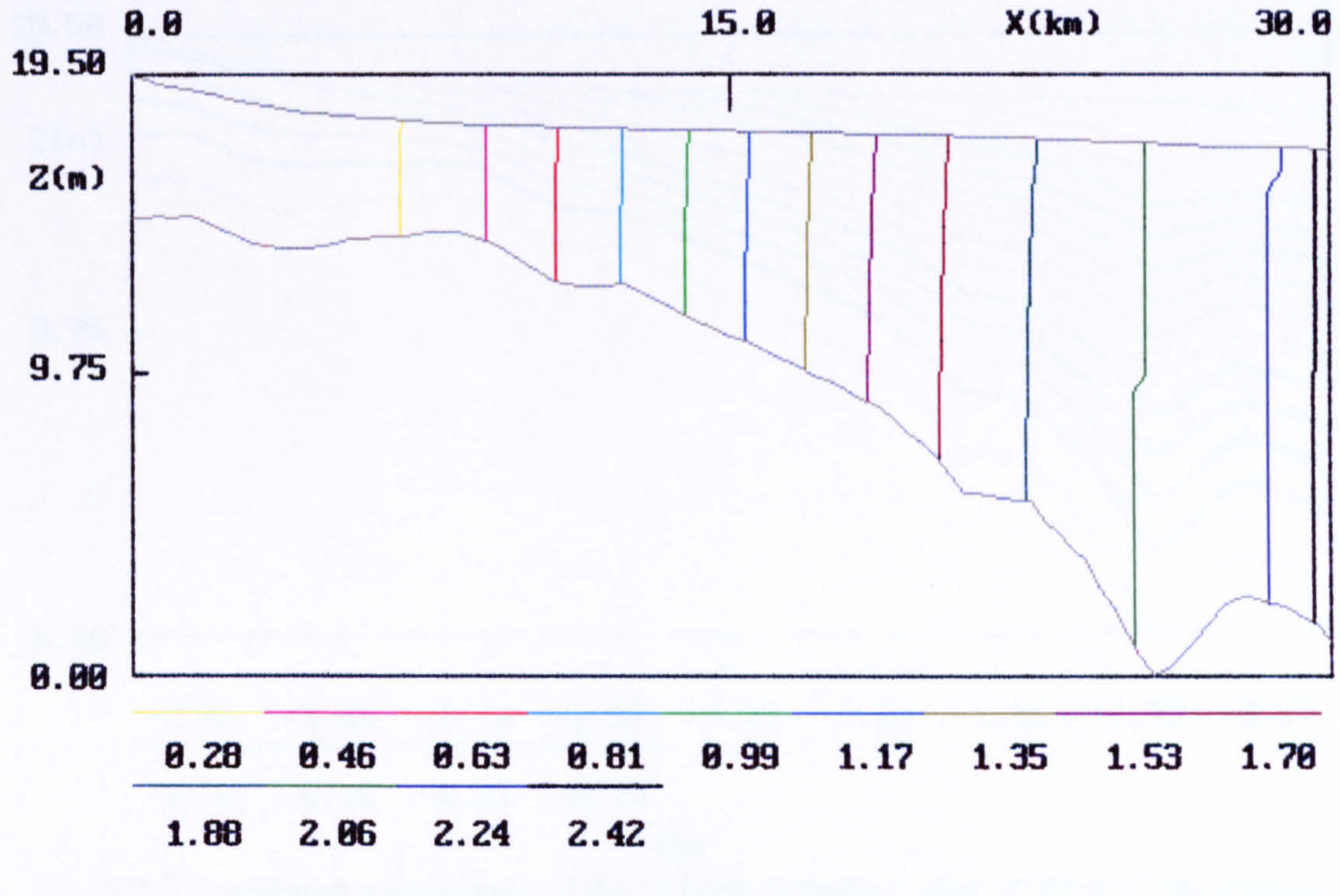

(b)

Fig. 5.3.1 Computed salinity after 10 days of integration (×10 ppt)
(a) river model only. (b) joined model.

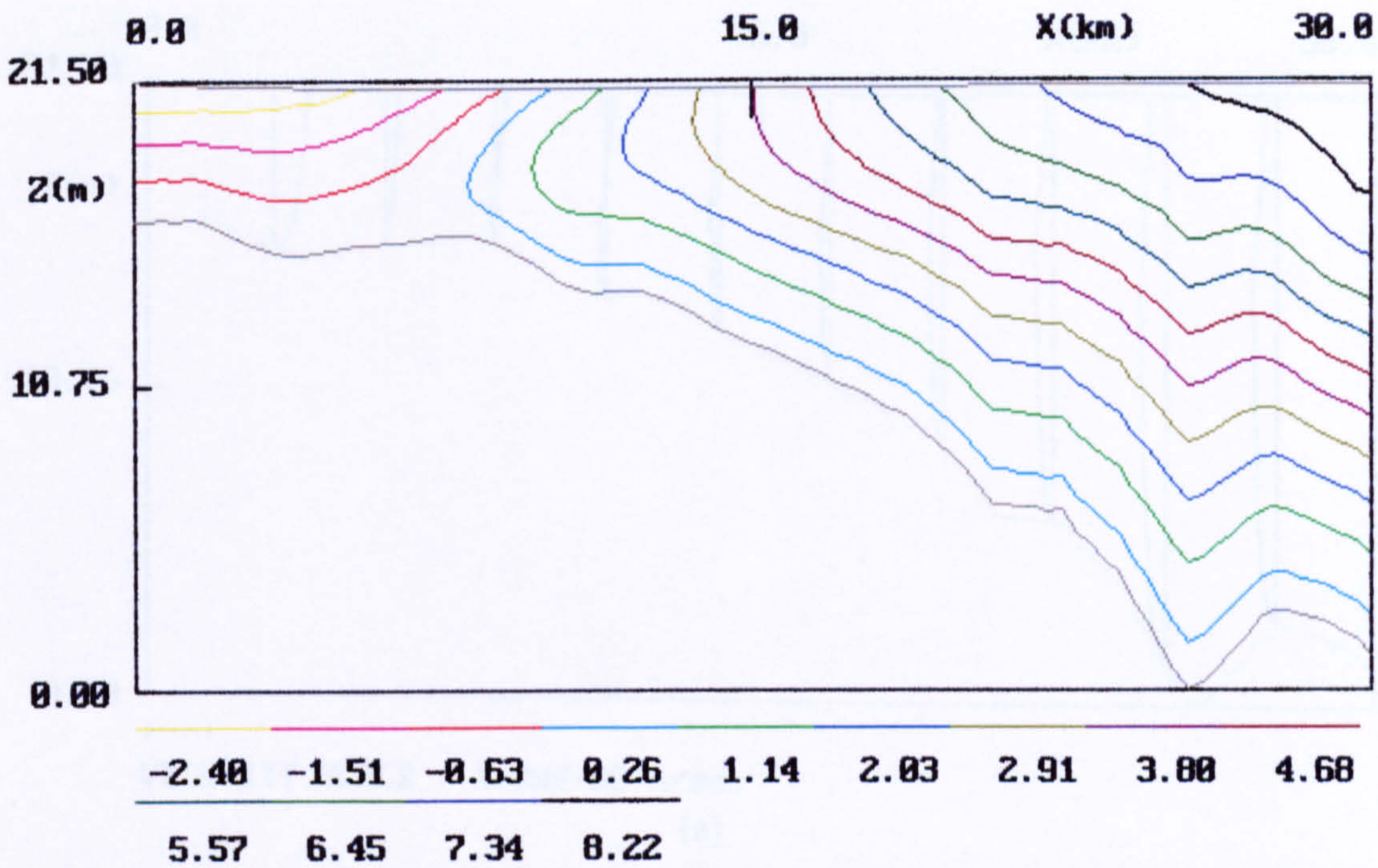

(a)

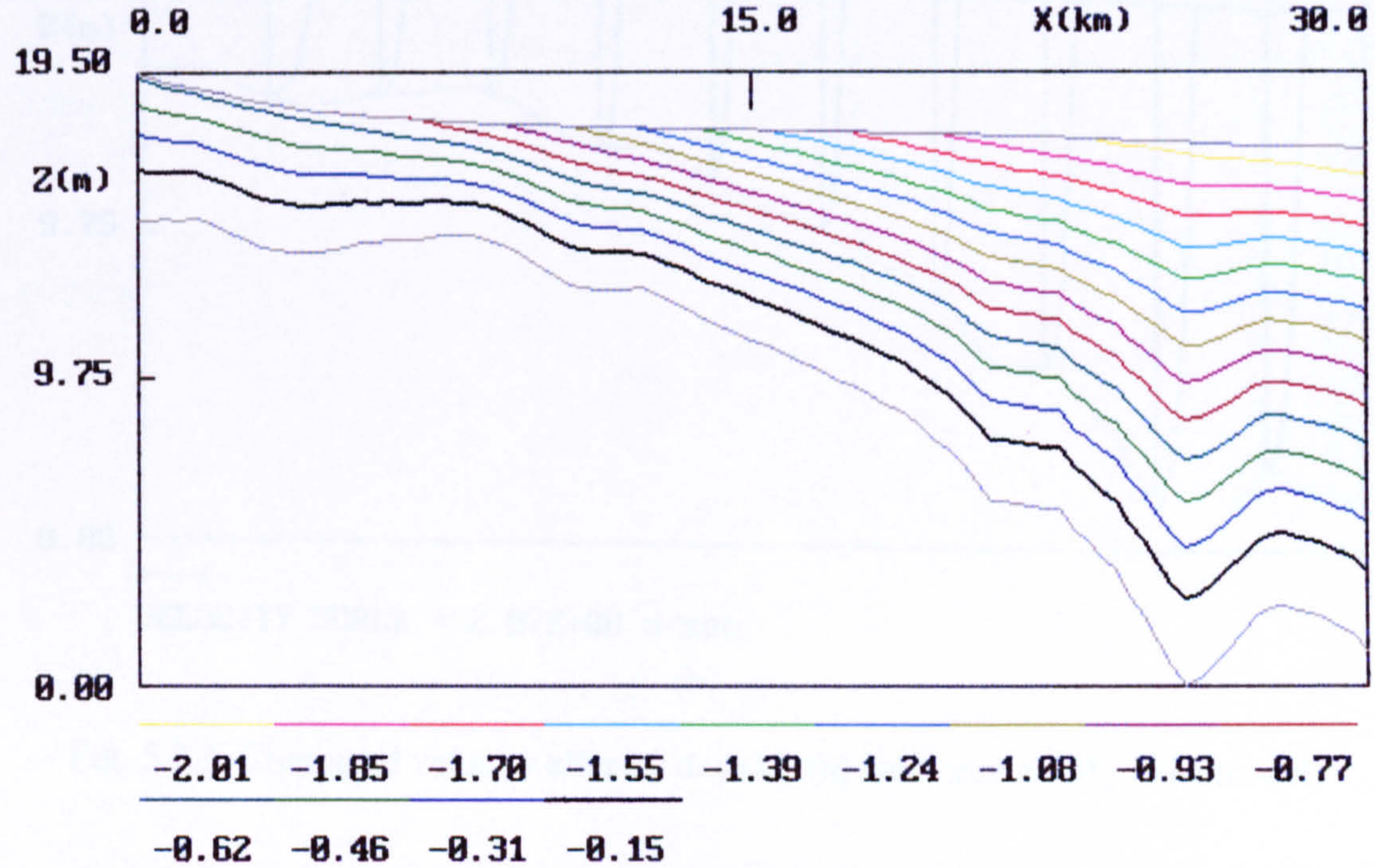

(b)

Fig. 5.3.2 Computed streamlines of the volume transport after 10 days of integration by (a)river model ($\times 10^3 m^3/s$). (b) joined model ($\times 10^4 m^3/s$).

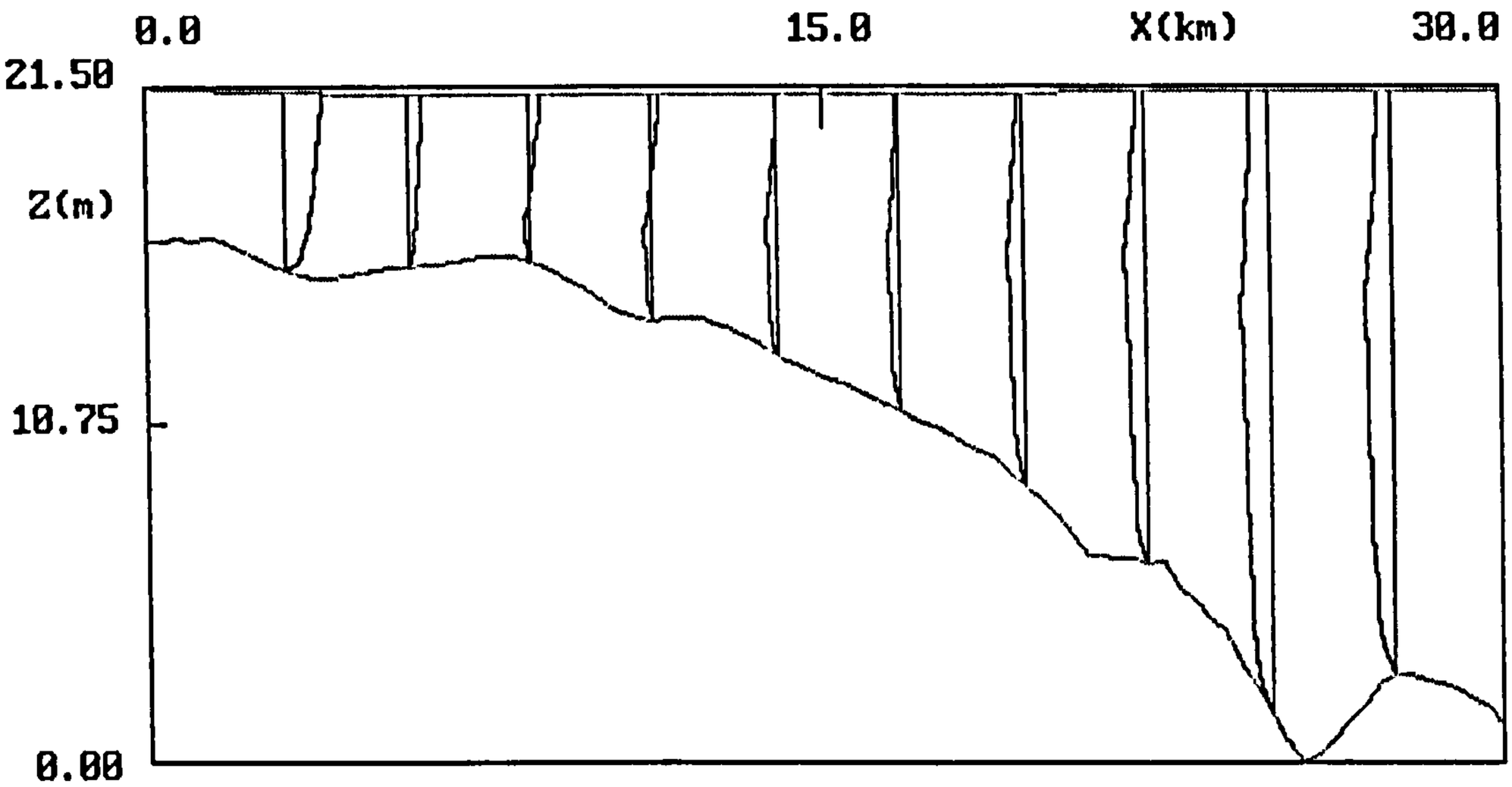

(a)

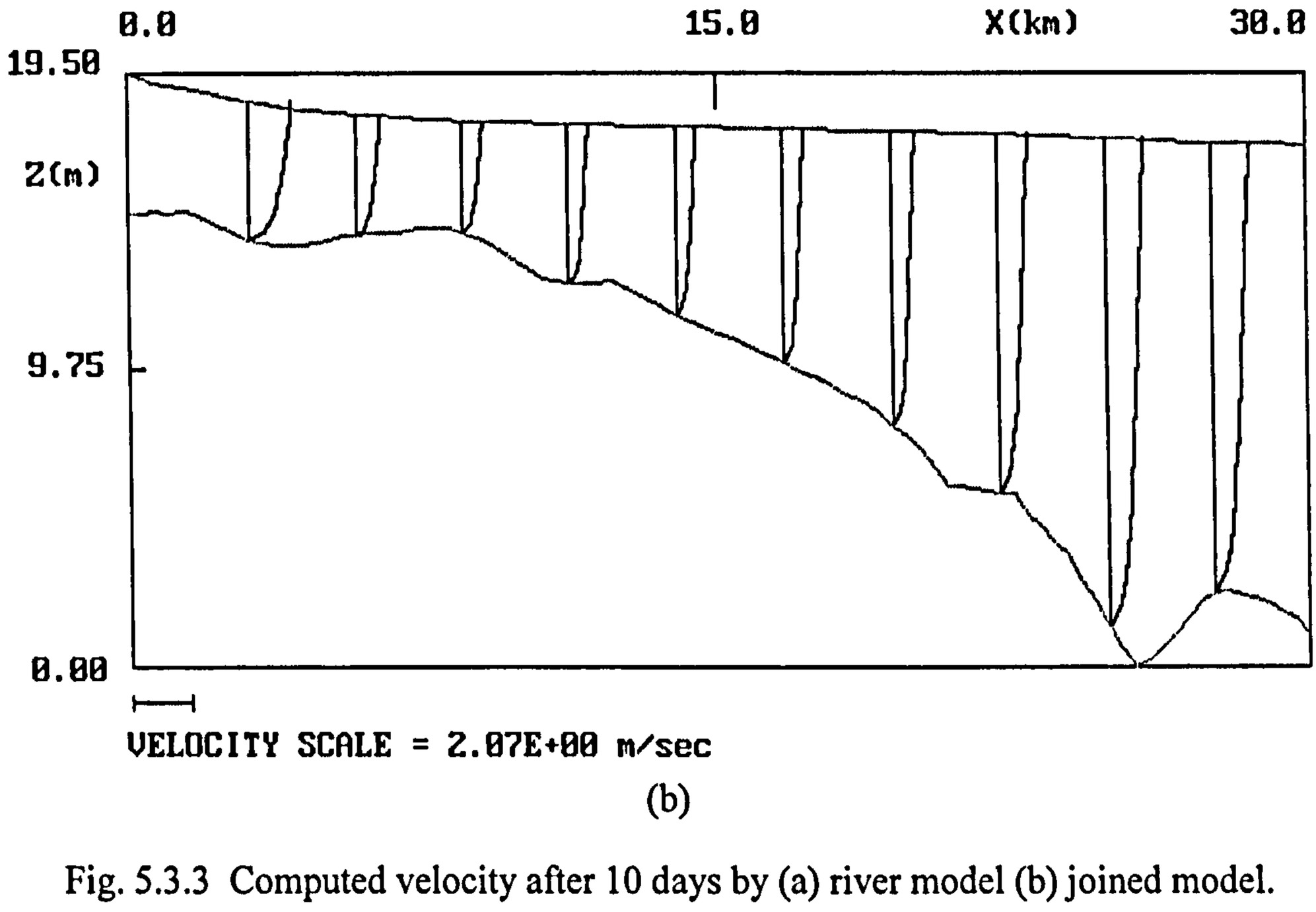

(b)

Fig. 5.3.3 Computed velocity after 10 days by (a) river model (b) joined model.

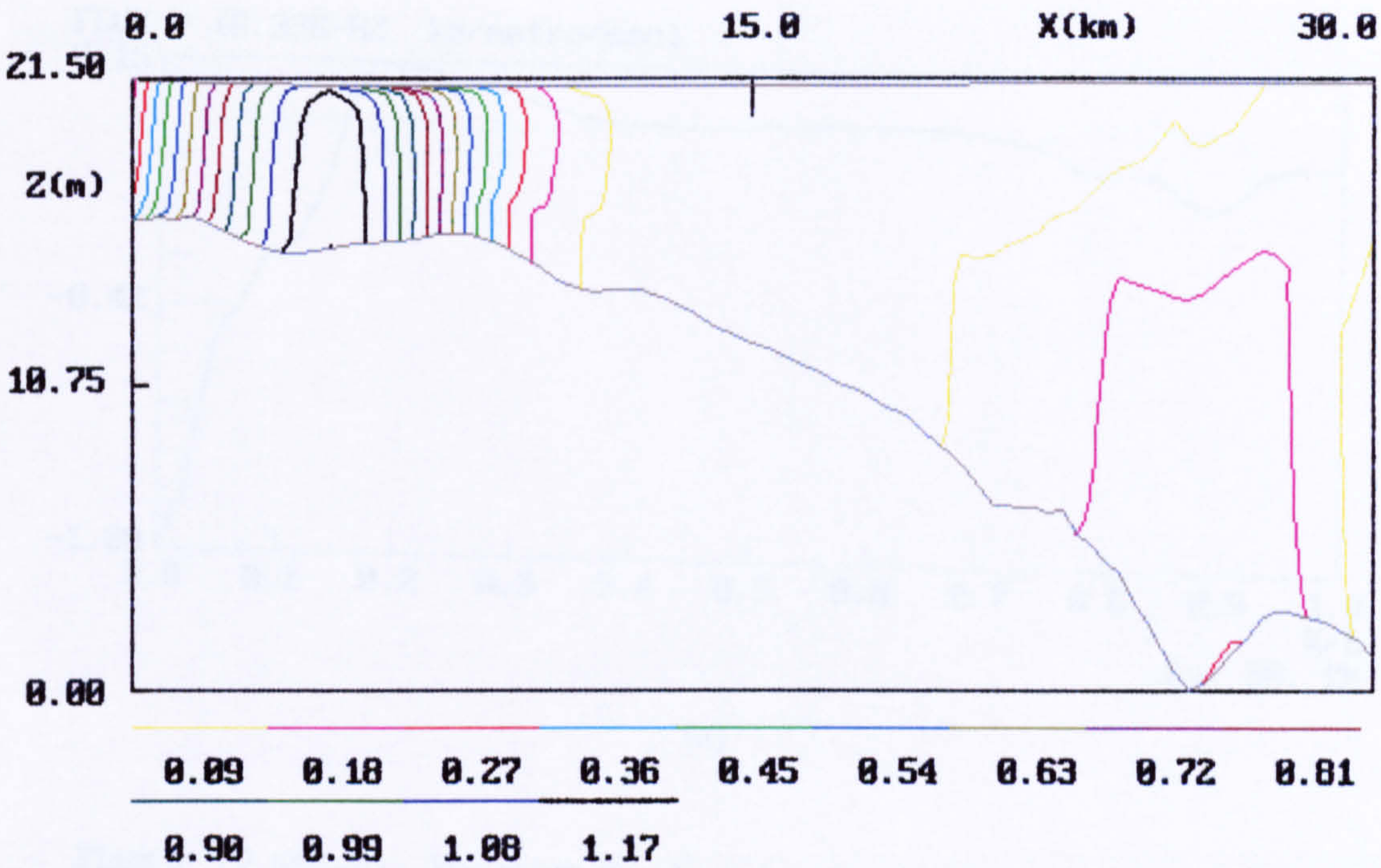

(a)

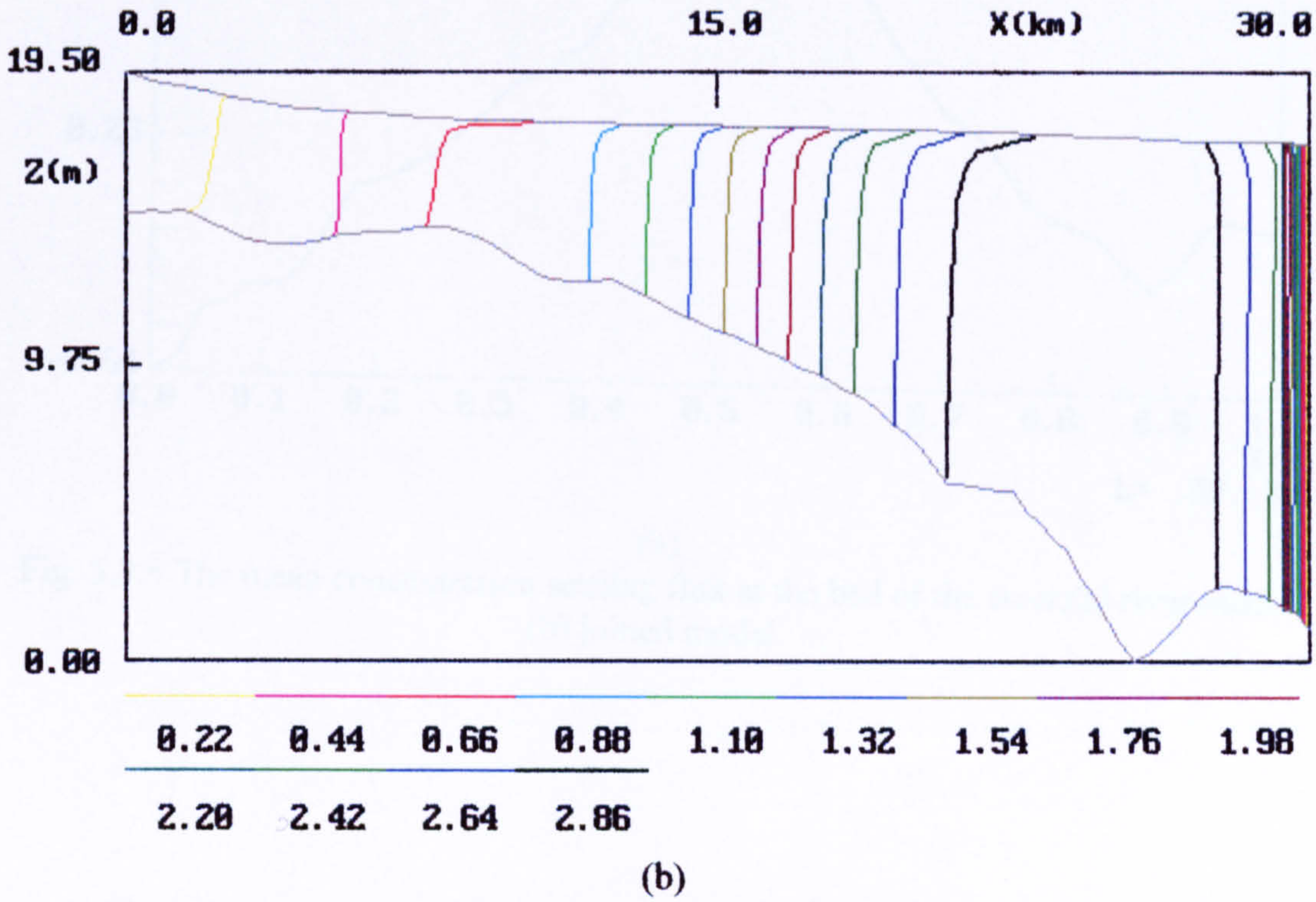

(b)

Fig. 5.3.4 Computed sediment concentration after 10 days (a) river model ($\times 10^2$mg/litre) (b) joined model ($\times 10^3$ mg/litre)

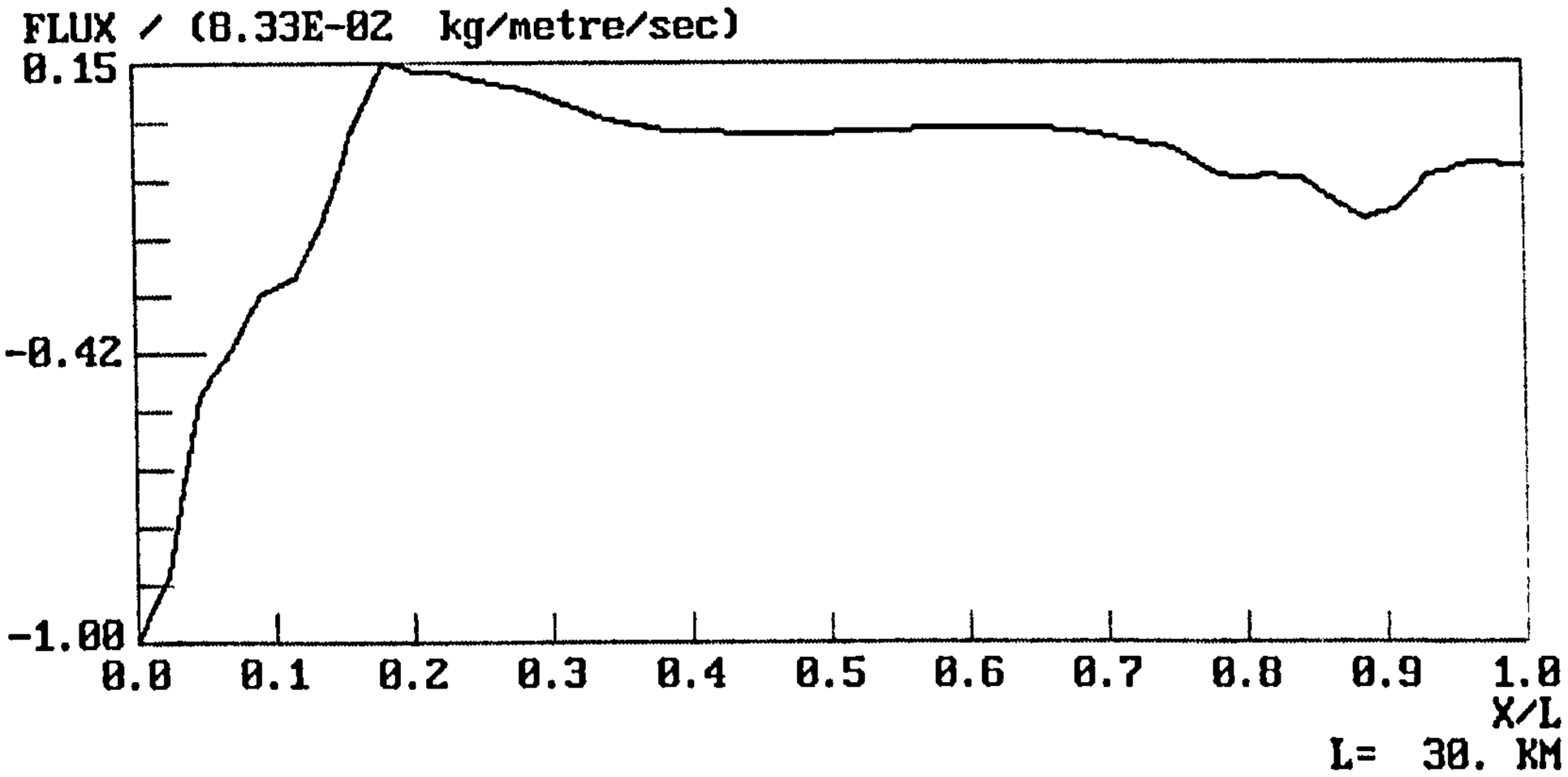

(a)

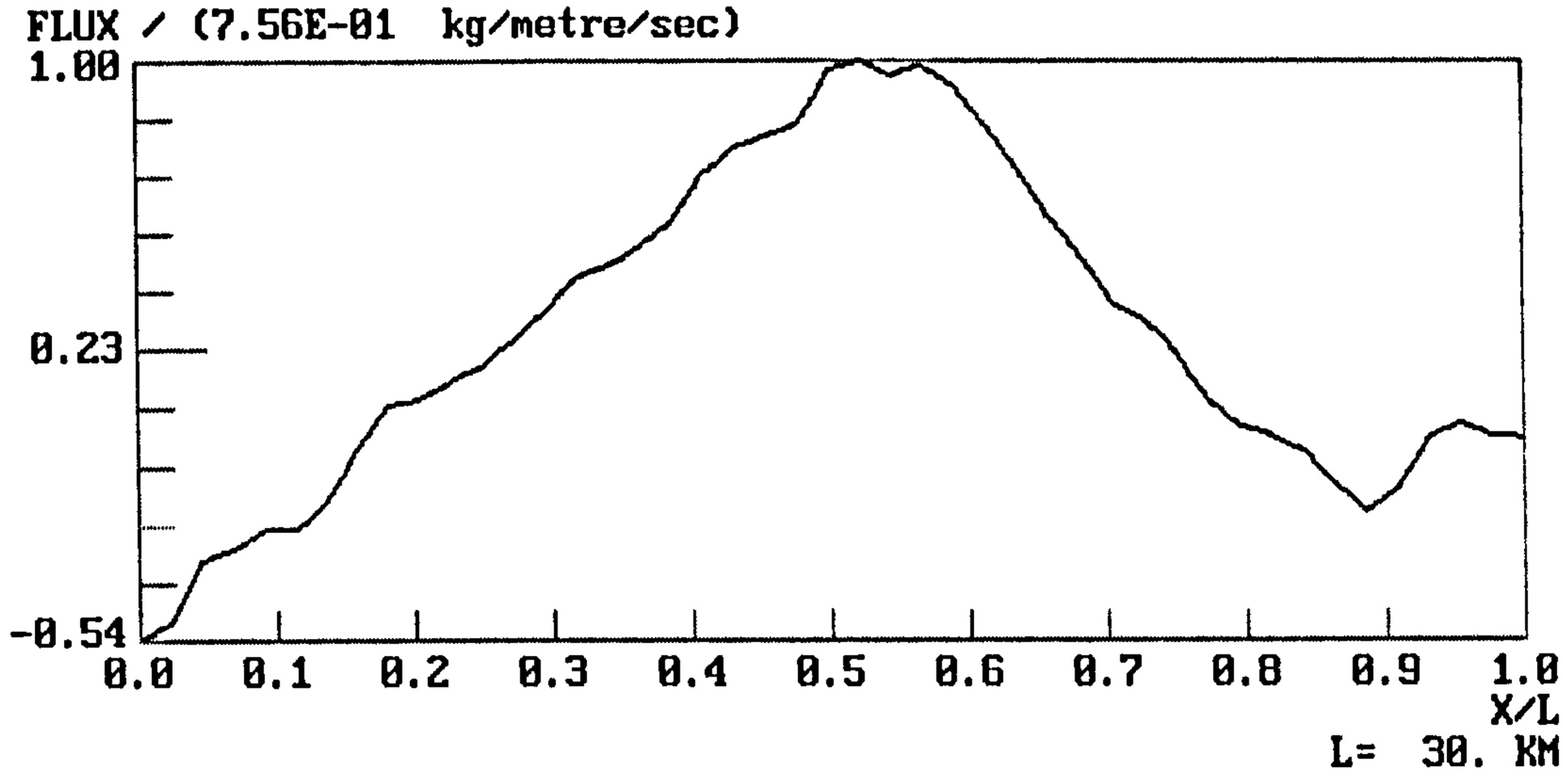

(b)

Fig. 5.3.5 The mean concentration settling flux at the bed of the river,(a) river model (b) joined model.

Figure 5.3.6(a) Surface current(m/s),after 10 days integration of bay model with M2 tide

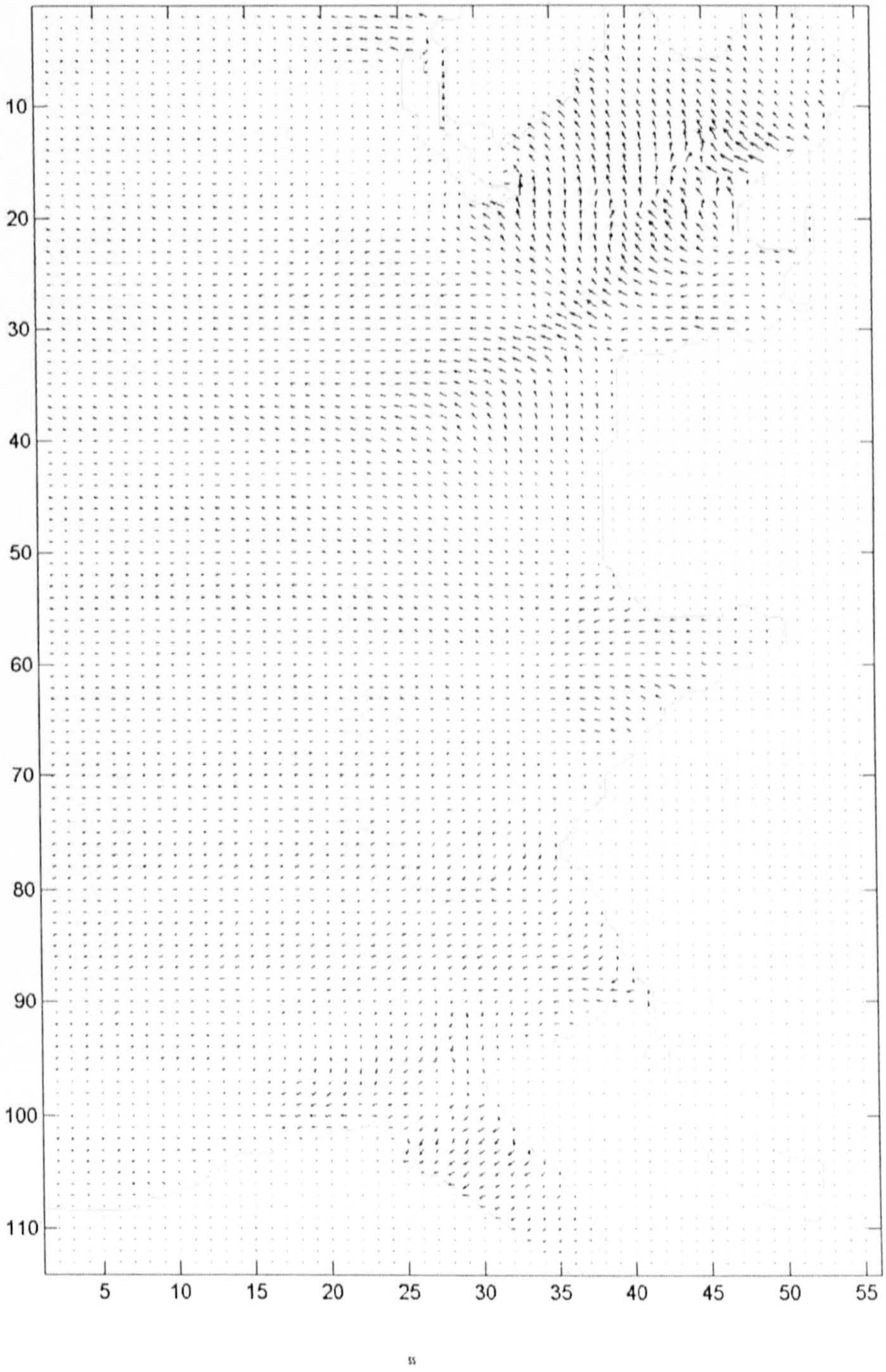

Figure 5.3.6(b)Surface current(m/s),after 10 days integration of joined model,M2 tide,freshwater 300m^3/s

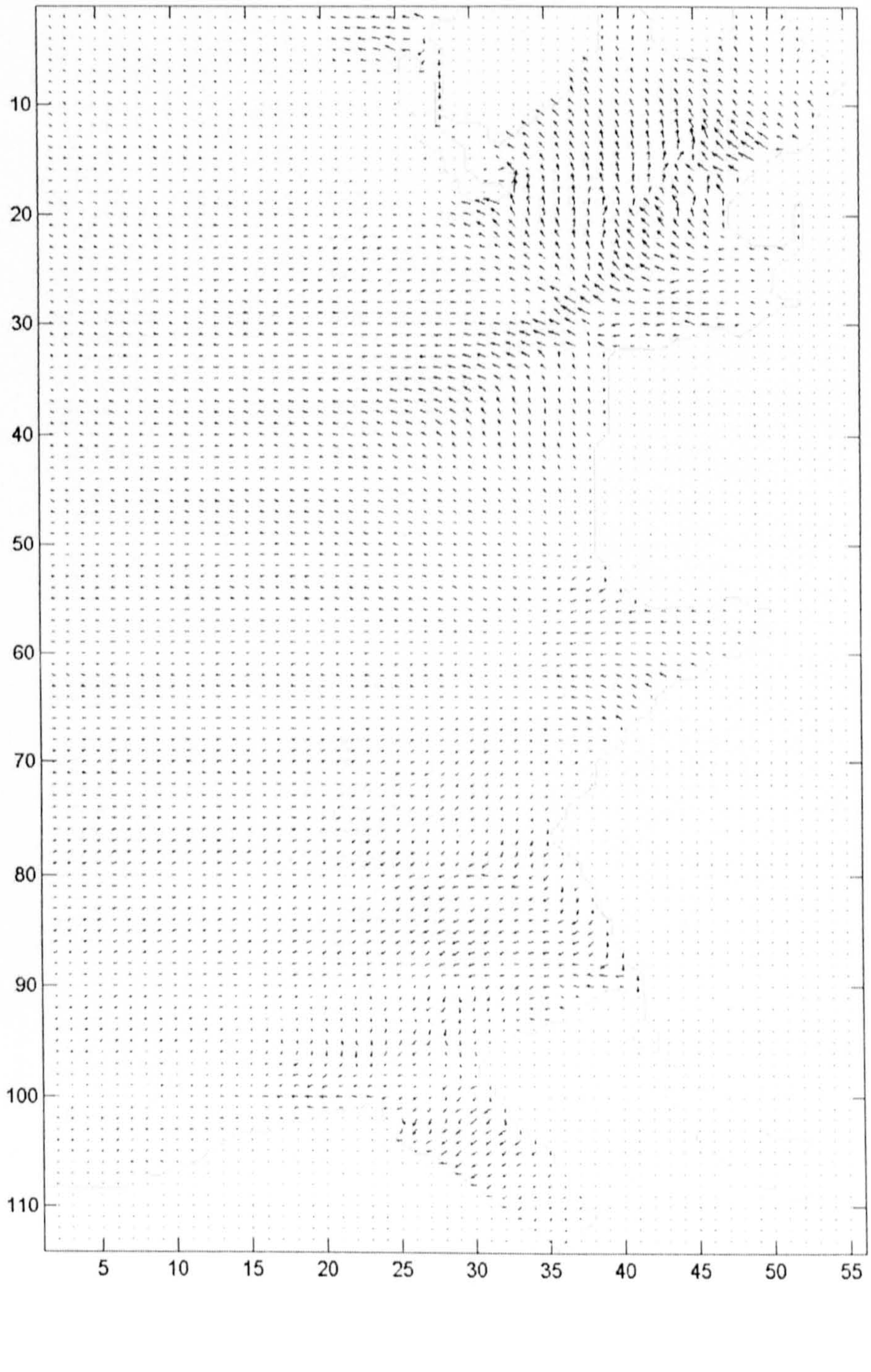

Figure 5.3.6(c)Surface current(m/s),after 10 days integration of joined model,M2 tide,freshwater 900m^3/s

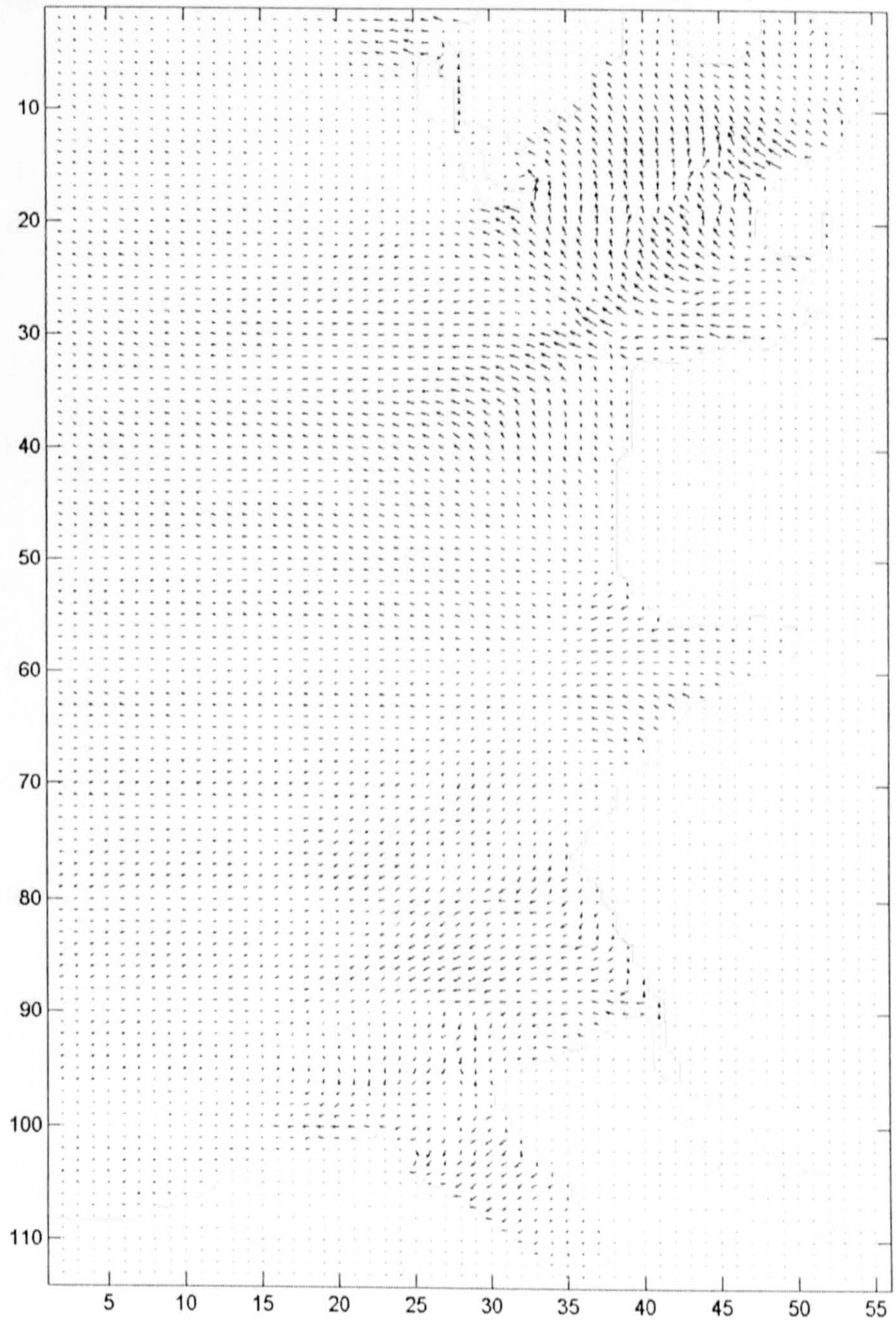

Figure 5.3.7(a)surface salinity,10 days integration of joined model with M2 tide, freshwater 300m3/sec

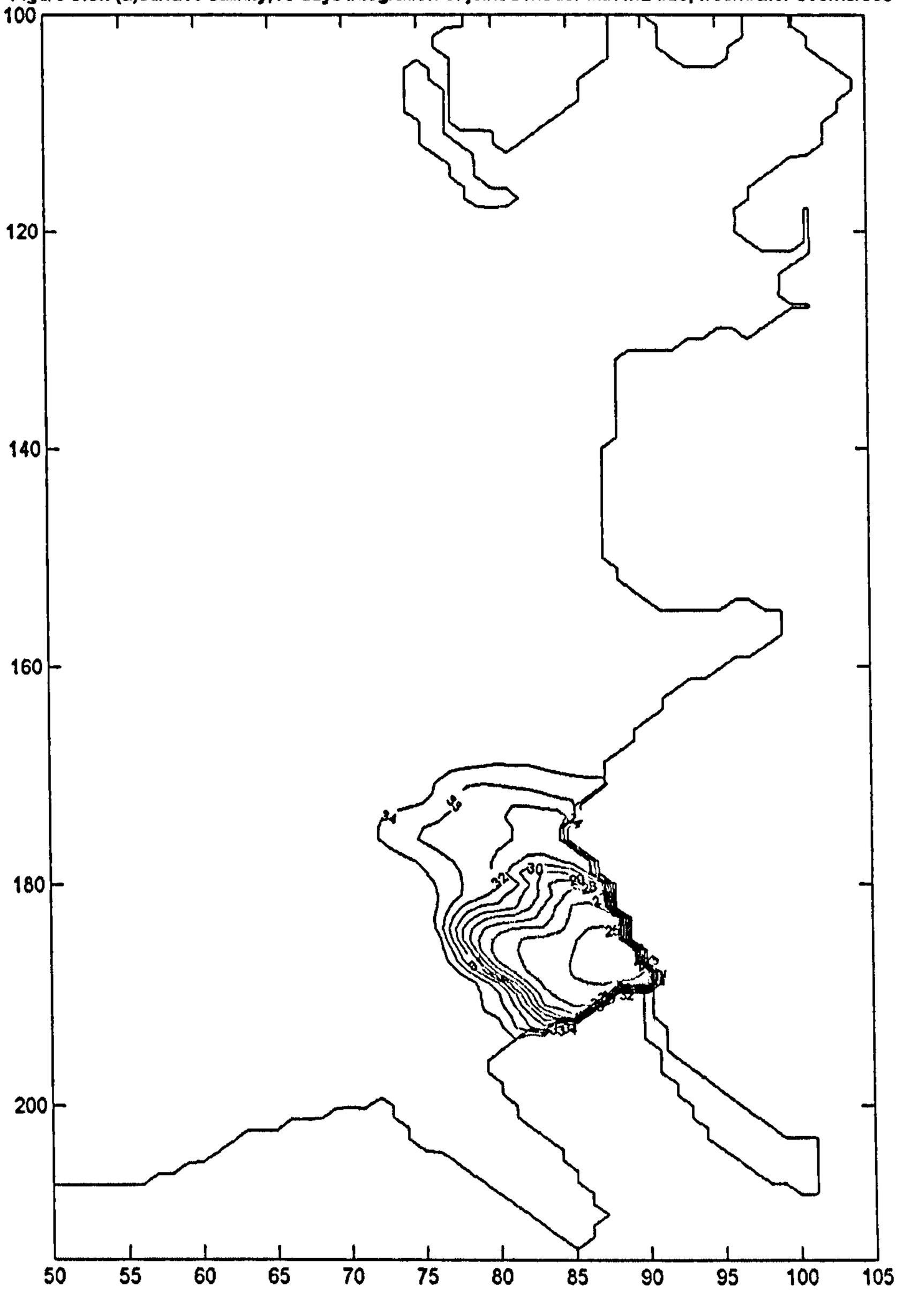

Figure 5.3.7(b)mid depth salinity,10 days integration of joined model with M2 tide, freshwater 300m3/sec

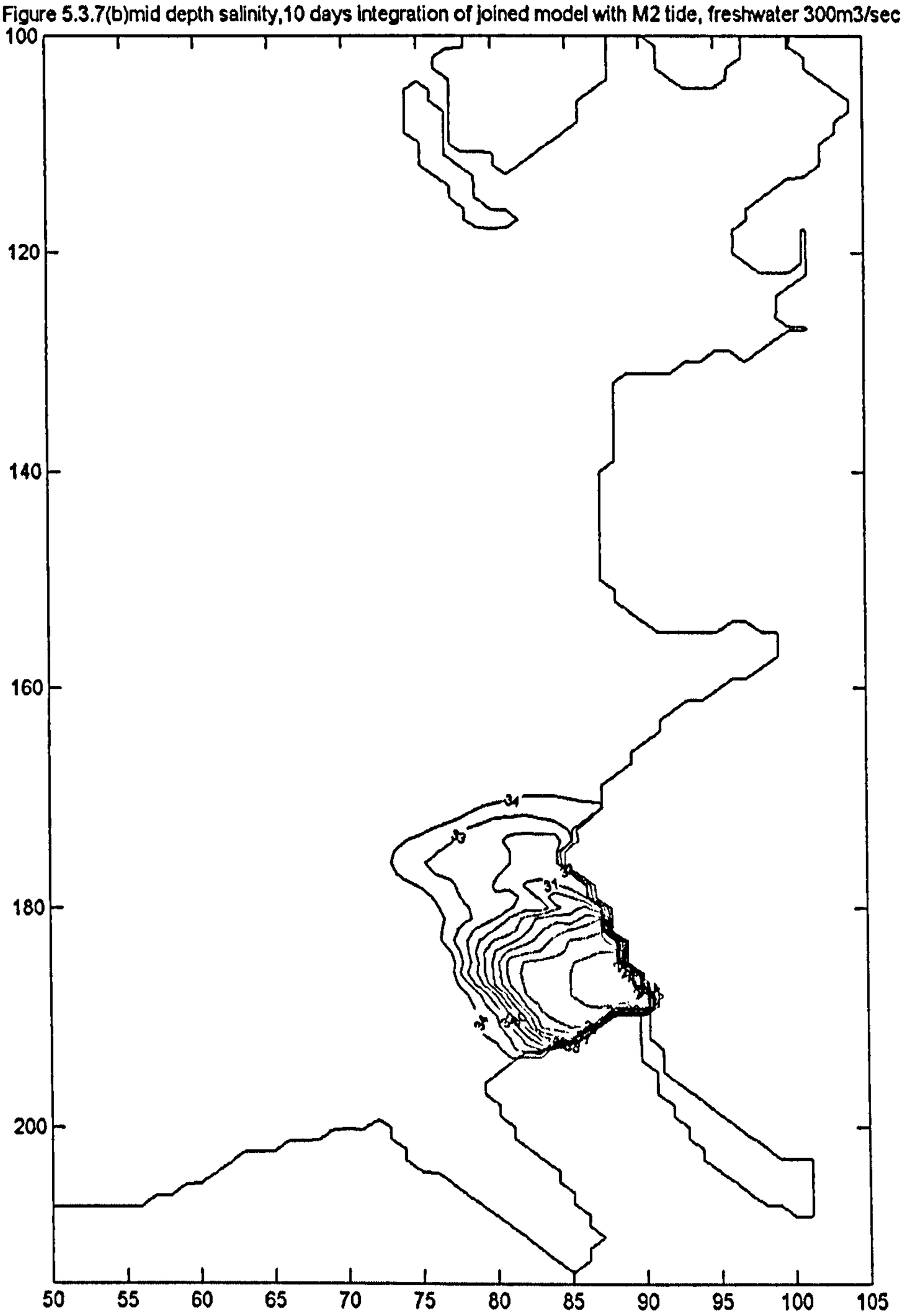

Figure 5.3.7(c)seabed salinity,10 days integration of joined model with M2 tide, freshwater 300m3/sec

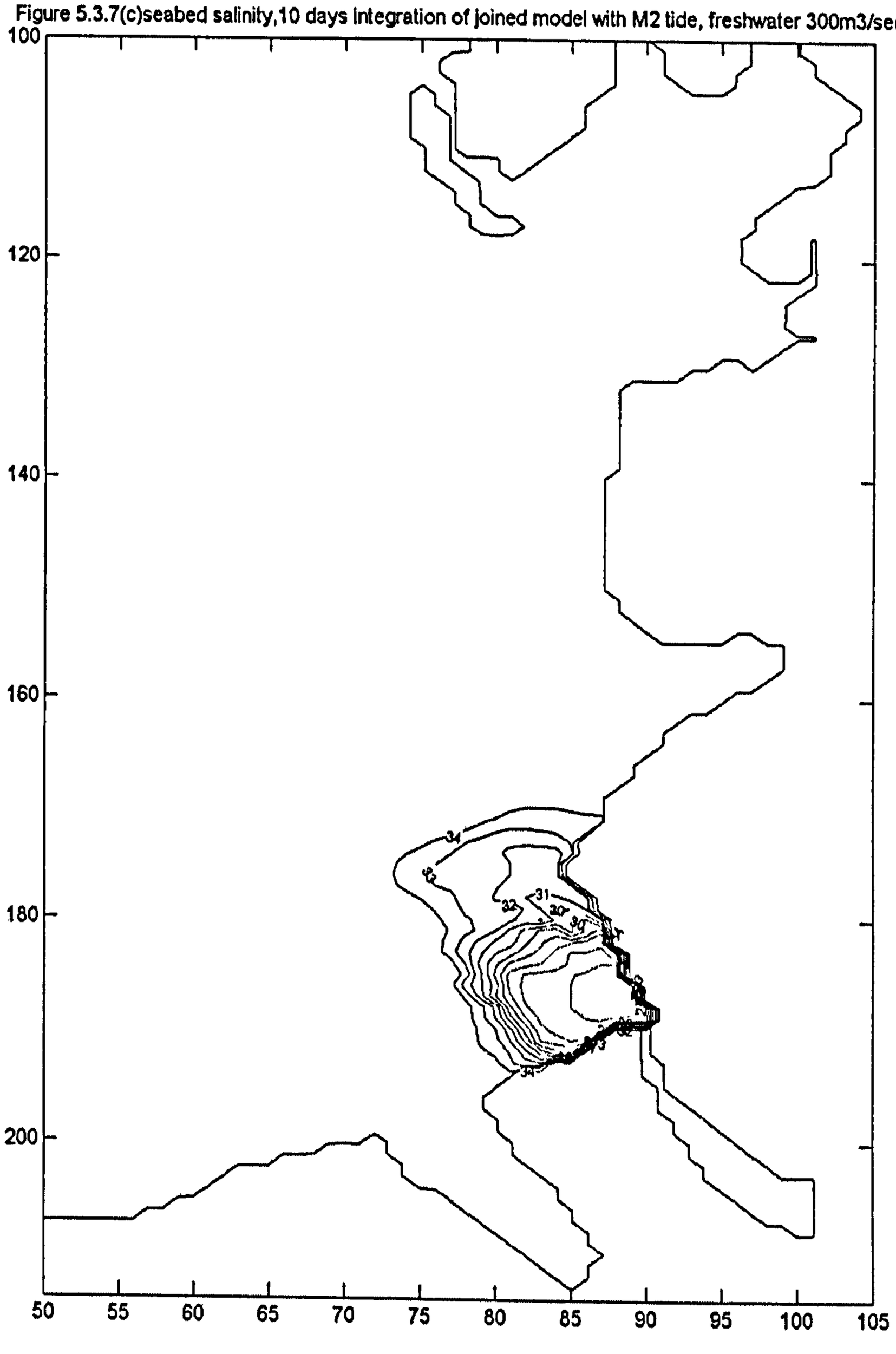

Figure 5.3.8(a)surface salinity,10 days integration of joined model with M2 tide, freshwater 1000m3/sec

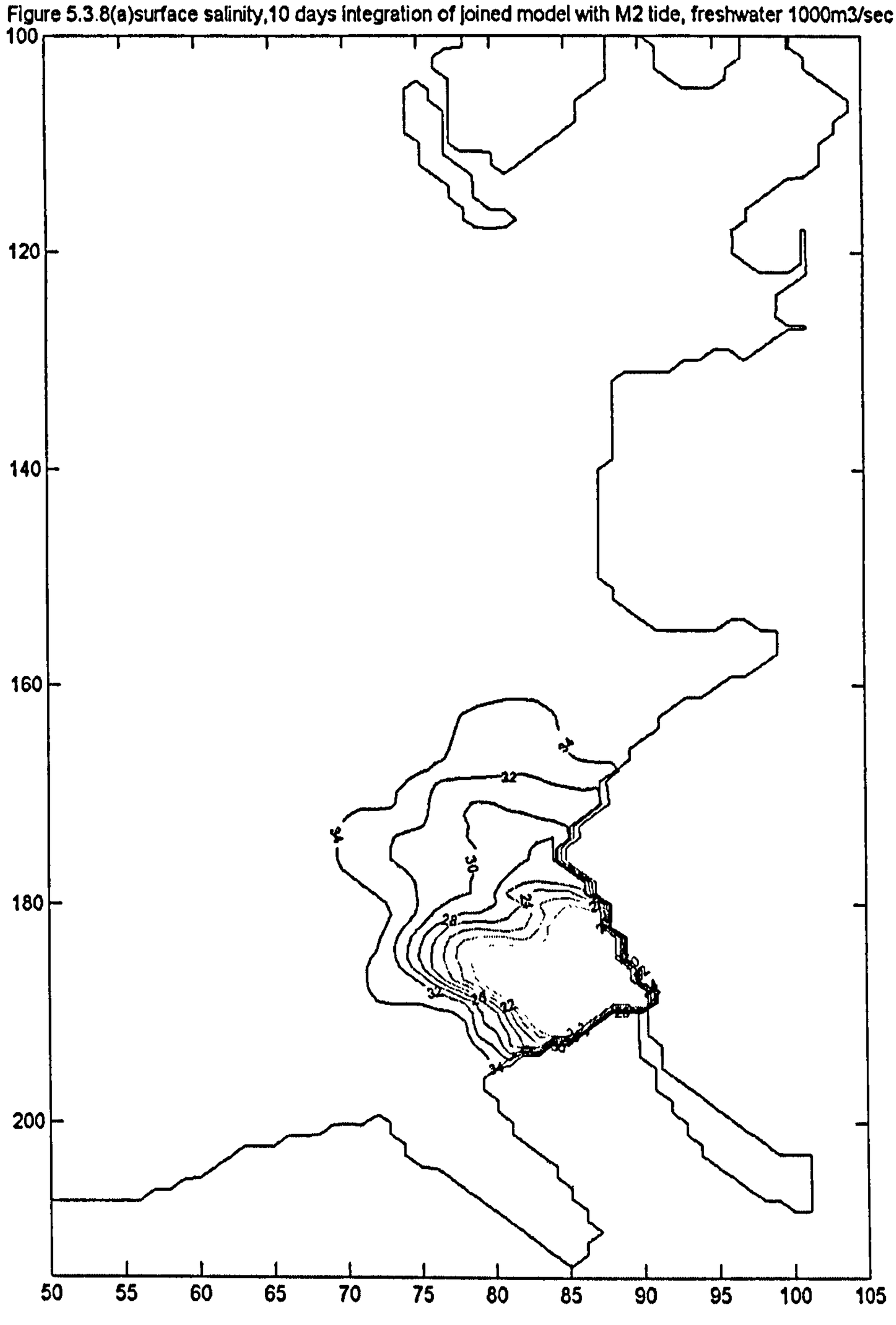

Figure 5.3.8(b)mid depth salinity,10 days integration of joined model with M2 tide, freshwater 1000m3/sec

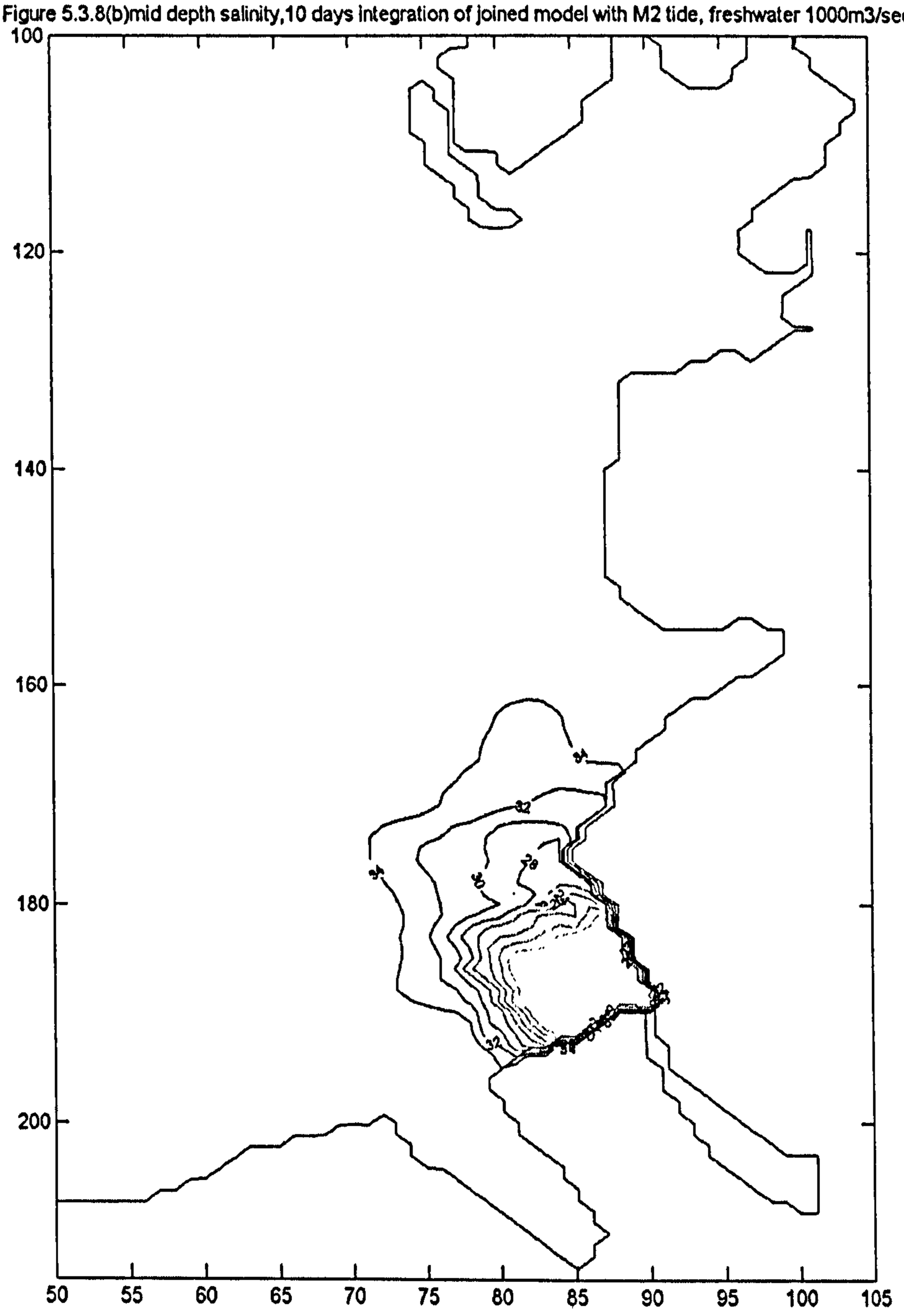

Figure 5.3.8(c)seabed salinity,10 days integration of joined model with M2 tide, freshwater 1000m3/sec

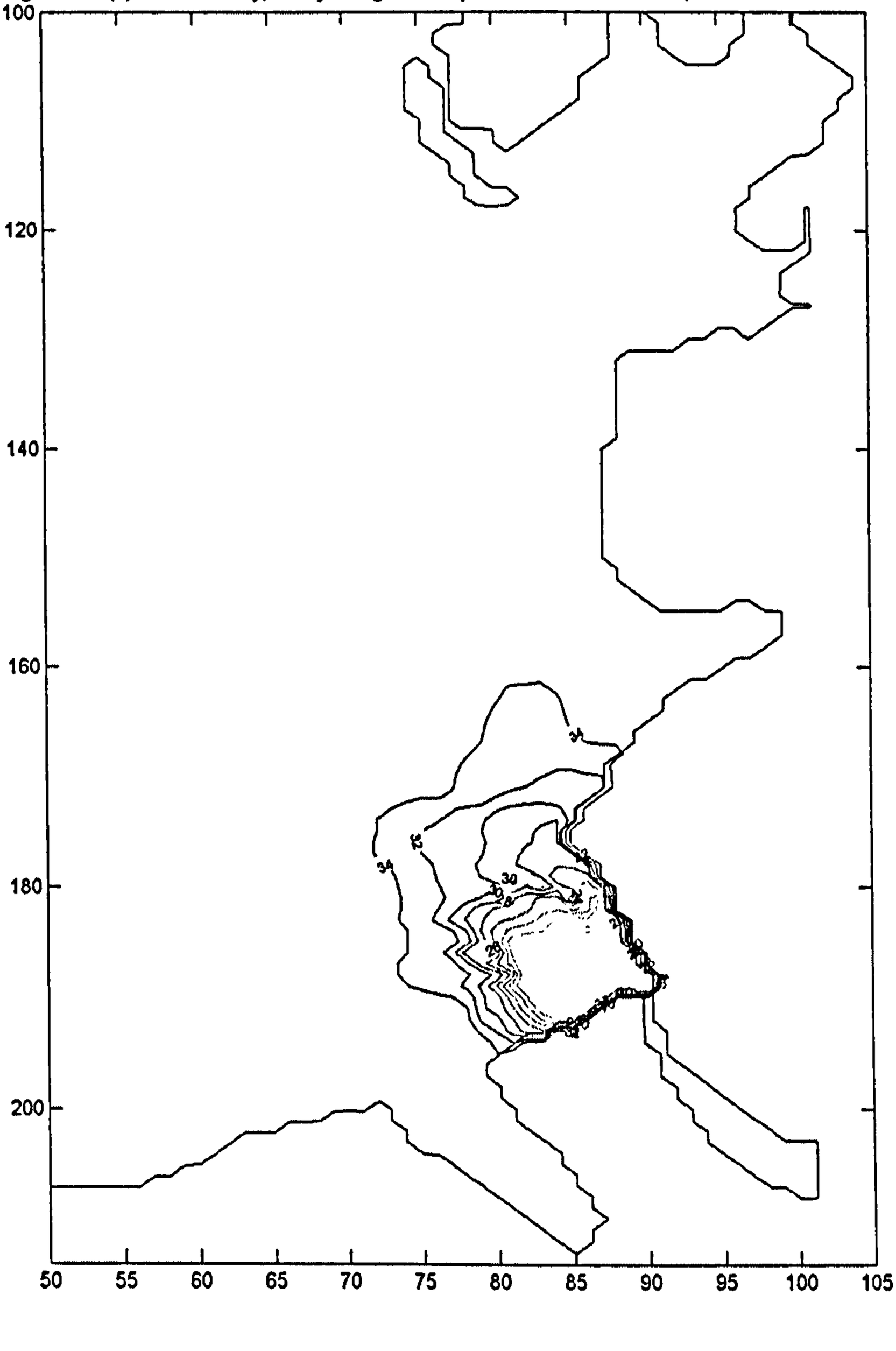

Figure 5.3.9(a)bottom salinity,10 days integration of joined model without tide, freshwater 900m3/sec

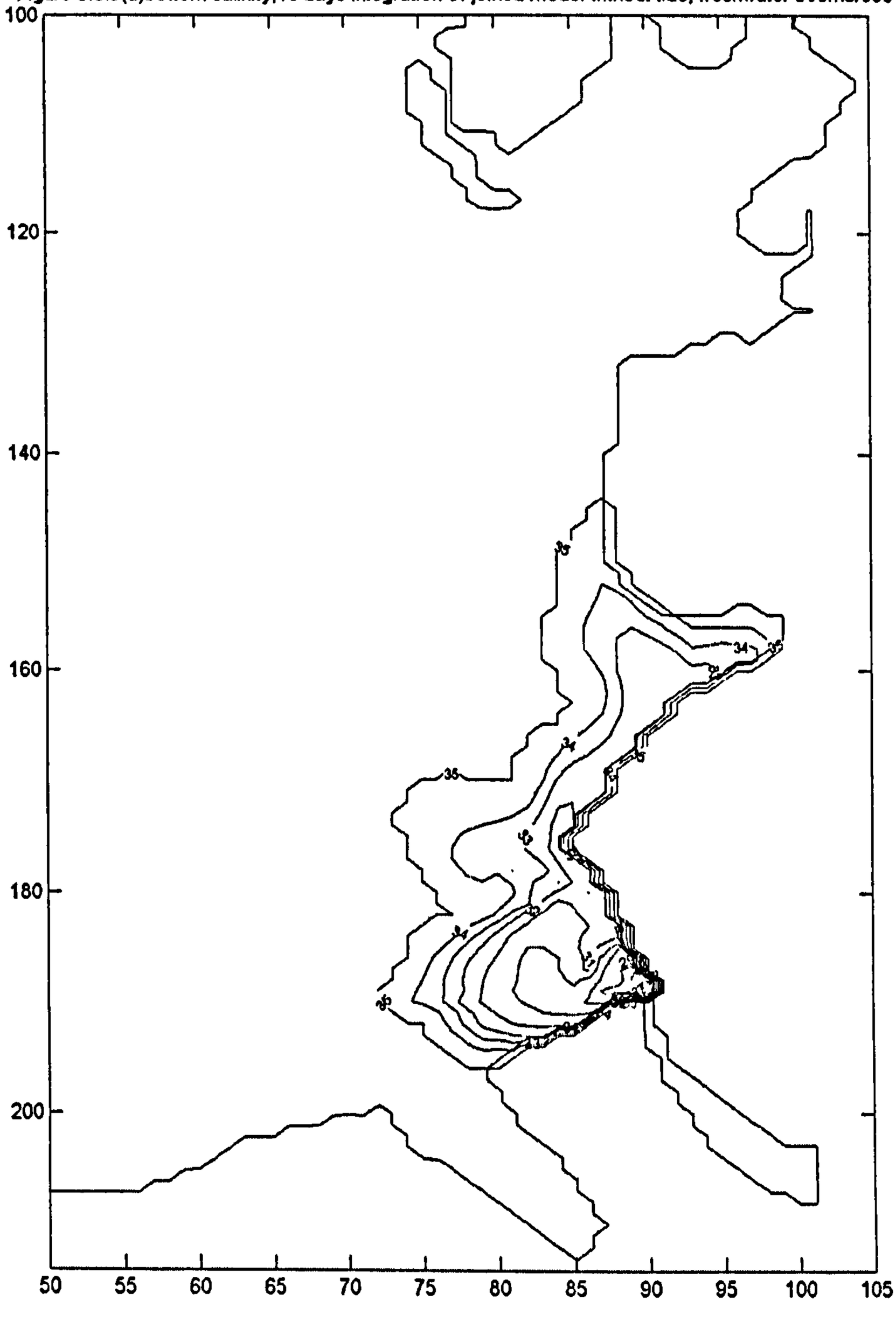

Figure 5.3.9(b)mid depth salinity,10 days integration of joined model without tide, freshwater 900m3/sec

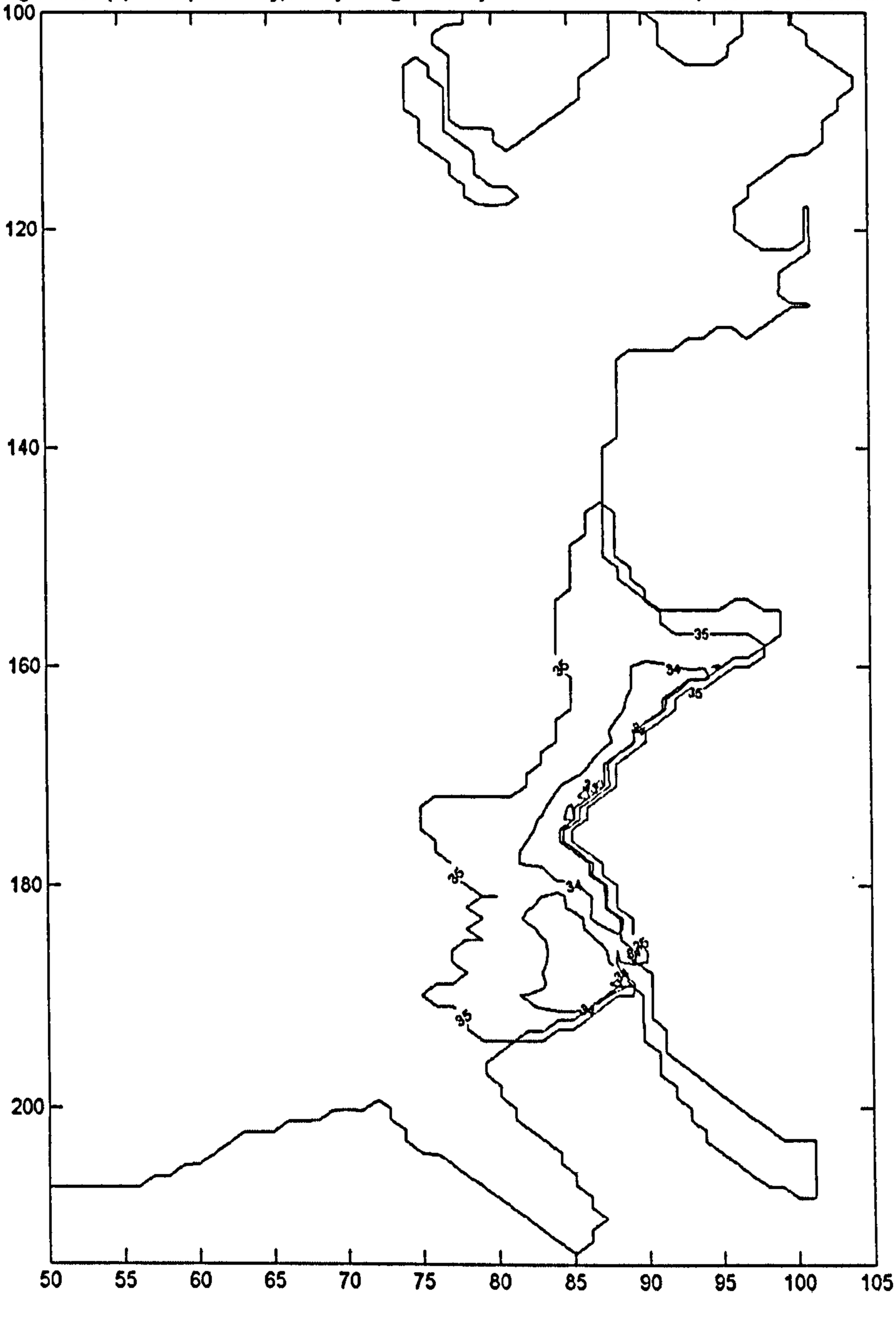

Figure 5.3.9(c)bottom salinity,10 days integration of joined model without tide, freshwater 900m3/sec

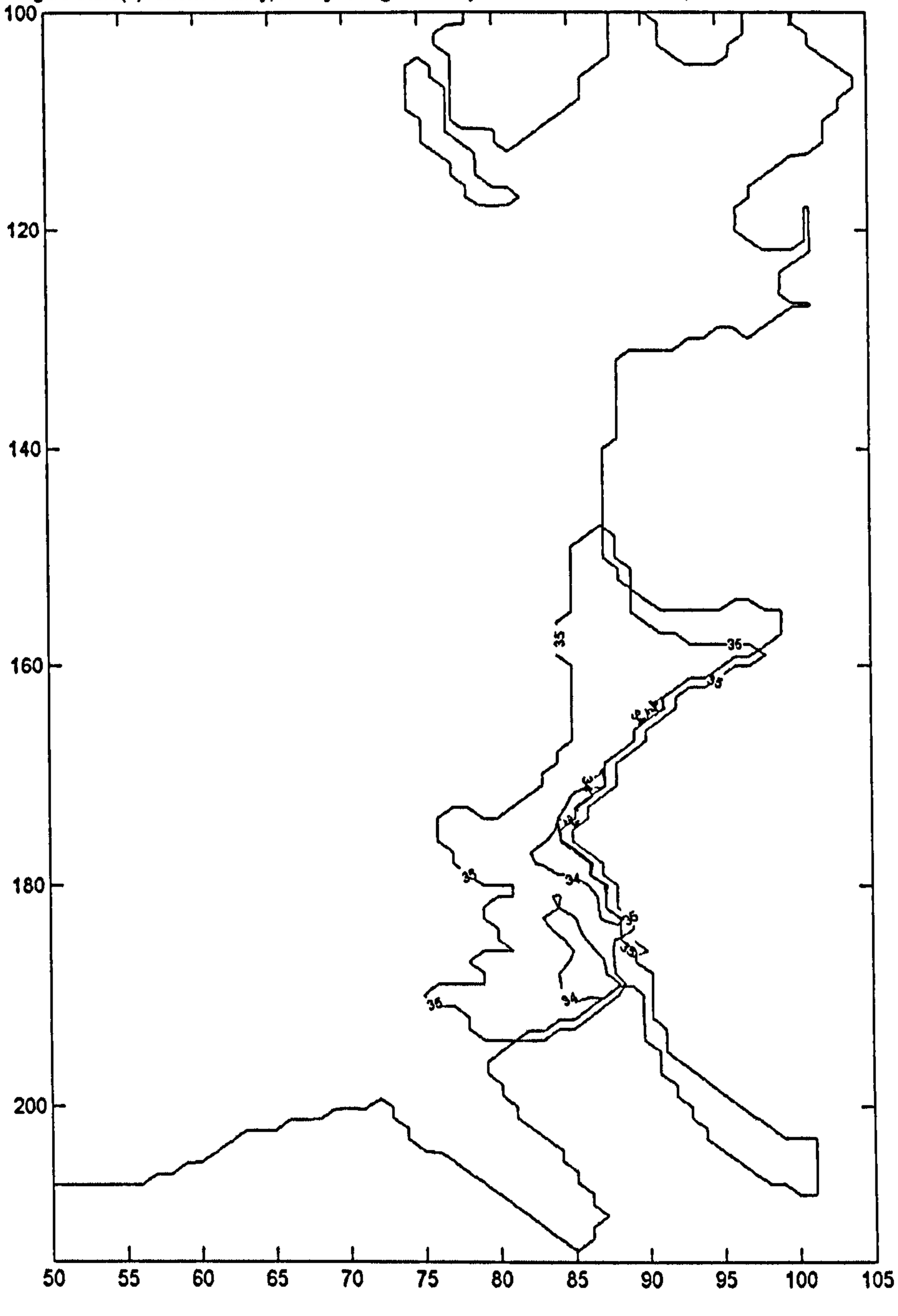

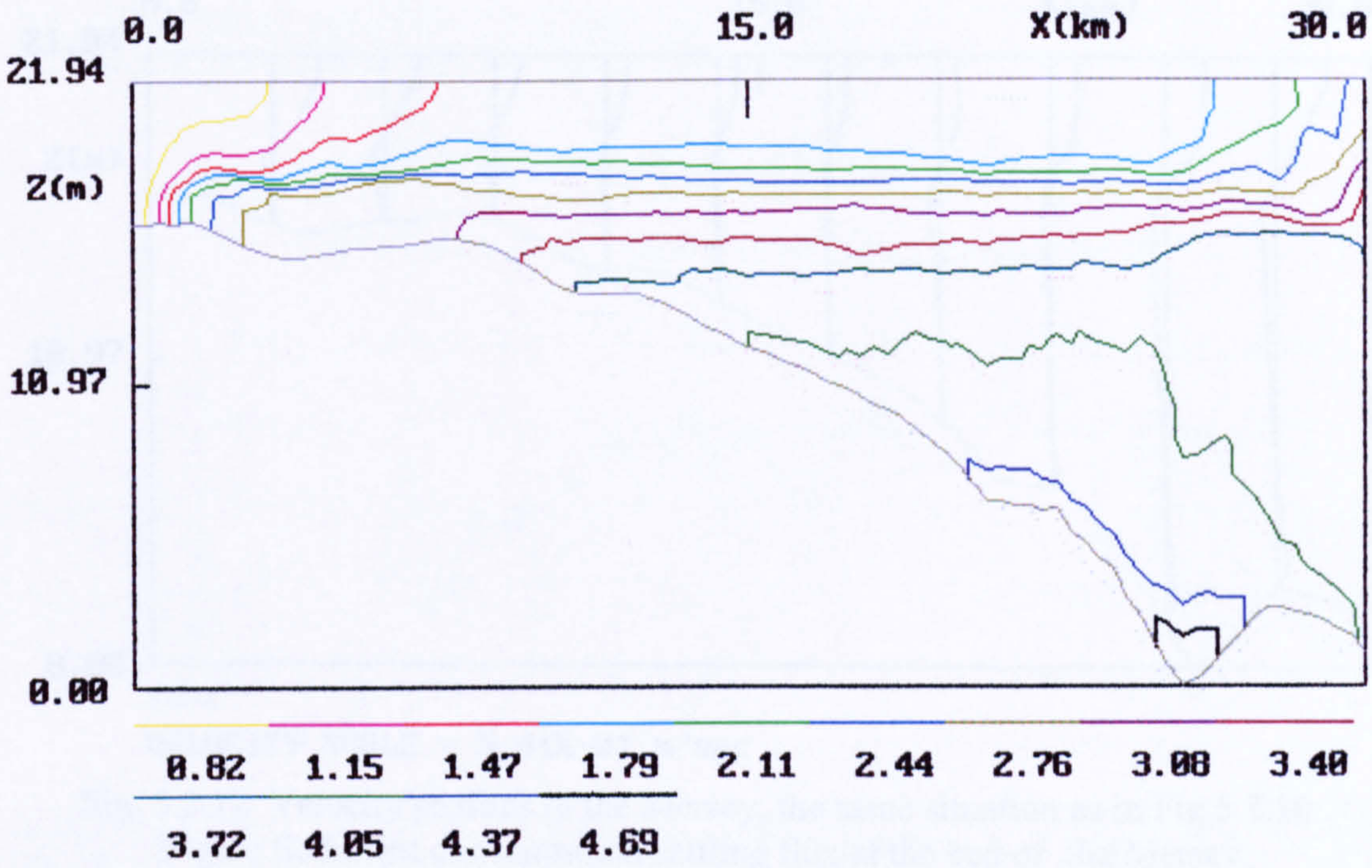

Fig. 5.3.10 Salinity in the Mersey when tidal force is absent from the joined model with freshwater of 1000 m^3/sec discharged from the Mersey (×10 ppt)

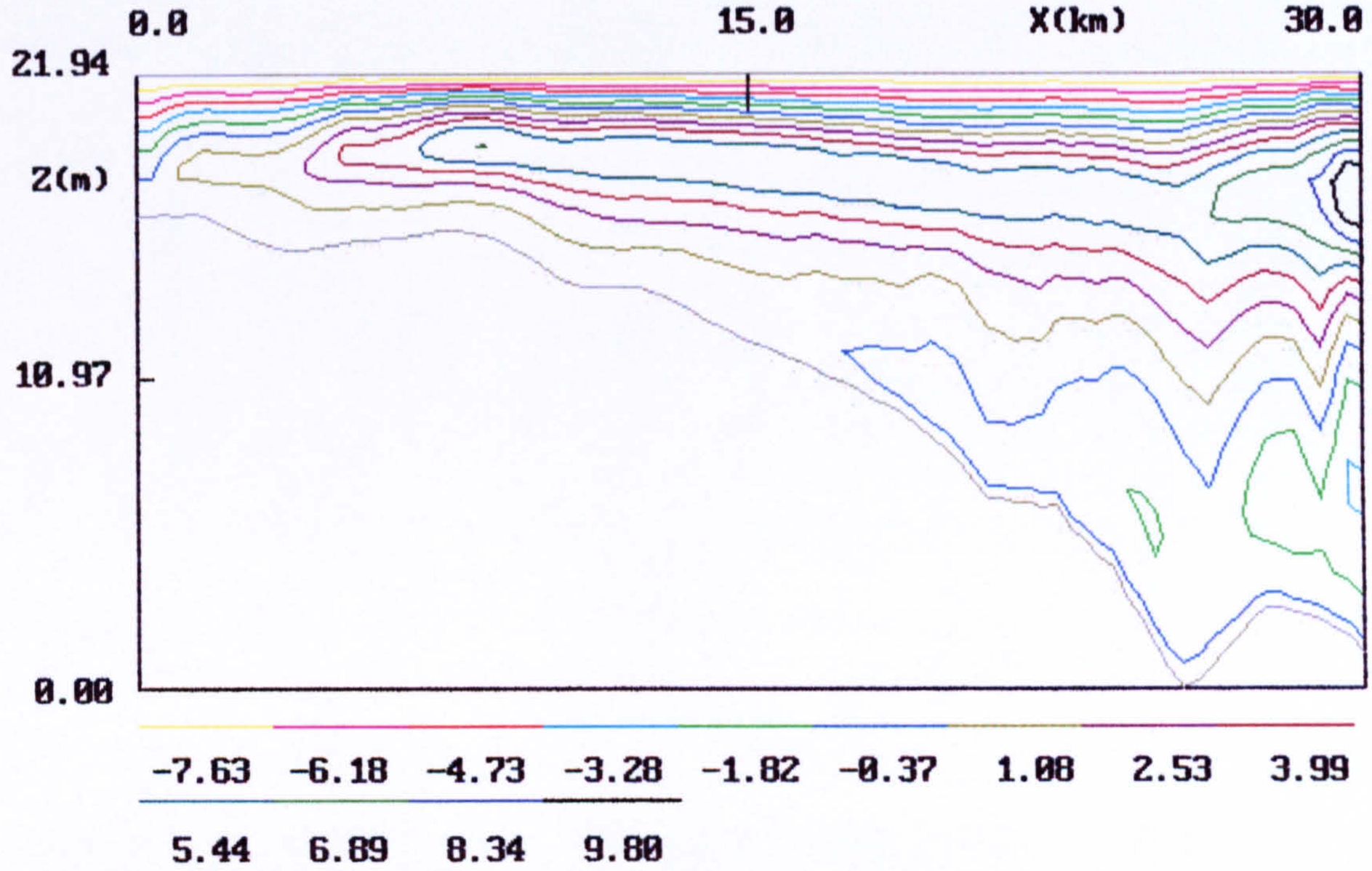

Fig. 5.3.11 Streamlines of Volume transport in the Mersey (×$10^2 m^3$/sec)

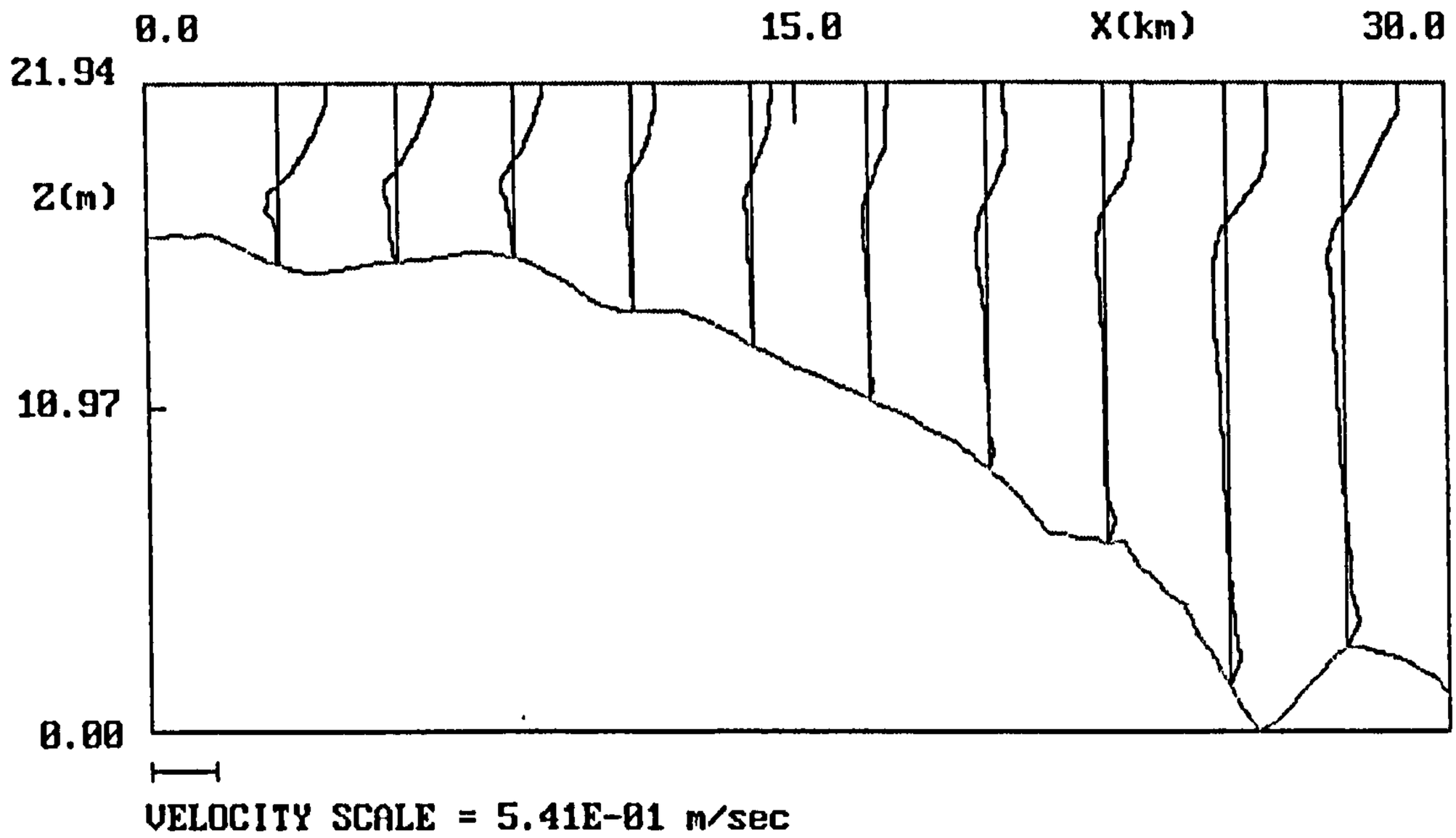

Fig. 5.3.12 Velocity profiles in the Mersey, the same situation as in Fig 5.3.10..
Figure Sediment concentration settling flux at the bed of the Mersey.

Fig 5.3.13a time series of surface current at MP

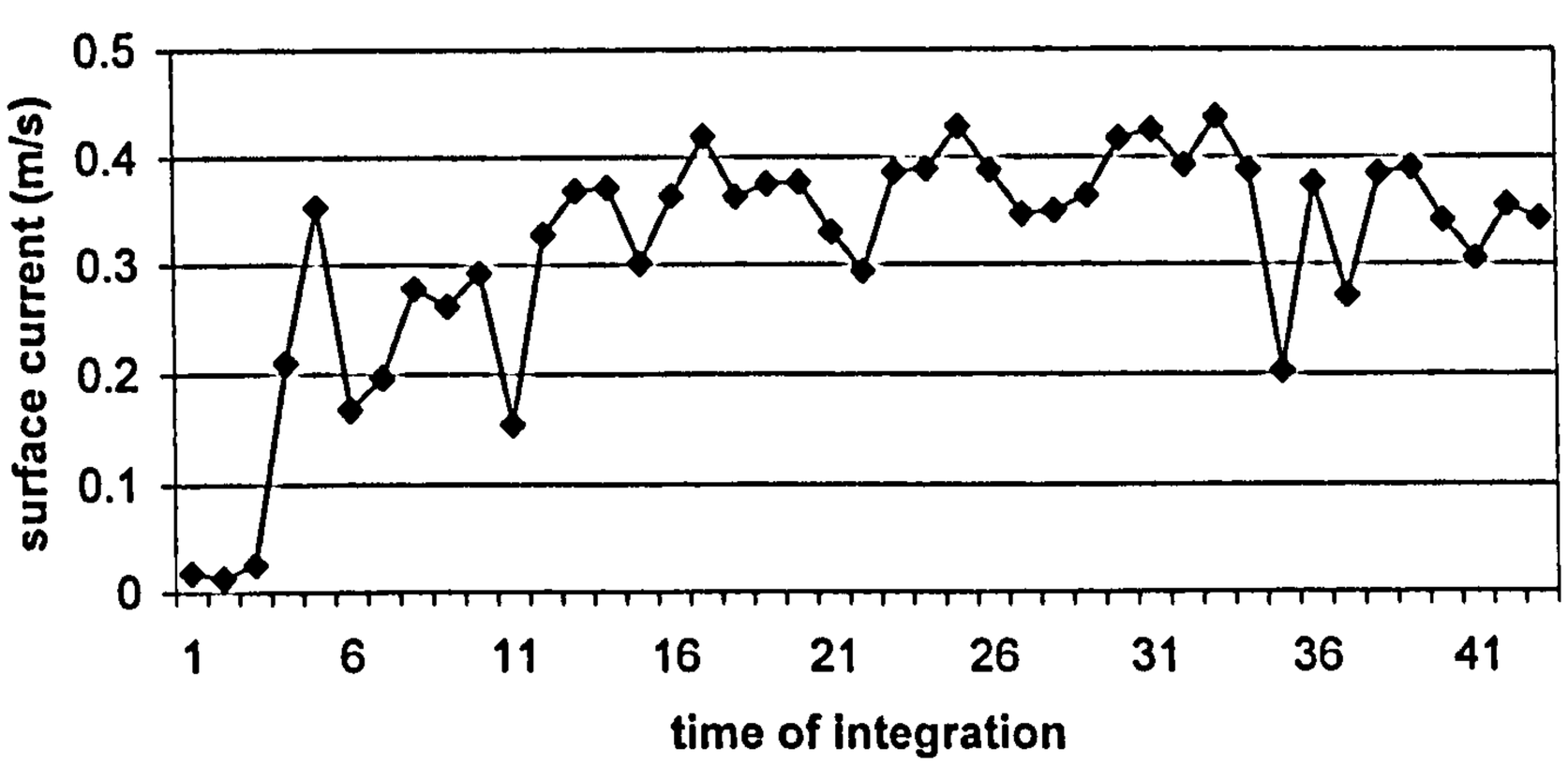

Fig 5.3.13b time series of seabed current at MP

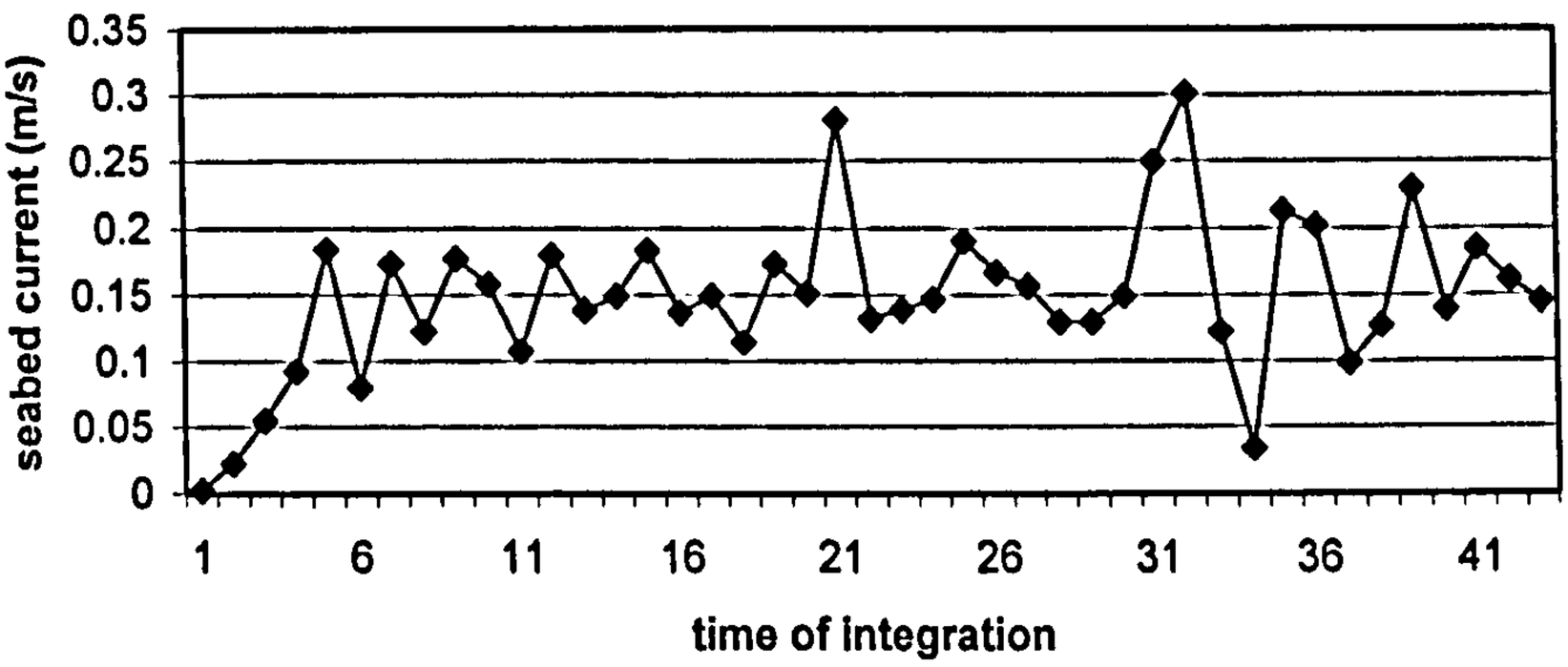

Chapter 6 Conclusions and Future Work

6.1 Conclusions

This thesis presents details of an interactive sigma co-ordinates splicing based numerical model of tidal flow interaction in estuarine and coastal waters. It is characterized by a combination of tidal forcing from the western open boundary of the Eastern Irish Sea and estuarially driven forcing from the river Mersey. The basic framework is implemented by the incorporation of an adaptation of an early river model described by Johns and Oguz (1990) with the bay model originally developed by the Proudman Oceanographic Laboratory for the Eastern Irish Sea. This high-resolution three-dimensional hydrodynamic tidal model is used as a bay model to provide the real-time tidal current profiles from sea surface to sea bed.

These two models are linked together at their common boundary through the surface elevation. The dynamic information is exchanged between the two models through continuity equations in both models. This is implemented by updating the boundary condition of one model using the output of the other. The model is capable of predicting a combination of the tidally- and estuarially- driven circulations of water flow in the nearshore regions.

The modelling of hydrodynamic processes in the estuary is performed by the river model. This model describes the computational domain by solving a set of governing equations numerically. An essential feature of this model is that it uses a turbulence energy equation in a scheme of parameterization for the vertical exchange coefficient. This involves the parameterization of the Reynolds stresses in terms of the turbulent energy density and velocity shear. The salinity and sediment concentrations have also

been incorporated in the model by the use of transport equations. Consequently, the local density of the water is also expressed in terms of the local salinity and sediment concentration. The governing equations are solved subject to a prescribed tidal oscillation at the mouth of the river. Other boundary conditions also have to be provided appropriately.

In the solution processes of the joined model, a difficulty is caused by the way that the discretization of the z variable is defined directly through the depth. As the computational levels are set with a fixed bottom and a free surface, they will not correspond to a set of the fixed physical levels. To avoid this difficulty, the sigma coordinate has been used in this model, so that the bottom of the river and the free surface always correspond to 0 and 1, respectively. This is then suitable for the fixed computational levels and numerical modelling can be implemented after transformation of the equations according to the new coordinates.

For the same reason, the basic equations of the bay model have been cast in a bottom following sigma coordinate system. In the transformed equations, the bottom of the water column and the free surface correspond to –1 and 0, respectively.

The bay model is used to simulate the tidal response in Liverpool bay and provide the real-time tidal elevations to the river model which is applied to the Mersey estuary. In the model, the hydrodynamic equations are solved in Liverpool bay and the surrounding shallow sea subject to the tidal forcing from the western open boundary. Other boundary conditions include land, sea surface, seabed and drying conditions. Salinity and temperature are incorporated in the model and the density is consequently expressed in terms of them. In this application the temperature is set to be constant.

The vertical eddy viscosity and eddy diffusivity are calculated by a one-equation turbulence model and it includes a prognostic equation for turbulence kinetic energy.

Although the sigma coordinate in the bay model is defined differently from that in the river model, they can be transformed from one to another when joining the models together.

In this thesis, the river model and the bay model are linked together through the surface elevation at the boundary between the Mersey river and Liverpool bay. The advantage of this work is to provide the river model with continuous dynamic information from the shelf sea. On the other hand, it is also possible to improve the understanding of the influence of estuary flow on the nearshore hydrodynamic processes.

The three-dimensional bay model was originally compiled using a Fortran complier using the Unix system and necessary adaptation of the model codes have been made in this study so that it can be run by the Fortran compiler on a PC. Then the model codes were modified for an efficient and correct exchange of information.

The first stage of the joining process is to combine the two models with an identical time step of 200 sec. During each time stepping procedure, the calculations in the bay model are performed one time step forward first and the result from this provides information of boundary condition to the river. This allows the variables to be updated so that they are ready to be used in the river model. Then the river model is called as a subroutine of the joined model, and the calculations in the river model can be performed one step forward to update the computed values in the river domain. The next step involves feeding back the values from the river model into the bay model along the common boundary. At this stage, both models have completed one time step

of forward integration. The variables along the common boundary are exchanged between two models at the same level of time. The result from previous step alone is enough for the calculation. This procedure goes back to the bay model to effect the next step of calculation and then to the river model and so on.

When both models are run with identical time steps the information can be exchanged directly between them if the σ-coordinate of each model are matched correctly at the same physical level. This is done by using a scheme to match two different sigma coordinates.

In order to obtain computational stability, the time step in the bay model needs to be chosen at about 200 sec for a 1 km space resolution. To consider the hydrodynamic processes in the estuary area, higher resolution is desirable. A solution to this is to treat the domain of the bay model and that of the river model with different time steps, so that the spatial resolution can be adjusted separately. Here the spatial resolution in the bay model is kept unchanged as before, while the resolution in the river is increased. The horizontal spatial resolution in the river has been increased by four times, which leads to a change of total staggered grid points from 21 to 89 and reduces the spatial grid increment from 3.0 km to 0.68 km.

The second stage of the joining procedure is to increase the total number of horizontal grid points while keeping the length of the computation domain unchanged in the river model to achieve a higher spatial resolution.

As a consequence of this, the time step of integration in the river model has to be changed in order to maintain the stability of the numerical scheme. This has been done by means of trial and error. The results show that the stability was very sensitive to the length of the time step. It was found that when the grid size was reduced to

25% of the original size, the time step required by the river model had to be reduced to 5% of the original time step.

In implementing the exchange of information between two models, we have introduced an interactive grid-splicing scheme to match the variables along the common vertical boundary. This scheme is able to convert the variables that are calculated in the topography following sigma coordinates and are therefore not at the same fixed physical levels along the time dimension. By using this scheme, the variables at a fixed physical level for two successive time steps are determined depending on the values that were originally calculated using the sigma coordinates. The variables for the next step of river model calculations are determined by linear extrapolation.

For each of the shorter time steps in the river model, variables, including the surface elevation and salinity at the common boundary of the two models need to be updated from the bay model. The variables from previous one step in the bay model are not enough to provide information to the river model. Instead, the results of the previous two steps are used to predict the boundary condition of each step for the river model.

During the development of the joined model with increased spatial resolution, it was found that the reduction of the time resolution was much more than that of the spatial resolution. With a reduction of about four times in spatial resolution, the time step has to be reduced by 20 times to achieve the stability of the calculations.

The joined model has been used in Liverpool Bay and the Mersey estuary and the results indicate that the model is effective at simulating (1) the circulation of tidal current approaching the coastal and estuary area; (2) The freshwater discharge from

the estuary into the bay; (3) The salinity structure caused by tidal forcing moving up the river; (4) The sediment transport from the river into the bay.

The joined model was first tested for predicting M_2 tidal elevation and currents. The results are compared with data from Aldridge and Davies (1993) at four locations in Liverpool bay. From the modelling results, it can be seen that a semi-diurnal harmonic has been correctly predicted by the joined model and is consistent with the observations. The tidal ranges in the area of interest in this study, namely, Liverpool bay and the Mersey estuary are large and represent a feature of macrotidal and well-mixed conditions in the vertical direction. The M_2 tidal component has a dominant influence on the dynamic structure of the Mersey estuary and coastal region of Liverpool bay.

The freshwater discharge from the river into the bay presents a feature of bulge in Liverpool bay around the mouth of Mersey. There is a very small difference in the vertical variation of salinity as a result of tidal mixing. The influence of tidal forcing is tested by comparison of the results of modelling with and without the tidal forcing. The results show that when the tidal forcing is absent from the model, the discharge of the freshwater will lead to a low salinity plume extending 40 km northwards from the mouth of the Mersey and spreading to the right as it extends north due to the Coriolis effect.

As the tide moves up the river, the joined model predicts a vertically well-mixed salinity structure in the Mersey estuary. There is almost no vertical salinity gradient. However, when there is no tidal forcing included in the joined model, the vertical gradient is very strong.

The joined model also includes sediment transport in the river and it can estimate the amount of sediment concentration that may be transported from the river into the bay. It is clear that the sediment transport in the Mersey and Liverpool bay is also strongly affected by the tidal forcing.

6.2 Future Work

From the foregoing numerical experiments using the joined model it is suggested that there are several ways the present results may be improved: (1) use an appropriate smoothing subroutine in the river model to reduce the effects of the nonlinear terms in the dynamic equation; (2) use different tidal components other than M_2 as driving forcing of the bay model; (3) incorporate the sediment concentration in the bay model.

The present model in the river is limited to one-dimension in the horizontal. It is suggested that the river model to be extended to two dimensions in the horizontal direction. There is one meeting point in the surface used in the present joined model, to improve the information exchange between the river model and bay model it is recommended to use more than one point as meeting point. One possible method is to embed the fine grid of river model within the coarse grid of bay model.

Further improvements can be made to the present joined model. The effort should be directed towards understanding the detail of the nonlinear instability in the river model when joining with fine horizontal resolution. It may be that there are short wave components input from the bay model which leads to a rapid spatial variation that necessitate the short time step. There is a need for further testing of the joined model with smoothing subroutine of the salinity in the river model.

References:

Aldridge, J.N., Davies, A.M., 1993. A high resolution three dimensional hydrodynamic tidal model for the eastern Irish Sea. J. Phys. Oceanography, **23**, 207-224.

Arakawa, A., Lamb, V.R., 1977. Computational design of the basic dynamical processes if the UCLA general circulation model. In: Methods of Computational Physics. Vol. **17**, Academic Press.

Baptista, A.M., Westerink, J.J., Turner, P.J., 1989. Tides in the English Channel and southern North Sea. A frequency domain analysis using model TEA-NL. Advance Water Resources, **12**, 166-183.

Baumert, H., Radach, G., 1992. Hysteresis of turbulent kinetic energy in nonrotational tidal flows: A model study. J. Geophys. Res., **97**, 3669-3677.

Beardsley, R.C., Hart, J., 1978. A simple theoretical model for the flow of an estuary on to a continental shelf. Journal of Geophysical Research, **83**, 873-883.

Beckers, J. M., 1991. Application of the GHER 3D general circulation model to the west Mediterranean. Journal of Marine System **1**, 315-332.

Berntsen, J., Kowalik, Z., Saelid, S., Soerli, K., 1981. Efficient numerical simulation of ocean hydrodynamics by splitting procedure. Modeling, Identification and Control, **4(2)**, 181-199.

Blumberg, A.F., 1975. A Numerical Investigation into the Dynamics of Estuarine Circulation, p. 59. Chesapeake Bay Institute Tech. Rep. 91, The Johns Hopkins University, Baltimore, MD, U.S.A.

Blumberg, A.F., Mellor, G.L., 1978. A coastal ocean numerical model, in Mathematical Modelling of Estuarine Physics, Proc. Int. Symp., edited by J. Sunderman and K.-P. Holtz, pp. 203-214, Springer-Verlag, Berlin.

Blumberg, A.F., Mellor, G.L., 1983. Diagnostic and prognostic numerical circulation studies of the South Atlantic Bight. J. Geophys. Res., **88**, 4579-4592.

Blumberg, A.F., Mellor, G.L., 1987. A description of a three-dimensional coastal ocean circulation model. In: Heaps, N. ed., Coastal Estuarine Science.4. Three Dimensional Coastal Ocean Models. American Geophysical Union, pp. 1-16.

Boussinesq, J., 1903. Theorie analytique de chaleur. Vol. 2. Gauthier-Villars, Paris.

Bowden, K.F., 1983. Physical Oceanography of Coastal Waters. Ellis Horwood, Chichester, 302pp.

Burchard, H., Petersen, O., Rippeth, T.P., 1998. Comparing the performance of the Mellor-Yamada and the k-ε two-equation turbulence model. Journal of Geophysical Research 103, **10**,543-10,554.

Chen, H., Dyke, P.P.G., 1996. Multivariable time series sediment dynamical transport and its identification in Rufiji Delta, Tanzania. Applied Mathematical Modelling, **20**, 756-770.

Chen, H., Dyke, P.P.G., 1998. Multivariate models for suspended sediment concentration. Continental Shelf Research, **18**, 123-150.

Craig, P.G., 1996. Vertical profiles and surface roughness under breaking waves. Journal of Geography Research **101**, 1265-1277.

Davies, A.M., Furnes, G.K., 1980 Observed and computed M_2 tidal currents in the North Sea. Journal of Physical Oceanography **10**, 237-257.

Davies, A.M., 1983a. Formulation of linear three-dimensional hydrodynamic sea model using a Galerkin-Eigenfunction method. International Journal for Numerical Methods in Fluids. **3**, 33-60.

Davies, A.M., 1983b Application of a three-dimensional shelf sea model to the calculation of North Sea currents. North Sea Dynamics, J. Sunderman and W. Lenz, Eds., Springer-Verlag, 44-62.

Davies, A.M., Stephens, C.V., 1983. Comparison of the finite difference and Galerkin methods as applied to the solution of the hydrodynamic equations. Appl. Math. Model., **7**, 226-240.

Davies, A.M., 1986. A three-dimensional model of the northwest European continental shelf, with application to the M_4 tide. Journal of Physical Oceanography **16**, 797-813.

Davies, A.M., 1987a. A three-dimensional numerical model of semi-diurnal tides on the European continental shelf. Three Dimensional Models of Marine and Estuarine Dynamics. J. C. J. Nihoul and B. M. Jamart, Eds., Elsevier, 573-590.

Davies, A.M., 1987b. Spectral models in continental shelf sea oceanography. Three Dimensional Coastal Ocean Models. N. S. Heaps, Ed., Amer. Geophys. Union, 71-106.

Davies, A.M., Flather, R.A., 1987. On computing extreme meteorologically induced currents with application to the north-west European continental shelf and wind forcing: Results from a three-dimensional hydrodynamic model. Journal of Geography Research **99**, 22665-22687.

Davies, A.M., 1988. On formulating two dimensional vertically integrated hydrodynamic numerical models with an enhanced representation of bed stress. J.Geophys. Res., **95**, 20,287-20,312.

Davies, A.M., Xing, J., 1995. An intercomparison and validation of a range of turbulence closure schemes used in three-dimensional tidal models. In Quantitative skill assessment for coastal ocean models, D. R. Lynch and A. M. Davies eds., Geophys. Union, Washington D. C., pp 97- 124.

Davies, A.M., Jones, J.E., Xing, J., 1997a. Review of recent developments in tidal hydrodynamic modelling. I: Spectral models. J. Hydraulic Eng., **123**, 278-292.

Davies, A.M., Jones, J.E., Xing, J., 1997b. Review of recent developments in tidal hydrodynamic modelling. II: Turbulence energy models. J. Hydraulic Eng., **123**, 293-302.

Davies, A.M., Xing, J., 1999. Sensitivity of plume dynamics to the parameterization of vertical mixing. Int. J. Numer. Meth. Fluids **30**, 357-405.

Davies, A.M., Xing, J., 2001. Modelling processes influencing shelf edge currents, mixing, across shelf exchange, and sediment movement at the shelf edge. Dynamics of Atmos. and Oceans. **34**, 291-326.

Davies, A.M., Hall, P., Howarth, M.J., Knight, P., Player, R., 2001. A detailed comparison of measured and modelled wind driven currents in the North Channel of the Irish Sea. Journal of Geophysical Research. **106**, 19683-19714

Davies, A.G., Soulsby, R.L., King, H.L., 1988 . A numerical model of combined wave and current bottom boundary layer. Journal of Geophysical Research **93**, 491-508.

Dyke, P.P.G., 2000. Coastal and shelf sea modelling. Kluwer Academic Publishers, 272pp.

Duxbury, A.C., 1965. The union of the Columbia river and the Pacific Ocean-general features. In Ocean Science and Ocean Engineering. Marine Technology Society, Washington, pp. 914-922.

Elliot, A.J., 1976. A Numerical Model of the Internal Circulation in a Branching Estuary, p. 85. Chesapeake Bay Institute, Spec. Rep. 54, The Johns Hopkins University, Baltimore, MD, U.S.A.

Fairbridge, R.W., 1980. in E. Olausson and I. Cato (eds.) Chemistry and Biogeography of Estuaries, John Wiley.

Flather, R.A., Heaps, N.S., 1975. Tidal computations for Morecambe Bay. Geophys. J. R. Astron. Soc., **42**, 489.

Flather, R.A., 1976. A tidal model of the north west European continental shelf. Mem. Soc. R. Sci. Liege **6**, 141-164.

Flather, R.A., Hubbert, K.P., 1990. Tide and surge models for shallow water-Morecambe Bay revisited. Modeling Marine Systems, Vol. 1, A. M. Davies, Ed., CRC Press, 135-166.

Foreman, M.G.G., Walters, R.A., 1990. A finite-element tidal model for the southwest coast of Vancouver Island. Atmospheric Oceanography, **18**, 261-287.

Foreman, M.G.G., Henry, R.F., Walters, R.A., Ballantyne, V.A., 1993. Afinite-element tidal model for British Columbia. J. Geophys. Res., **98**, 2509-2531.

Freeman, N.G., Hale, A.M., Danard, 1972. A modified sigma equations approach to the numerical modelling of Great Lake hydrodynamics. J. Geophys. Res., **77**, 1050-1060.

Furnes, G.K., 1983. A three-dimensional numerical sea model with eddy viscosity varying piecewise linearly in the vertical. Contin. Shelf Res., **2**, 231-242.

Furnes, G.K., Mork, M., 1987. Formulation of a continuously stratified sea model with three-dimensional representation of the upper layer. Coastal Eng., **11**, 415-445.

Gary, J.M., 1973. Estimate of truncation error in transformed co-ordinate, primitive equation atmospheric models. Journal of Atmospheric Sciences, **30**, 223-233.

Gopala Krishna, V.V., Sastry, J.S., 1985. Surface circulation over the shelf off the east coast of India during the Southwest Monsoon. Indian Journal of Marine Sciences, **14**, 62-65.

Gordon, R.B., Spaulding, M.L., 1987. Numerical simulations of the tidal- and wind-driven circulation in Narragansett Bay. Estuar. Coastal Shelf Sci., **24**, 611-636.

Hamilton, P., 1975. A numerical model of vertical circulation of tidal estuaries and its application to the Rotterdam waterway. Geophys. J. Roy Astron. Soc., **40**, 1-12.

Haney, R.L., 1991. On the pressure gradient force over steep topography in sigma co-ordinate ocean models. Journal of Physical Oceanography. **21**, 610-619.

Harleman, D.R.F., 1971. One-Dimensional Model. Estuarine Modeling: An Assessment, pp. 34-85. TRACOR, Inc., New York, NY, U.S.A.

Heaps, N.S., 1972. On the numerical solution of the three-dimensional hydrodynamical equations for tides and storm surges. Mem. Soc. Roy. Soc. Sci. Liege Coll. Huit, **2**, 143-180.

Heaps, N.S., 1974. Development of a three-dimensional numerical model of the Irish Sea. Rapp. P.-V. Reun. Cons. Int. Explor. Mer., **167**, 147-162.

Heaps, N.S., 1983. Storm surges, 1967-1982. Geophys. J.R. Astronom. Soc. **74**, 331-376.

Hess, K.W., 1985. Assessment model for estuarine circulation and salinity. NOAA Tech. Memo. NESDIS AISC 3, Mar. Envir. Ass. Div. Washington D.C.

Hinze, J.O., 1975. Turbulence. McGraw-Hill, New York, N.Y., 790 pp.

Hsu, M.H., Kuo, A.Y., Liu, W.C., Kuo, J.T., 1999. Numerical simulation of circulation and salinity distribution in the Tanshui estuary. Proc. Natl. Sci. Counc. ROC(A) Vol. **23**, 2, 259-273.

James, I.D., 1990. Numerical modelling of density-driven circulation in shelf seas. Modelling Marine Systems, Vol. II, A.M. Davies, ed., CRC Press, Boca Raton, Fla., 345-373.

Johns, B., 1978. The modelling of tidal flow in a channel using a turbulence energy closure scheme. J . Phys. Oceanogr., 8, 1042-1049.

Johns, B., 1983. Physical Oceanography of Coastal and Shelf Seas, Chap. 3, Elsevier Amsterdam, Oxford, New York, Tokyo, 470pp.

Johns, B., Sinha, P.C., Mohanty, U.C., Rao, A.D., 1983. Simulation of storm surges using a three-dimensional numerical model: an application to the 1977 Andhra cyclone. Q. J. R. Meteorl. Soc., 109, 211-224.

Johns, B., Oguz, T., 1990. The modelling of flow of water through the Bosphorus.Dynamics of Atmospheres and Oceans. 14, 229-258.

Johns, B., 1991. The modelling of the free surface flow of water over topography. Coastal Engineering .15, 257-278.

Johns, B., Rao, A.D., Dube, S.K., Sinha, P.C., 1991. An application of a wind-driven coastal upwelling model in the western Bay of Bengal. Continental Shelf Research, 11, 295-319.

Johns, B ., Rao, A.D., Rao, G.S., 1992. On the occurrence of upwelling along the east coast of India. Estuarine, Coastal and Shelf Science 35, 75-90.

Johns, B., 1997. Expert lectures in coastal hydrodynamics/computation.

Johnson, B.H., 1980. VAHM-Vertically averaged hydrodynamic model using boundary-fitted coordinates. Paper HL-80-3, U.S. Army Engineer Waterways Experiment Station, Vicksburg, Miss.

Kolmogorov, A. N., 1941 Compt. Rend. Acod. Sci. U.R.S.S. 30,301.

Koutitas, C.G., O'Connor, B.A., 1980. Modelling three dimensional wind-induced flows. *J. Hydr. Div.*, ASCE, 106, 1843-1865.

Kowalik, Z., Murty, T.S., 1993. Numerical Modeling of ocean dynamics. Advanced series on ocean Engineering- Volume 5. World Scientific, 481pp.

Landau, L.D., Lifshitz, E.M., 1959. Fluid Dynamics. Pergamon Press, 536 pp.

Lardner, R.W., Song, Y., 1992. A comparison of spatial grids for numerical modelling of flows in near coastal seas. Int. J. Numer. Methods in Fluids. 14(1), 109-124.

Launder, B.E., Spalding, D.B., 1972. Mathematical models of turbulence. Academic Press, New York, N.Y., 169pp.

Launder, B.E., Spalding, D.B., 1972. Mathematical Models of Turbulence. Academic Press, London, 170pp.

Leendertse, J.J., Alexander, R.C., Liu, S.K., 1973. A three-dimensional model for estuaries and coastal seas: Volume I, Principles of Computation. RAND Corporation. R-1417-OWRR.

Leendertse, J.J., Liu, S.K., 1975. A three-dimensional model for the estuaries and coastal seas: Volume II, Aspects of Computation. RAND Corporation. R-1764-OWRT.

Le Provost, C., Genco, M.L., Lyard, F., 1995. Modelling and predicting tides over the World ocean. Quantitative skill assessment for coastal ocean models. D.R. Lynch and A.M. Davies, eds., Am. Geophys. Union, Washington, D.C. 175-202.

Le Provost, C., Fornerrino, M., 1985. Tidal spectroscopy of the English Channel with a numerical model. J. Phys. Oceanography, **15**, 1009-1031.

Liu, S.K., Leedertse, J.J., 1978. Multidimensional Numerical Modeling of Estuaries and Coastal Seas. 95-164. In: Ven Te Chow (ed.), Advances in Hydro-science, Vol. **11**.

Luettich, R.A., Westerink, J.J., 1994. Continental shelf scale convergence studies with a barotropic tidal model. Quantitative skill assessment for coastal ocean models. D.R.

Lynch, D.R., Naimie, C.E., 1993. The M_2 tide and its residual on the outer banks of the Gulf of Maine. J. Phys. Oceanography, **23**, 2222-2253.

Lynch, D.R., Ip, J.T.C., Naimie, C.E., Wernere, F.E., 1995. Convergence studies of tidally-rectified circulation on Georges Bank. Quantitative skill assessment for coastal ocean models. D.R. Lynch and A.M. Davies, eds., Am. Geophys. Union, Washington, D.C., 153-174.

Madala, R.V., Piacsek, S.A., 1977. A semi-implicit numerical model for baroclinic oceans. J. Comp. Phys., **23**, 167-178.

Mellor, G.L., 1973. Analytic prediction of the properties of stratified planetary surface layers. J. Atmos. Sci., **30**, 1061-1069.

Mellor, G.L., Blumberg, A.F., 1985. Modelling vertical and horizontal diffusivities with the sigma coordinate system. Mon. Wea. Rev, **113**, 1380-1383.

Mellor, G.L., Ezer, T., Oey, L.Y., 1994. The pressure gradient conundrum of sigma coordinate ocean models. J. Atmos. Oceanic. Technol., **11**, 1126-1134.

Mellor, G.L., Oey, L.Y., Ezer, T., 1998. Sigma coordinate gradient errors and the seamount problem. J. Atmos. Oceanic. Technol., **12**, 1122-1131.

Mesinger, F., Arakawa, A., 1976. Numerical Methods Used in Atmospheric Models. GARP Publications Series, No.17. 64pp.

Murty, T.S., 1984. Storm surges- Meteorological Ocean Tides, Bull. No.212, Dept. Fish. Oceans, Ottawa, 897 pp.

Nihoul, J.C.J., 1977. Three-dimensional model of tides and storm surge in a shallow well-mixed continental sea. Dyn. Atmos. Oceans, **2**, 29-47.

Ozer, J., Padilla-Hernandez, R., Monbaliu, J., 2000. A coupling module for tides, surges and waves. Coastal Engineering. **41**, 95-124.

Pedlosky, J., 1982. Geographical Fluid Dynamics. Springer-Verlag, New York. 624 pp.

Phillips, N.A., 1957. A coordinate system having some special advantages for numerical forecasting. J. Meteorol., **14**, 184-185.

Pietrzak, J., Jakobson, J.B., Burchard, H., Vested, H.J., Petersen, O., 2002. A three-dimensional hydrodynamic model for coastal and ocean modelling using a generalised topography following co-ordinate system. Ocean Modelling, **4**, 173-205.

Proudman, J.W., 1953. Dynamical Oceanography. Methuen, J. Willey, London, 409 pp.

Ramming, H.G., Kowalik, Z., 1980. Numerical Modeling of Marine Hydrodynamics Elsevier, Amsterdam.

Rao, A.D., 1995. A numerical modelling study of the flow and salinity structure in the Godavari estuary, east coast of India. International Journal for Numerical Methods in Fluids, **21**, 35-48.

Rodi, W., 1980. Turbulence models and their application in hydraulics. Report, International Association for Hydraulic Research, Delft, Netherlands.

Rotta, J., 1951. Statistical theory of inhomogeneous turbulence. Part I.. Zeitschrift fur Physik. **129**, 257-272.

Sharples, J., Simpson, J.H., 1995. Semi-diurnal and longer period stability cycles in the Liverpool Bay region of freshwater influence. Continental Shelf Research. Vol. **15**, 295-313.

Smith, T.J., Takhar, H.S., 1977. The calculation of oscillatory flow in open channels using mean turbulence energy models. Unpublished report, Simon Engineering Laboratories, University of Manchester.

Simons, T.J., 1974. Verification of numerical models of Lake Ontario: Part I. Circulation in spring and early summer. J. Phys. Oceanogr., **4**, 507-523.

Simons, T.J., 1980. Circulation models of lakes and inland seas. Can. Bull. Fish. Aquat. Sci., Bull. 203, Ottawa, 146pp.

Simpson, J.H., Brown, J., Matthews, J., Allen, G., 1990. Tidal straining, density currents, and stirring in the control of estuarine stratification. Estuarines, **13**, 125-132.

Spaulding, M.L., 1984. A vertically averaged circulation model using boundary fitted coordinates. J. Phys. Oceanography, **14**, 973-982.

Spaulding,M.L., Isaji, T., 1987. Three-dimensional continental shelf hydrodynamic model including wave current interaction. Pp 405-426 In: Nihoul, J.C.J., Jamart, B.M.,(Eds.), Three-dimensional Models of Marine and Estuarine Dynamics, Elsevier, Amsterdam, 629pp.

Stacey, M.W., Pond, S., 1997. On the Mellor-Yamada Turbulence Closure Scheme: the surface boundary condition for q2 . Journal of Physical Oceanography **27**, 2081-2086.

Stelling, G.S., Wiersma, A.K., Willemse, J.B.T.M., 1986. Practical aspects of accurate tidal computations. J. Hydraul. Eng. ASCE, **112**, 802-817.

Van Rijn, L.C., 1984. Sediment pickup functions. J. Hydraulic Eng., **110**(10), 1494-1502.

Van Rijn, L.C., 1986. Mathematical modelling of suspended sediment in non-uniform flows. Proc. ASCE, J. Hydraul. Eng. **112**(6), 1613-1641.

Walters, R.A., Werner, F.E., 1991. Nonlinear generation of overtides, compound tides, and residuals. Tidal hydrodynamics, B.B. Parker, ed., John Wiley and Sons, New York, N.Y., 297-320.

Wang, D.P., Kravitz, D.W., 1980. A semi-implicit two-dimensional model of estuarine circulation. Journal of Physical Oceanography, **10**(3), 441-454.

Westerink, J.J., Stolzenback, K.D., Connor, J.J., 1989. General spectral computation of the nonlinear shallow water tidal interactions within the Bight of Abaco. J. Phys. Oceanography. **19**, 1348-1371.

Wilders, P., van Stijn, Th.L., Stelling,G.S., Fokkema, G.A., 1988. A fully implicit splitting method for accurate tidal computations. Int. J. Numer. Methods Eng., **26**, 2707-2721.

Wolf, J., 1983. A comparison of a semi-implicit with an explicit scheme in a three-dimensional hydrodynamic model. Contin. Shelf Res., **2**, 215-229.

Xing, J., Davies, A.M., 1995a. Application of a range of turbulence energy models to the determination of M_4 tidal current profiles. Continental Shelf Res., **16**, 517-547.

Xing, J., Davies, A.M., 1995b. Application of three-dimensional models to the determination of tidal mixing and currents in a shallow sea. Progress in Oceanography, **35**, 153-205.

Xing, J., Davies, A.M., 1996a. The influence of mixing length formulation and stratification upon tidal currents in shelf seas. Estuarine Coastal and Shelf Science **42**, 417-456.

Xing, J., Davies, A.M., 1996b. Application of a range of turbulence models to the determination of M_4 tidal current profiles. Continental Shelf Research **7**, 643-683.

Xing, J., Davies, A.M., 1998. Application of a range of turbulence energy models to the computation of the internal tide. International Journal for Numerical Methods in Fluids **26**, 1055-1084.

Xing, J., Chen, F., Proctor, R., 1999. A two-dimensional slice model of the shelf edge region off the west coast of Scotland: Model response to realistic seasonal forcing and the role of M_2 tide. Continental Shelf Research **19**, 1353-1386.

Xing, J., Davies, A.M., 2003. A model study of tidally induced suspended sediment transport in the Iberian shelf edge region. Estuarine, Coastal and Shelf science, **58**, 321-333.